SENSOR AND SIMULATION NOTES

Note 305

COMMON AND DIFFERENTIAL TEM MODES
FOR TWO WIRES ABOVE A GROUND PLANE

C. Zuffada
N. Engheta

CLEARED FOR PUBLIC RELEASE

PL/PA 7 FEB 97

Kaman Sciences Corporation
Dikewood Division/Santa Monica
2800 28th Street, Suite 370
Santa Monica, California 90405

July 1987

Abstract

The analysis presented in this document predicts the field produced by
two parallel wires over a perfectly conducting, infinite ground plane. Both
common mode and differential mode excitation of the wires are considered. The
field uniformity is quantified by calculating the 2-norm and the ∞-norm
errors. Impedance calculations are also presented.

PL 96-1152

SENSOR AND SIMULATION NOTES

Note 305

COMMON AND DIFFERENTIAL TEM MODES
FOR TWO WIRES ABOVE A GROUND PLANE

C. Zuffada
N. Engheta

Kaman Sciences Corporation
Dikewood Division/Santa Monica
2800 28th Street, Suite 370
Santa Monica, California 90405

July 1987

Abstract

The analysis presented in this document predicts the field produced by
two parallel wires over a perfectly conducting, infinite ground plane. Both
common mode and differential mode excitation of the wires are considered. The
field uniformity is quantified by calculating the 2-norm and the ∞-norm
errors. Impedance calculations are also presented.

1

PREFACE

The starting point in the present analysis was a work originally performed by C.E. Baum which is here extended to cover four possible excitation configurations. We wish to acknowledge the helpful discussions C.E. Baum had with one of the authors as well as his comments on the work performed at its intermediate stage.

Many thanks are expressed to S. Kokorowski for his continuous cooperation, valuable suggestions, and advice in the organization of the material. Comments and discussions with Capt. T. Smith of AFWL and K.S.H. Lee, F.C. Yang and L. Marin of Kaman Sciences, Dikewood Division are also gratefully acknowledged. We availed ourselves of the computer skills of C.C. Cheung and T. Weimer for writing the software used to produce the figures.

CONTENTS

I. INTRODUCTION

Figure 1 shows the geometry of the antenna which is being analyzed. It consists of two wires in a configuration similar to a rhombus, with a CW source at one vertex and a matched termination load at the other vertex. The wires are supported by a dielectric cord stretched between two poles. The mechanical design allows the wire separation at the poles, denoted by 2a, and the wire height at the poles, denoted by b, to be varied. The CW source can drive the illuminator in either a common mode or a differential mode. In the common mode both wires are driven with the same voltage, and the electric field produced in the region of interest between wires and ground, referred to as the working volume, has predominantly vertical polarization with respect to ground. In the differential mode the wires are driven with voltages of opposite polarity, and the electric field in the working volume has a strong horizontal polarization with respect to ground.

One of the main objectives of this analysis is to determine optimum wire heights and wire separations, for both the common and differential modes, which produce the most uniform fields in the working volume of the antenna. Such volume has a transverse section of size 2A x B, as shown in Fig.1. Another objective is to determine the expected electromagnetic field distributions, and the characteristic impedances at these optimum wire heights and separations. To this end four different cases are investigated. These are illustrated in Figure 2. Case 1 considers the common mode excitation with a test object near the ground. Case 2 considers the common mode excitation with a test object above the ground to better approximate in-flight conditions. Case 3 considers the differential mode with the test object near the ground, and Case 4 considers the differential mode with the test object above the ground.

The analysis presented in the following sections builds on the analysis originally performed by C. Baum (Ref. 1). Section II gives an overall description of the mathematical model. Section III describes the optimization study performed to determine optimum values for wire heights and separations for the four cases mentioned above. Section IV describes the impedance calculations, and Section V presents field calculations.

TERMINATION

SOURCE

WORKING VOLUME

b

B

WORKING VOLUME

2a

2A
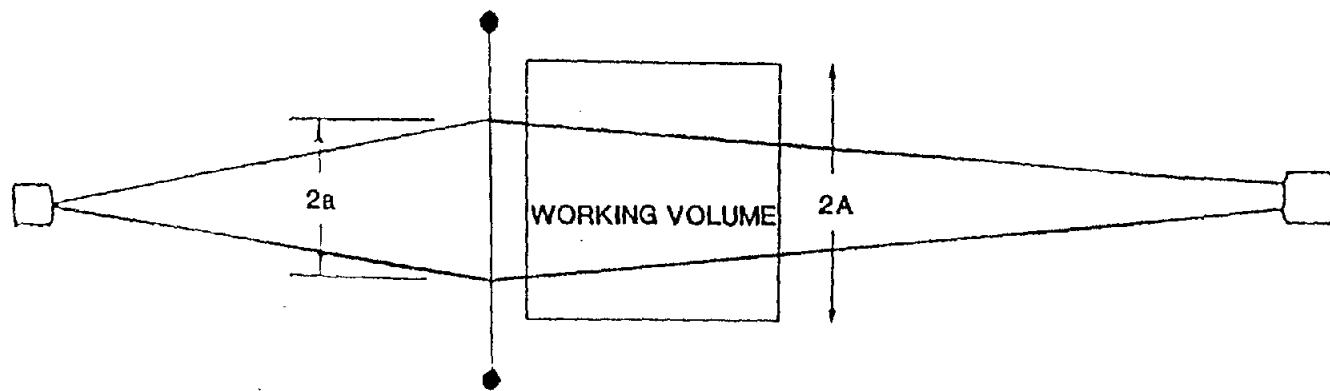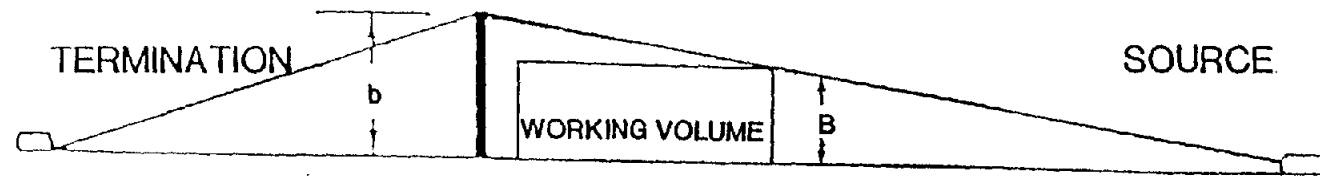
Figure 1. Antenna configuration
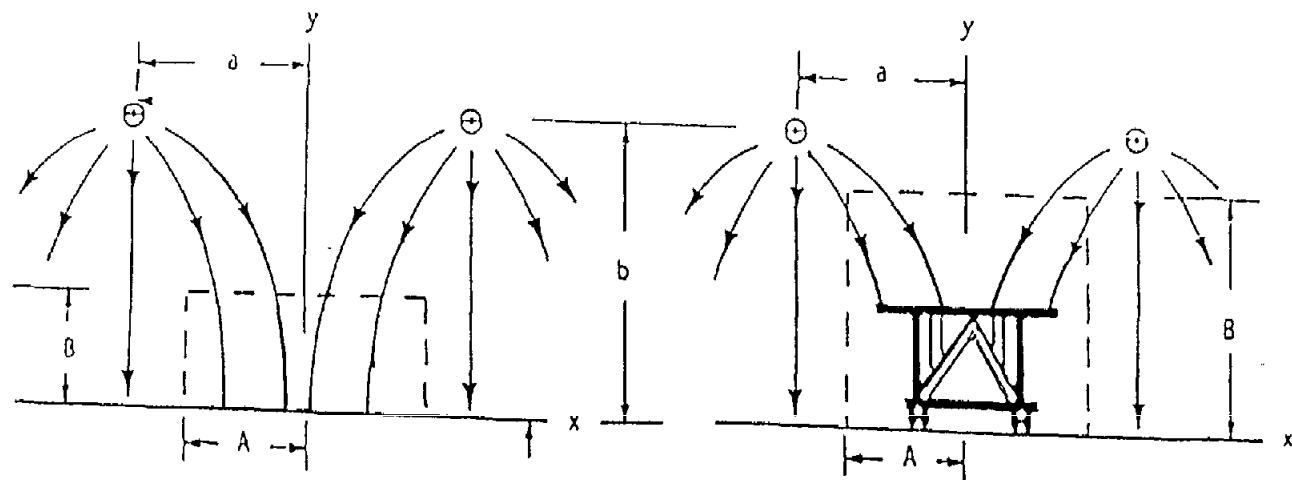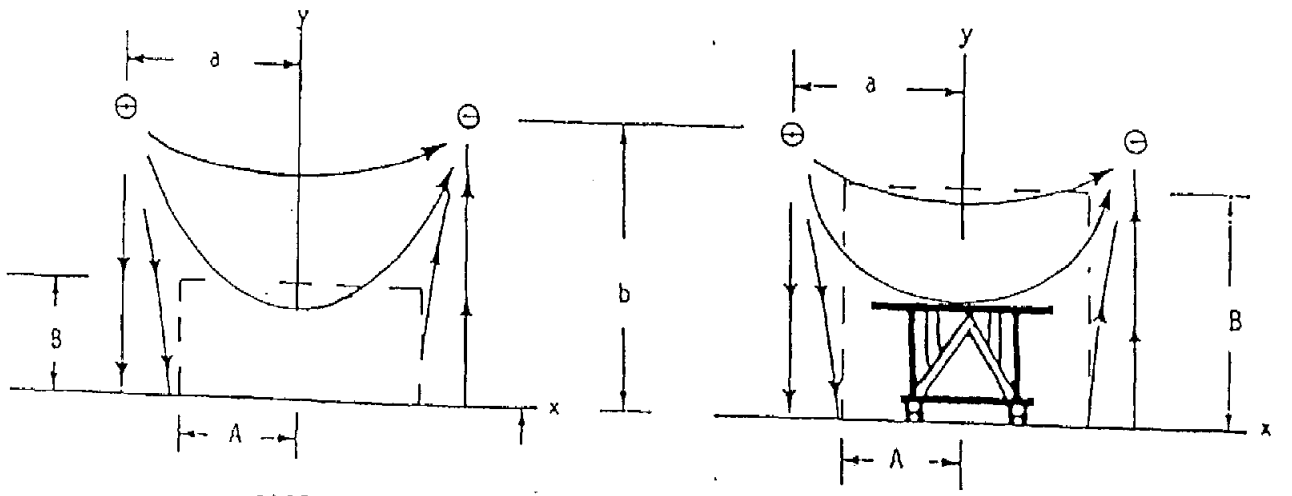
Figure 2. Dimensions of the four cases being investigated.

II. DESCRIPTION OF THE ANALYTICAL MODEL

Given the configurations presented in Figures 1 and 2 the problem of
determining the electromagnetic fields inside the working volume is
approximated by the ideal static problem(s) of finding the electric (magnetic)
field due to two parallel infinite line charges (currents) separated by a
distance 2a and located above a perfectly conducting and infinitely extended
plane at a height b. Such an approximation is adequate provided the
frequencies of interest are sufficiently low so that higher order modes can be
neglected. In addition, the reflections and scattering originating from bends
in transmission lines and load terminations are not described by this model.
The analysis simplifies the three dimensional problem by assuming a two-
dimensional, quasi-static, transverse electromagnetic (TEM) approximation.
The solution to this problem can be obtained by the method of images and is
well documented in the literature (see, for instance, Ref. 2). Figure 2 shows
the four cases being considered, two using common mode and two using
differential mode excitations, together with the Cartesian coordinate system
introduced to describe the two-dimensional analysis.

In the common mode excitation the configuration of the antenna i.e., a
and b, are chosen in such a way that the electric field in the working volume,
which is predominantly directed along y, is made to be as uniform as
possible. For the differential mode the electric field has a large component
directed along x. For this type of excitation, a and b are therefore chosen
to maximize the uniformity of the x-component. These relevant components of
the electric field are given by the following expressions obtainable from the
potential presented, for instance, in Ref. 3, in conjunction with the method
of images.

$$E_y = \frac{q}{2\pi\varepsilon_0} \left\{ \frac{y-b}{(x-a)^2 + (y-b)^2} + \frac{y-b}{(x+a)^2 + (y-b)^2} - \frac{y+b}{(x-a)^2 + (y+b)^2} - \frac{y+b}{(x+a)^2 + (y+b)^2} \right\} \text{ (common mode)} \tag{1}$$

and

$$E_x = \frac{q}{2\pi\epsilon_0} \left\{ \frac{x+a}{(x+a)^2 + (y-b)^2} - \frac{x-a}{(x-a)^2 + (y-b)^2} - \right.$$

$$\left. \frac{x+a}{(x+a)^2 + (y+b)^2} + \frac{x-a}{(x-a)^2 + (y+b)^2} \right\} \quad \text{(differential mode)} \qquad (2)$$

where q is the charge per unit length of the line and $\epsilon_0 = 8.85 \times 10^{-12}$ F/m is the vacuum permittivity. The ratio $q/(2\pi\epsilon_0)$ can be related to the source power W of the transmitter; the reader is referred to Section IV for this detailed derivation.

In order to visualize the behavior of the fields in a cross section of the working volume, equipotential and electric field lines can be plotted for any given choice of a and b. The analytical expressions for such curves are found by constructing conformal transformations in addition to applying the method of images. According to References 2 and 3, the expression used to generate the curves are:

$$u = \frac{1}{2} \left\{ \ln\left[\frac{(x+a)^2 + (y+b)^2}{(x+a)^2 + (y-b)^2} \right] \pm \ln\left[\frac{(x-a)^2 + (y+b)^2}{(x-a)^2 + (y-b)^2} \right] \right\} \qquad (3)$$

$$v = \arctan\left[\frac{2b(x+a)}{(x+a)^2 + y^2 - b^2} \right] \pm \arctan\left[\frac{2b(x-a)}{(x-a)^2 + y^2 - b^2} \right] \qquad (4)$$

where the variable u represents equipotentials and v represents electric field lines. In this problem u may also represent magnetic field lines. The + signs in Equations 3 and 4 apply to the common mode and the - signs apply to the differential mode.

The above equations have been normalized to line charges of values $q = \pm 2\pi\epsilon_0$.

III. CONFIGURATION'S OPTIMIZATION

The purpose of this section is to investigate how fields vary in the working volume depending on the choice of a and b, and identify ranges of values for a and b over which the electric field is reasonably uniform within this volume for the two identified excitation modes. For simplicity we normalize all the linear quantities with respect to h, thus defining a' = a/h, b' = b/h.

To quantify the extent of uniformity we introduce a functional $F(E_\delta,a',b',D)$ which gives the relative error, in the sense of the 2-norm, of any of the relevant components of the field with respect to the average value taken within a specified region. In its general form $F(E_\delta,a',b',D)$ is defined as:

$$F(E_\delta,a',b',D) = \{\frac{1}{D} \int_D (E_\delta(a',b',\xi) - E_\delta^{ave}(a',b'))^2 d\xi\}^{1/2} / E_\delta^{ave}(a',b') \quad (5)$$

where ξ is either x' = x/h or y' = y/h, depending on the excitation region being considered, and D may be any of the following one-dimensional domains: -A/h < x'< A/h ; -C/h < y'< C/h. For the convenience of the reader these domains are visualized in Figure 3. The variable E_δ is E_y for the common mode or E_x for the differential mode. The integration in y is performed over a domain 2C which is smaller than the maximum height B of the working volume. Moreover, E_δ^{ave} is defined as:

$$E_\delta^{ave} = \frac{1}{D} \int_D E_\delta(a',b',\xi)d\xi \quad (6)$$

Explicit expressions for the 2-norm relative errors which have been derived for the four cases being considered in this report are shown in Appendix A.

As an alternative, or perhaps an addition, to the 2-norm error, an infinity-norm error can be constructed. The ∞-norm error is given, in its general form, by the expression
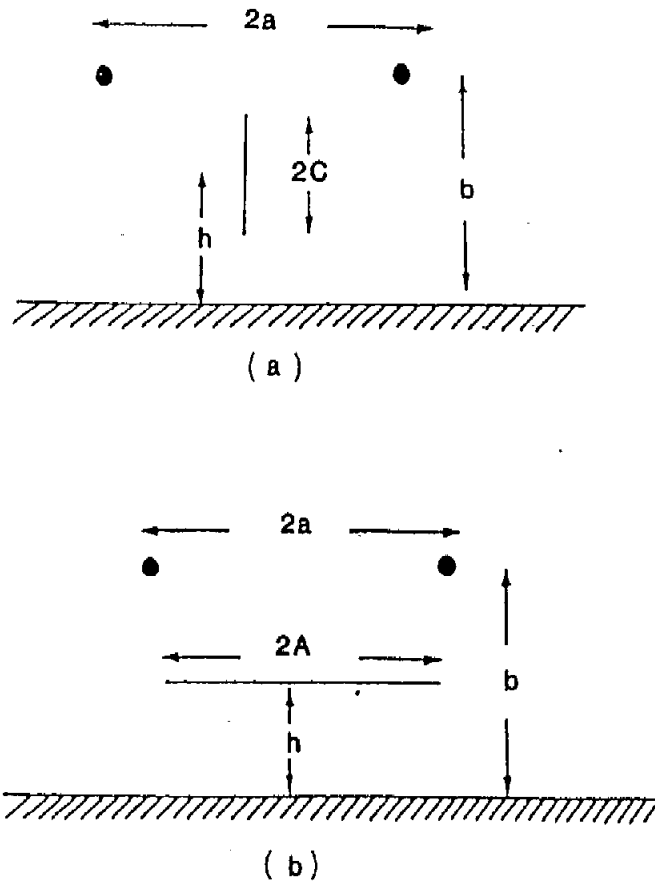
Figure 3. Domains of integration for uniformity errors.
(a) along y
(b) along x

$$P(E_\delta, a', b', D) = \max_D \left| \frac{E_\delta(a', b', \xi) - E_\delta^{ave}(a', b')}{E_\delta^{ave}(a', b')} \right| \tag{7}$$

where the meaning of ξ, δ and D is the same as in Equation 5. Starting with Equations A2, A4, A6 and A8 given in Appendix A, Equation 7 was used to calculate the ∞-norm for the four cases being considered. The ∞-norm functionals were maximized within their domain of definition; the maximization was done numerically. The calculations are presented in the following sections. The ∞-norm error provides a rougher estimate of field uniformity than the 2-norm error in that it is a measure of the maximum deviation from the average field, while the 2-norm error is a root-mean-square quantity. For each case the following inequality is always true:

$$\infty\text{-norm error} > 2\text{-norm error}$$

As previously noted the relative error F or P, for any given D, is a function of two independent parameters: a' and b'. Given a certain working volume, and given a relationship between a and b based on some conditions placed on the field or its derivatives at a given point, the uniformity errors can be evaluated as a function of either a' or b', only. This allows one to choose a suitable range of values for a and b (for a given value of h) for which the errors are at or close to their minimum and the degree of uniformity of the field at the test object is contained within a few percent error. Alternatively, a' and b' can be determined in such a way that one of the errors is made minimum. In the following sections we describe how the field uniformity may be optimized in terms of the minimization of one of the error calculations based upon the parameters a', b', for the four cases being considered in this study.

1. CASE 1: COMMON MODE - TEST OBJECT NEAR THE GROUND

For the common mode excitation (see Figure 2) it turns out that, when the relationship $a/b = 1/\sqrt{3}$ holds, the first three derivatives of E_y with respect to x and y at the point (x = 0, y = 0) are zero (calculations are provided in Reference 1). According to Reference 1 this criterion was chosen to optimize the field uniformity in the local region near this point. Indeed the origin of the coordinate system is a point of symmetry for this excitation mode, and

11

the field is strong there relative to other points in the working volume. Figures 4 and 5 illustrate the 2-norm errors computed along x and y, respectively, for this case. In Figure 4 the variable on the abscissa axis is a/A, i.e., the ratio of a to the half-width A of the working volume (see Figure 2). In Figure 5 the variable on the abscissa axis is b/B, where B is the height of the working volume. Here A and B are normalization parameters; the results for the uniformity errors do not change provided A/h, B/h, a/h and b/h are kept constant. In the Figures presented in this section A/h was chosen equal to 7 and B/h was 6.7.

Figures 6 and 7 give the ∞-norm errors along x and y, respectively, and they should be compared with Figures 4 and 5, respectively.

Once a and b have been determined, it might be interesting to see how the 2-norm errors vary when the dimensions of the working volume are allowed to change. Figure 8 and 9 illustrate the resulting 2-norm errors along the x and y directions when $b/h = 9$, $a/b = 1/\sqrt{3}$, $0 < A/h < 8$, and $0 < B/h < 9$. The variable on the abscissa axis is A/a in Figure 8 and B/b in Figure 9. Figure 10 and 11 plot the ∞-norm errors for the same case.

Finally, we report in Figures 12 and 13 the 2-norm errors for different values of the ratio b/a, other than $\sqrt{3}$. The plots show that the choice of b/a is not very critical within the range $1.5 < b/a < 2$ to limit the uniformity error at 10 percent.

2. CASE 2: COMMON MODE - TEST OBJECT ABOVE THE GROUND

An optimum field uniformity may be achieved in a small local region near the center of the test object (i.e. $x = 0$, $y = h$) by choosing a' and b' so that the first derivative of E_y with respect to y is zero at that point. By imposing that $\partial E_y/\partial y = 0$ at $(x = 0, y = h)$, the following relationship between a' and b' is obtained from Equation 1

$$a'^2 = \frac{-(b'^2 + 1) + \sqrt{(b'^2 + 1)^2 + 8(1 - b'^2)^2}}{4} \tag{8}$$

Equivalently, solving for b' gives:

$$b'^2 = 1 + a'^2 + 2a'^2\sqrt{1 + a'^2} \tag{8a}$$

common mode – test object near the ground
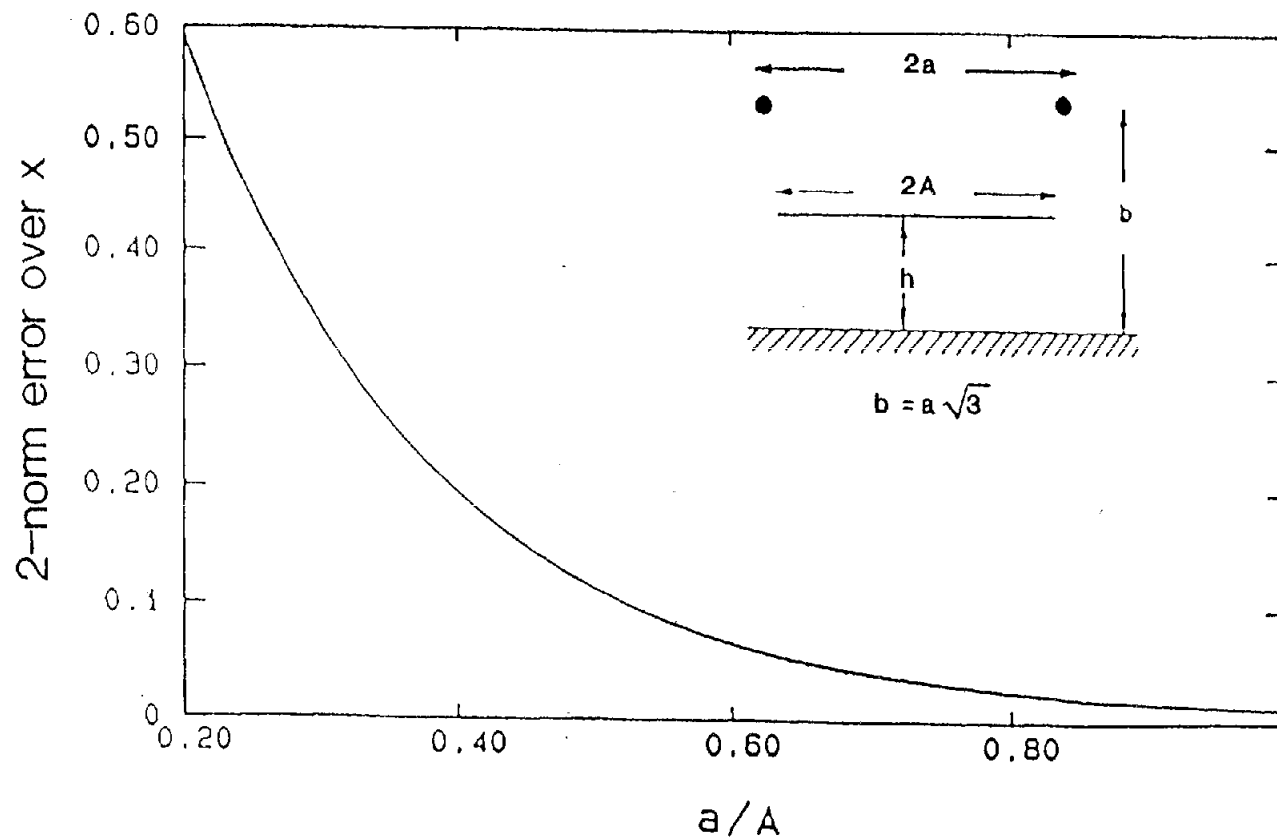
Figure 4.   2-norm error over x (from eq A1).   A is the half-width of the
working volume (see Fig. 2) and A/h = 7.

common mode − test object near the ground
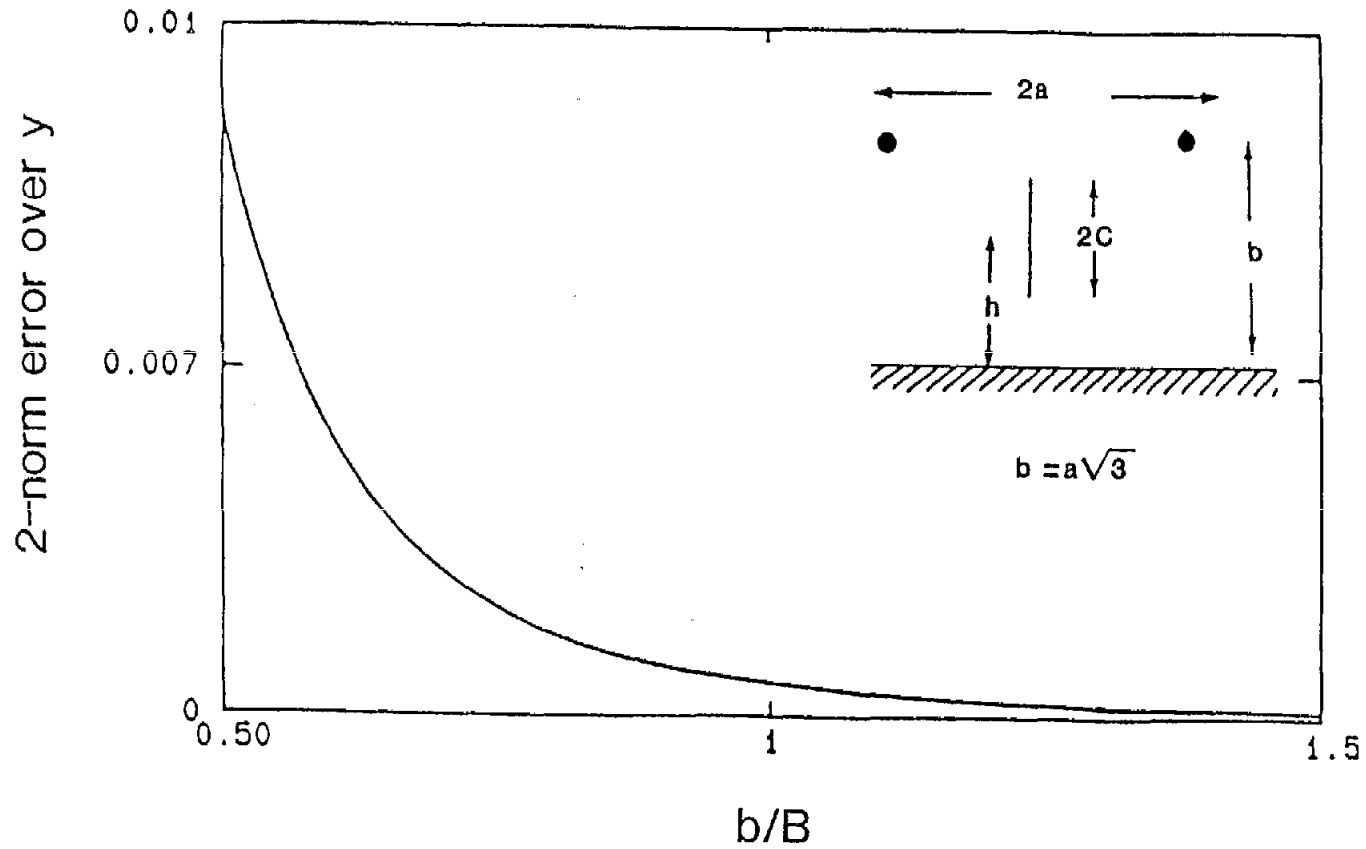
Figure 5.   2-norm error over y (from eq. A3).   B is the height of the working volume (see Fig. 2) and B/h = 6.7.

common mode – test object near the ground
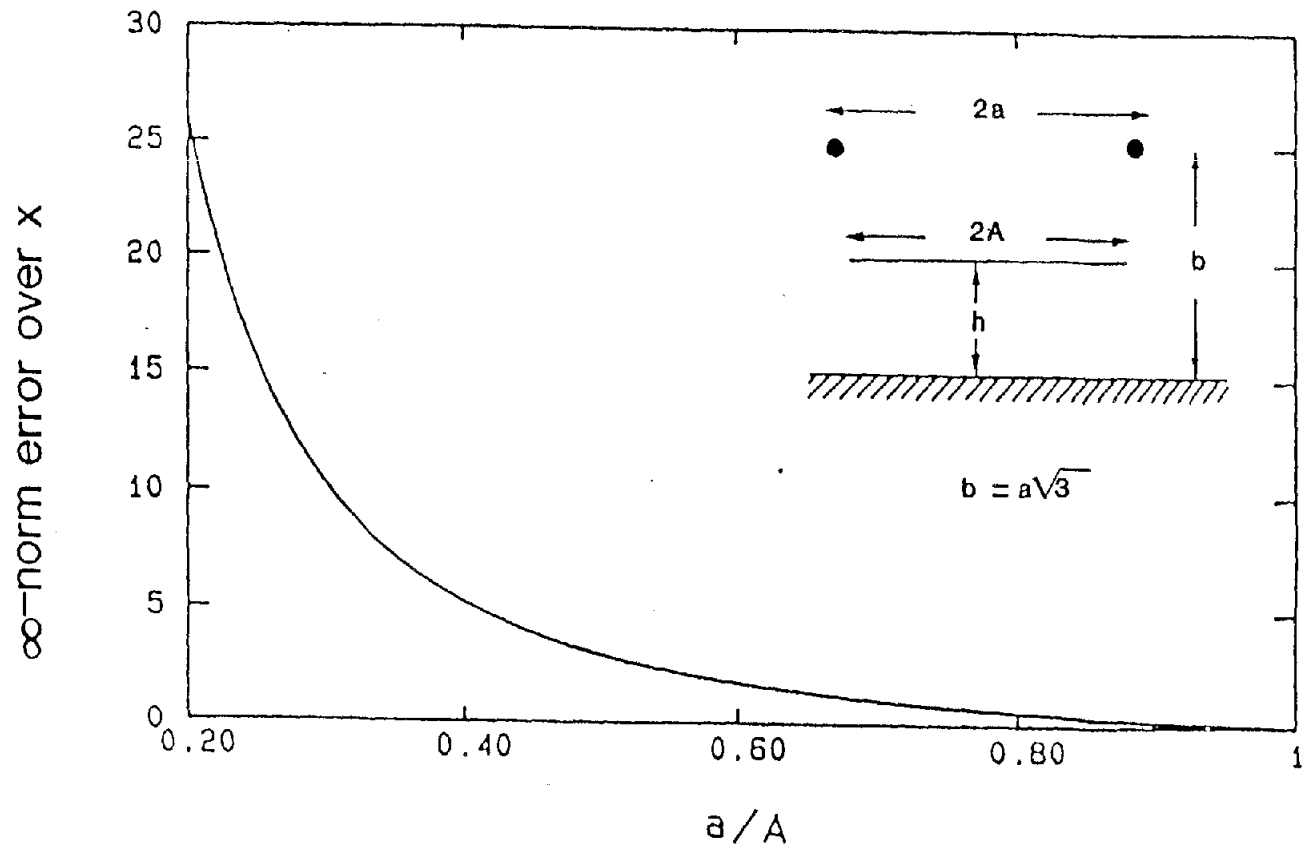
Figure 6. ∞-norm error over x. A is half-width of the working volume (see Fig. 2) and A/h = 7.

common mode – test object near the ground
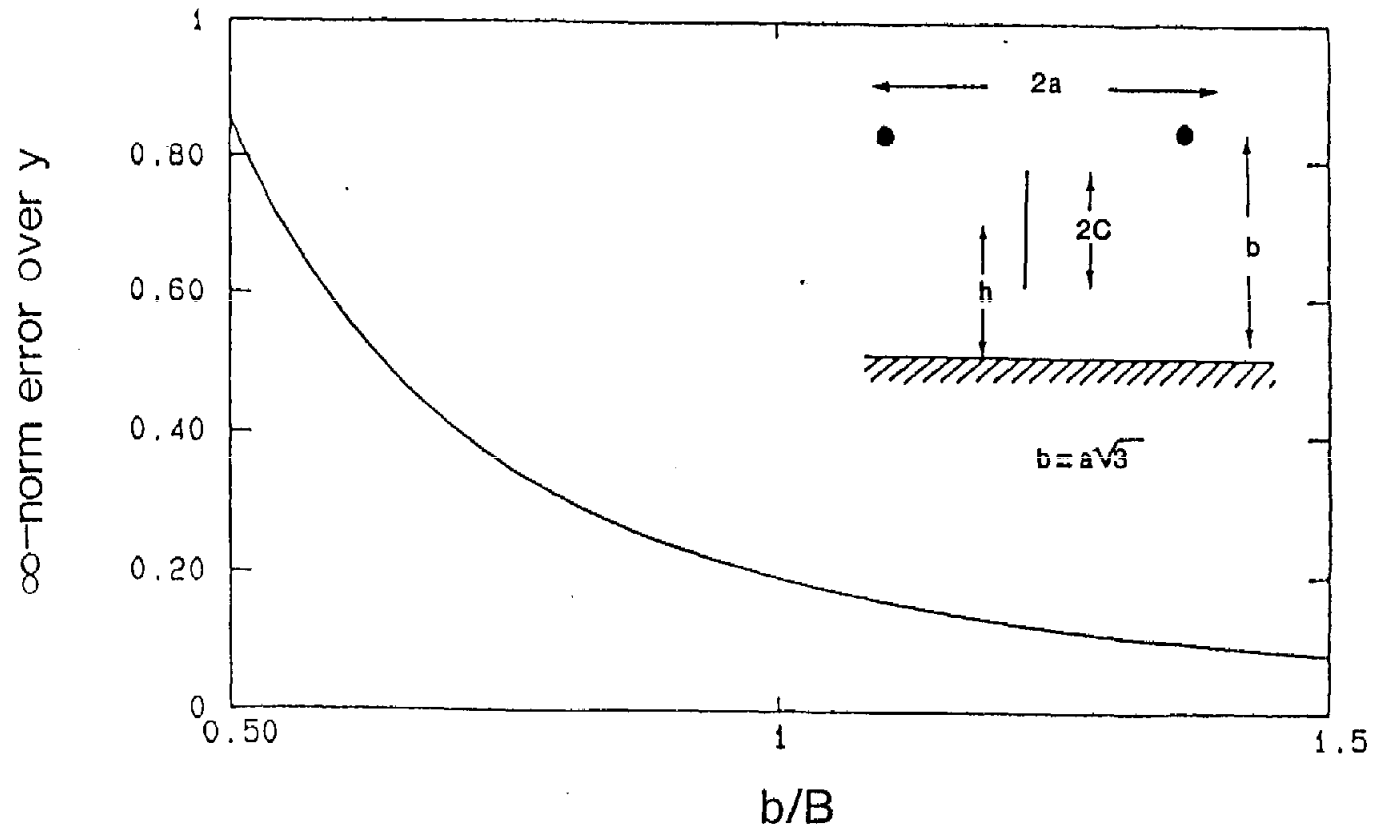
Figure 7.   ∞-norm error over y.   B is the height of the working volume
(see Fig. 2) and B/h = 6.7.
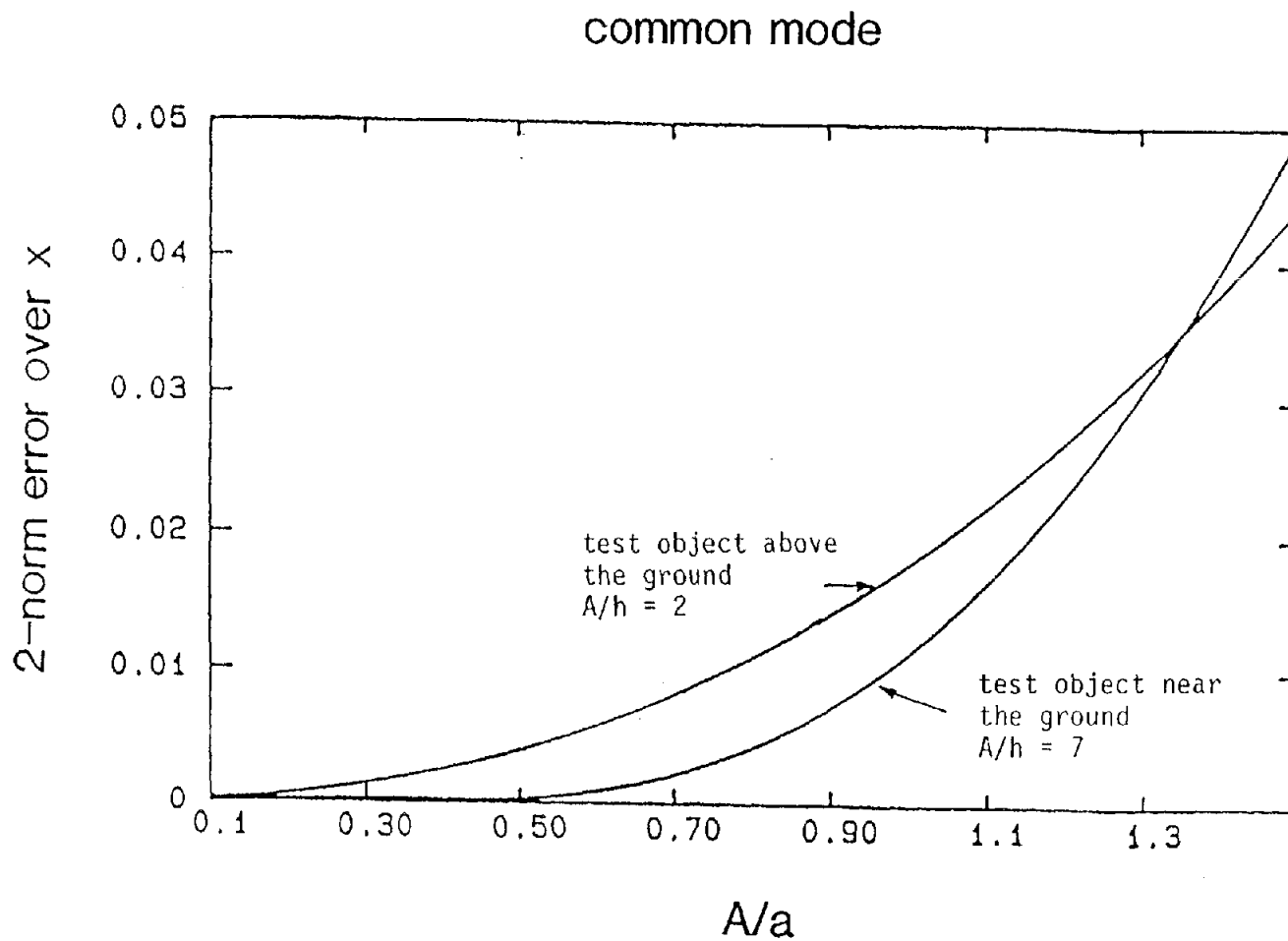
Figure 8. 2-norm error over x; a/h = 5, b/h = 9 when the test object is near the ground and a/h = 1.5, b/h = 2.5 when the test object is above the ground.
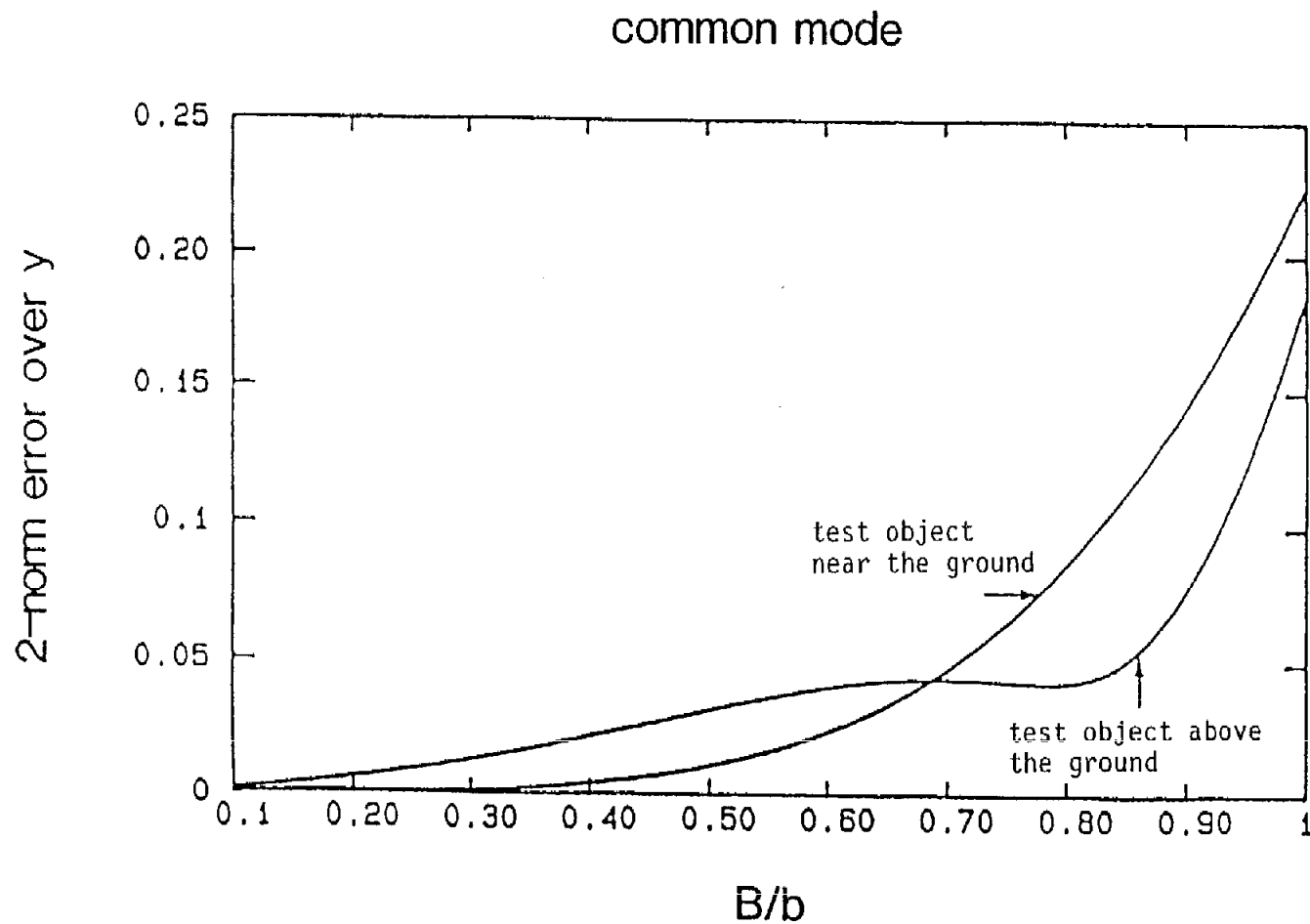
common mode

Figure 9. 2-norm error over y; a/h = 5, b/h = 9 for the test object near the ground; a/h = 1.5, b/h = 2.5 for the test object above the ground.
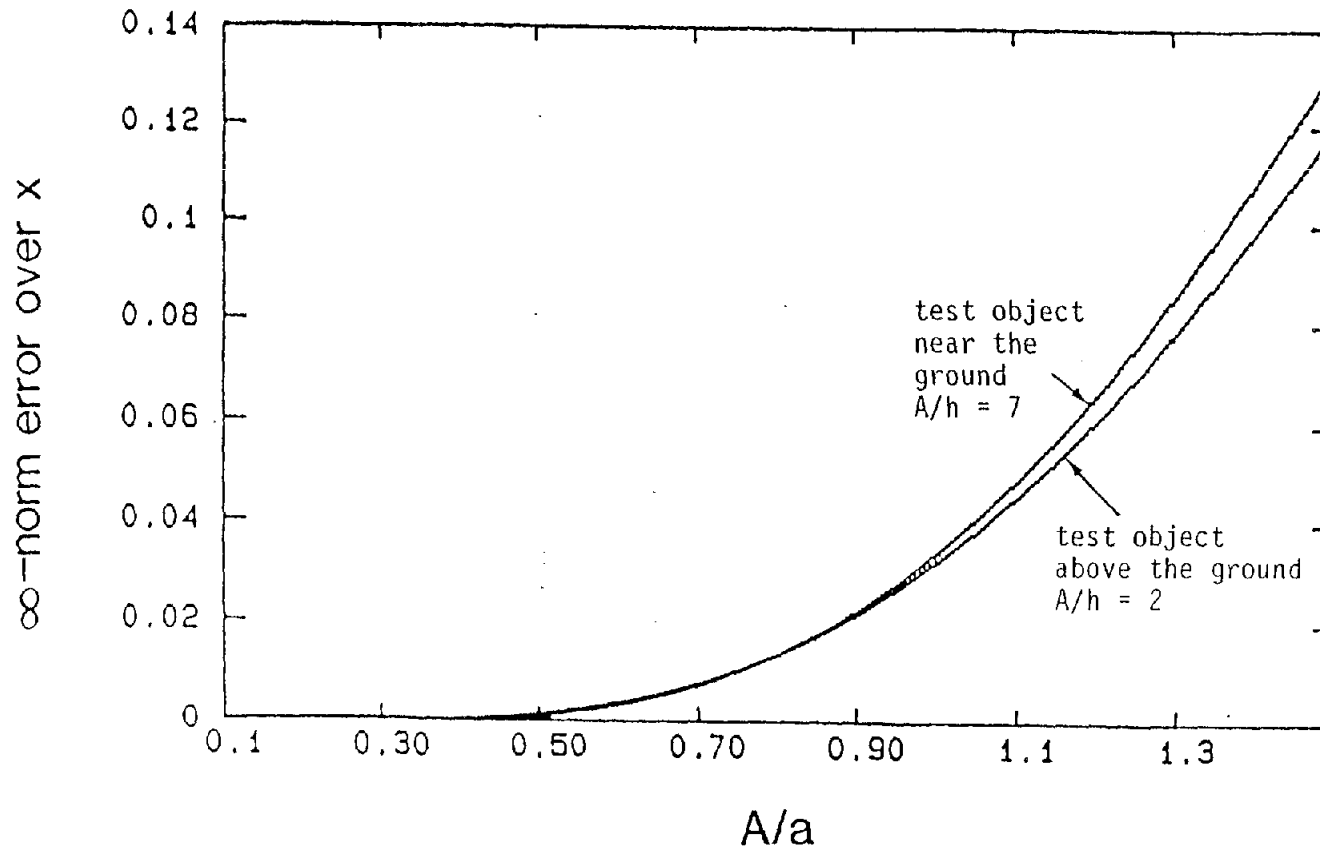
common mode

Figure 10. ∞-norm error over x; a/h = 5, b/h = 9 for the test object near the ground; a/h = 1.5, b/h = 2.5 for the test object above the ground.
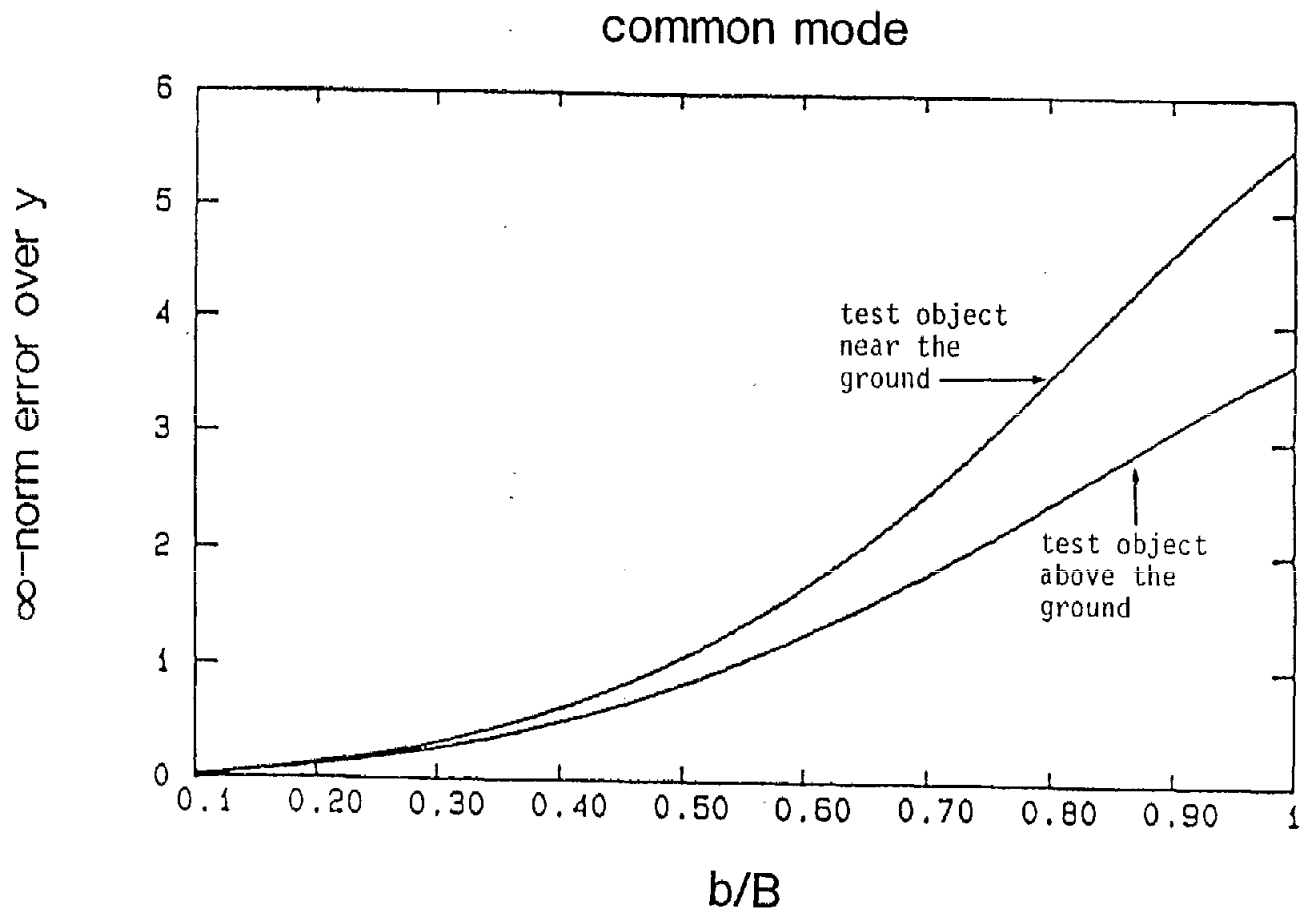
common mode

Figure 11. ∞-norm error over y; a/h = 5, b/h = 9 for the test object near the ground; a/h = 1.5, b/h = 2.5 for the test object above the ground.

common mode – test object near the ground
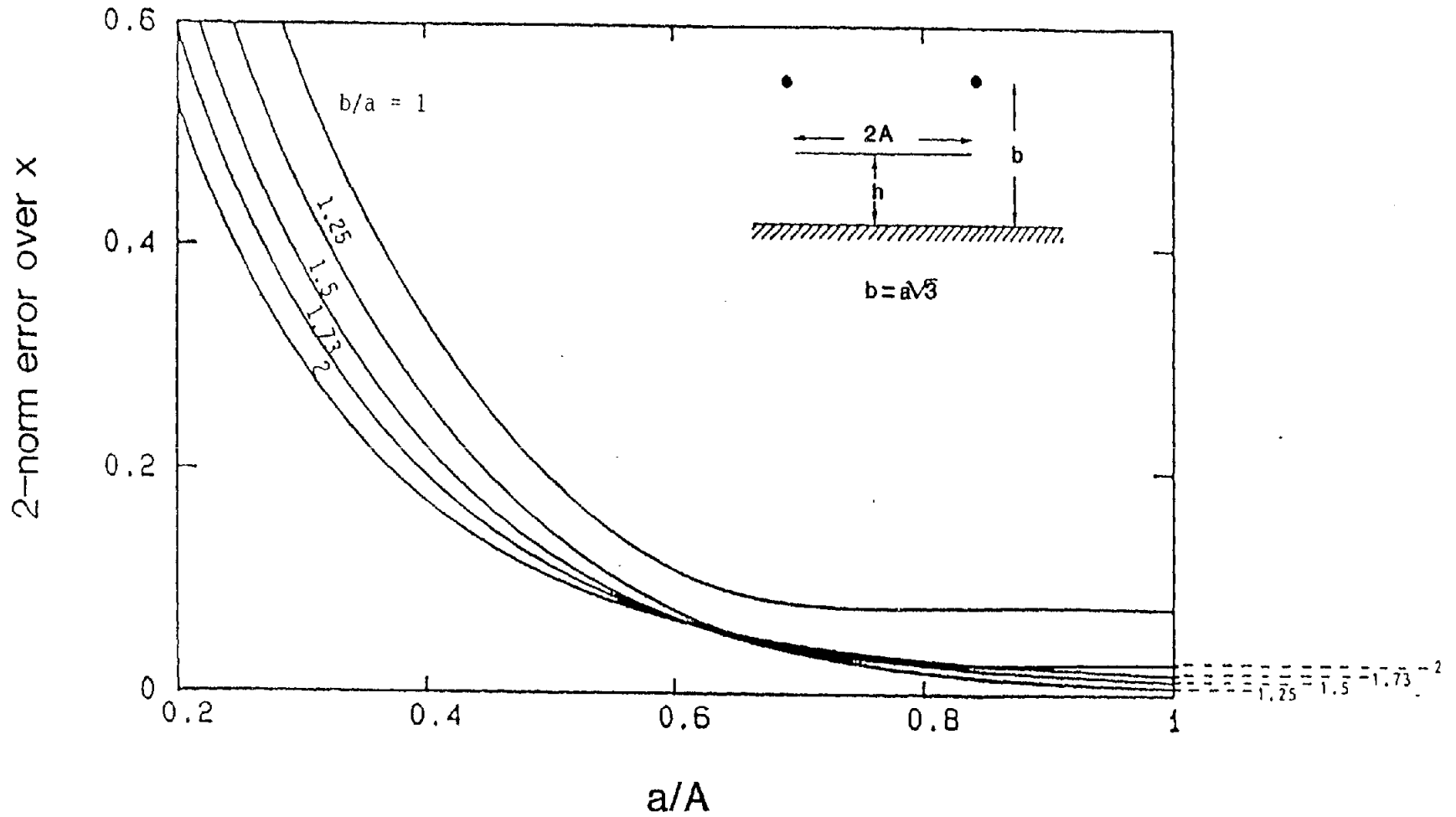
Figure 12. 2-norm error over x for different values of the ration b/a.
A is the half-width of the working volume and A/h = 7.

common mode – test object near the ground

b/a = 1

1.25

1.5

1.73

2

2-norm error over y

b/B

$b = a\sqrt{3}$

2c

h

b
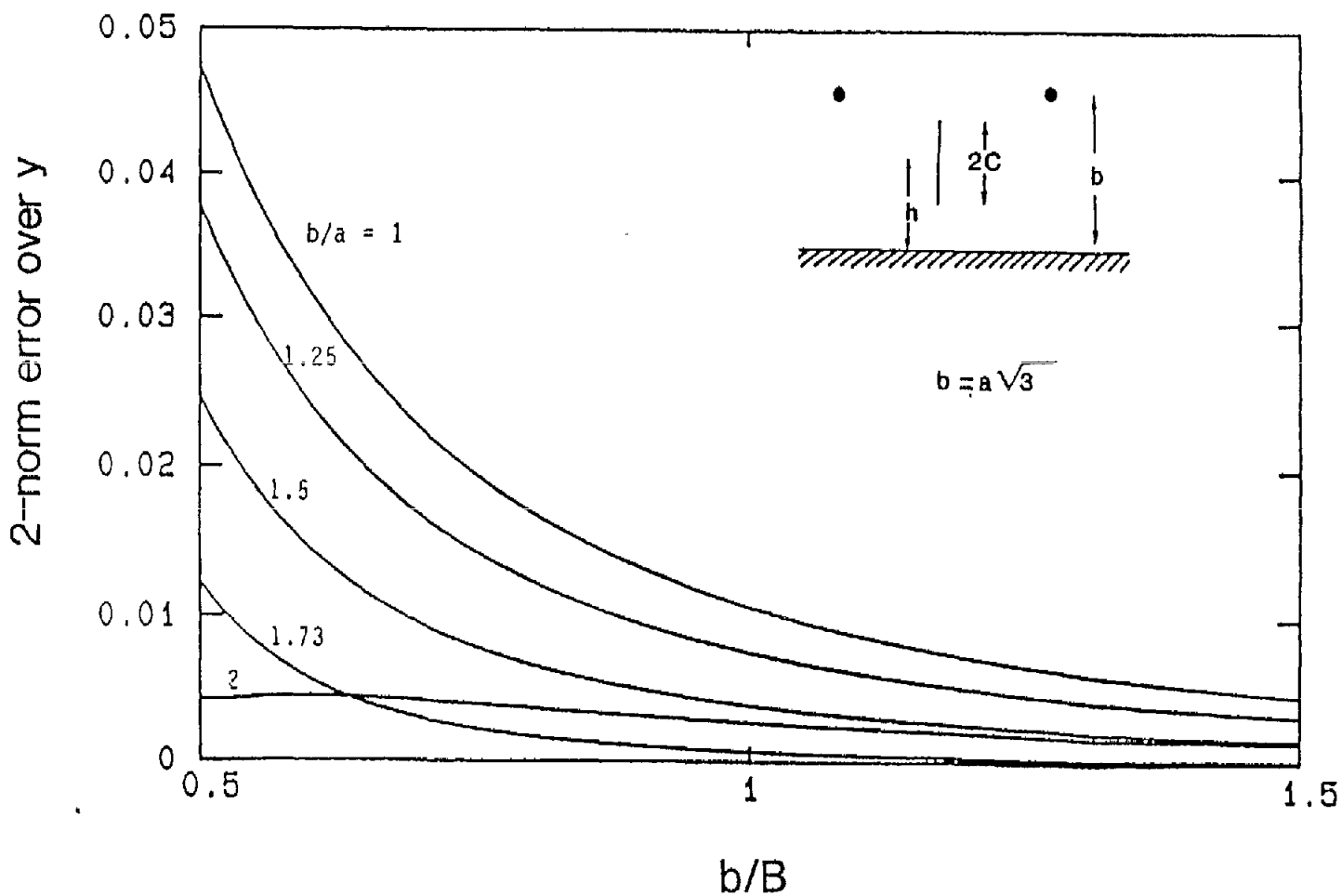
Figure 13.   2-norm error over y for different values of the ratio b/a.
B is the height of the working volume and B/h = 6.7.

22

Figure 14 and 15 represent the 2-norm errors along x and y, respectively, for the case of the test object located on top of a stand at an average height h. From Figure 15 we see that the error along y can become small (a few percent), provided b is made sufficiently large. For the plots in this section A/h = 2 and B/h = 1.8.

Figures 16 and 17 plot the ∞-norm errors calculated along the x and y directions, respectively.

Figures 8 through 11, mentioned before, plot 2-norm and ∞-norm errors as functions of A/a and B/b for the present case also. The value of b/h and a/h were fixed at 2.5 and 1.6, respectively, whereas A and B were actually varying.

Before concluding this part we would like to include the analytical expressions for the 2-norm error and the ∞-norm error calculated along the x-axis for an infinitesimal interval 2ε about the point (x = 0, y = h), in the case when the test object is located above the ground. The 2-norm error is given by

$$\{\frac{1}{\varepsilon}(\frac{\partial^2 E_y}{\partial \varepsilon^2}\Big|_{y=h})^2 \frac{\varepsilon^5}{20}\}^{1/2} / (E_y\Big|_{y=h}) =$$

$$\{\frac{\dfrac{4(1-b')[3a'^2-(1-b')^2]}{[a'^2+(1-b')^2]^3} - \dfrac{4(1+b')[3a'^2-(1+b')^2]}{[a'^2+(1+b')^2]^3}}{\dfrac{2(1-b')}{a'^2+(1-b')^2} - \dfrac{2(1+b')}{a'^2+(1+b')^2}}\} \frac{\varepsilon^2}{\sqrt{20}} \qquad (9)$$

The ∞-norm error is given by

$$\frac{\partial^2 E_y}{\partial \varepsilon^2} \frac{\varepsilon^2}{2} / (E_y\Big|_{y=h}) =$$

$$\{\frac{\dfrac{4(1-b')[3a'^2-(1-b')^2]}{[a'^2+(1-b'^2)]^3} - \dfrac{4(1-b')[3a'^2-(1+b')^2]}{[a'^2+(1+b')^2]^3}}{\dfrac{2(1-b')}{a'^2+(1-b')^2} - \dfrac{2(1+b')}{a'^2+(1+b')^2}}\} \frac{\varepsilon^2}{2}$$
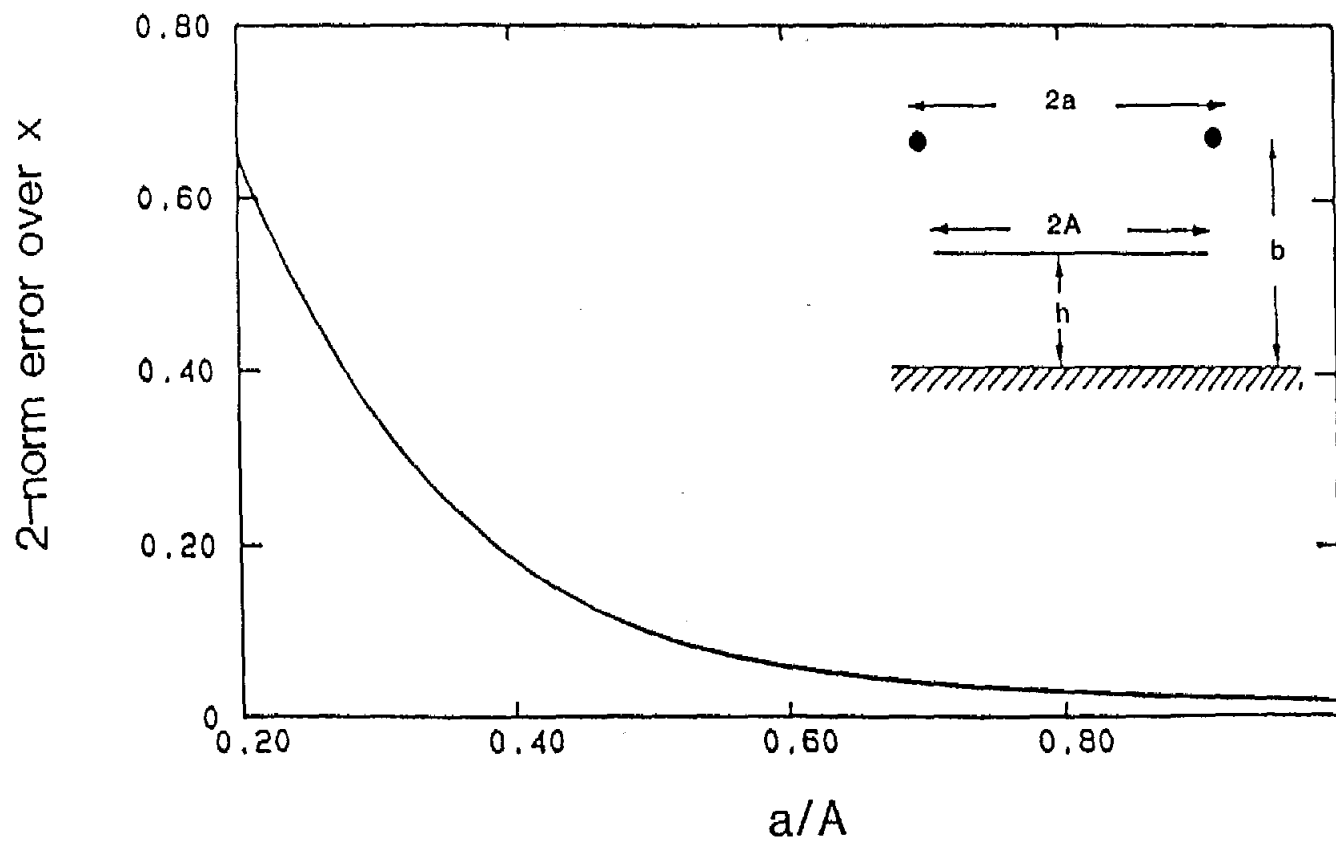
Figure 14. 2-norm error over x (from eq. A1). A is the half-width of the working volume (see Fig. 2) and A/h = 2.
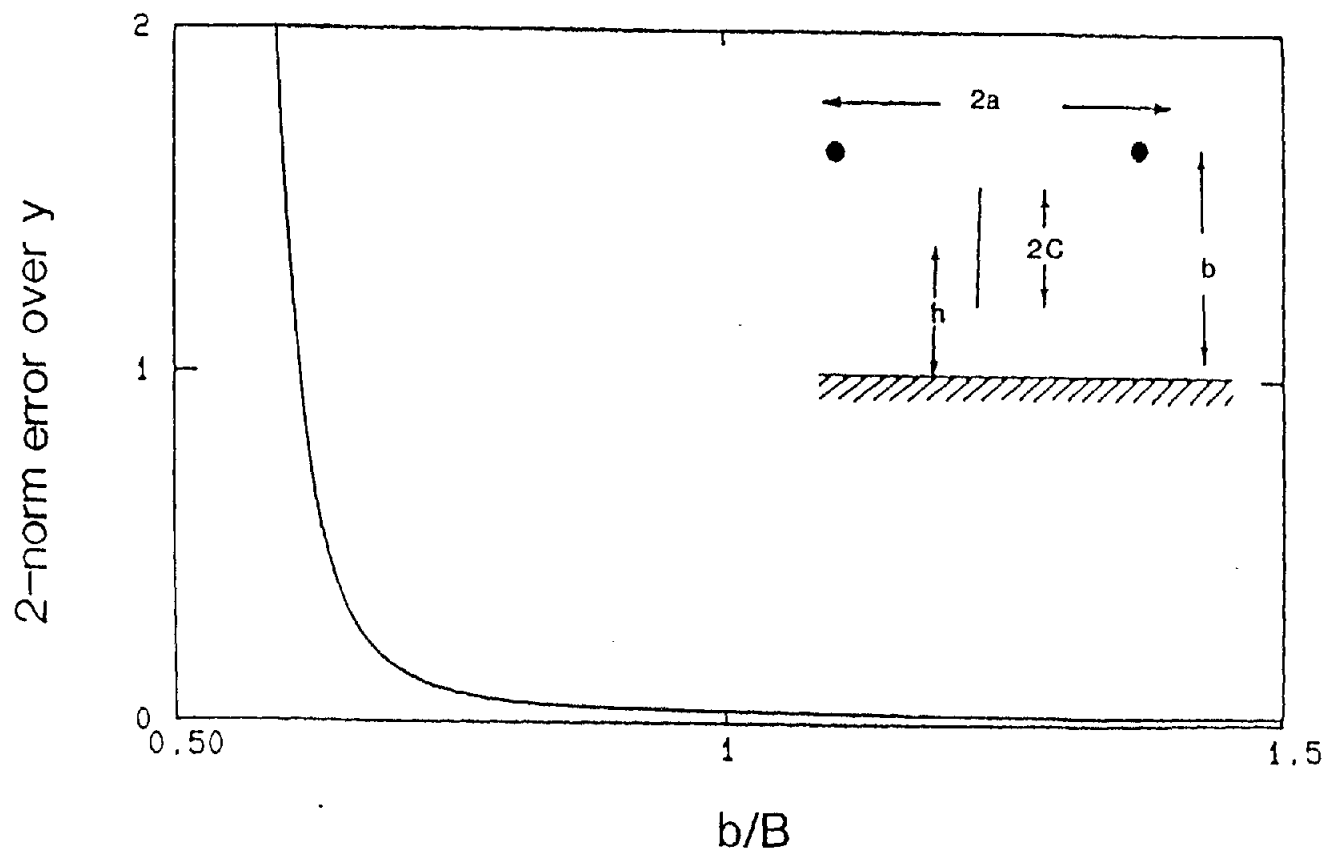
Figure 15.   2-norm error over y (from eq A3).   B is the height of the
working volume (see Fig. 2) and B/h = 1.8.

$$= \frac{1}{\sqrt{5}} \{2\text{-norm error}\} \tag{10}$$

3.   CASE 3:   DIFFERENTIAL MODE - TEST OJBECT NEAR THE GROUND

For the differential mode excitation the criterion used for obtaining an optimum field distribution was to determine a' and b' so that the 2-norm error in Equation A5 or, alternatively, Equation A7 becomes minimum.   To accomplish this numerical minimization we plot a family of curves representing the 2-norm error along x or y as a function of either a/A or b/B, while holding the other variable constant as a parameter.   Figures 18 and 19 illustrate two such families of curves when the error is computed along the x-axis, whereas Figures 20 and 21 provide the error along y.   Again, the ratio A/h was fixed at 7 while B/h was assumed equal to 6.7.   Figures 18 and 19 show that the curves are very flat about their absolute minima.   This implies that the choice of the actual values of a and b is not very critical within a certain range about their minima, especially if one is interested in finding an upper bound for the allowed uniformity error (for instance 10%).   However, we notice that the minimum error along y is fairly large ($\approx$ 55 percent) .   This can be explained by the fact that this excitation mode produces an intrinsically weaker and less uniform field than the common mode does, because of the presence of the perfectly conducting ground which tends to make the horizontal E-field go to zero near the ground.   Hence, since the horizontal electric field varies from zero at the surface y = 0 to non-zero values along the y-direction, this results in large 2-norm errors over the fuselage.   Therefore, the 2-norm error of Figures 20 and 21 should be taken as a worst-case result.

Figures 22 through 25 illustrate the ∞-norm errors calculated along x (Figs. 22 and 23) and y (Figs. 24 and 25) and they should be compared with Figures 18 thro. jh 21.   We point out that the same values of a and b which minimize the 2-norm errors also minimize the ∞-norm errors.

Finally, if it is desired to keep a/h and b/h fixed at 12 and 9, respectively, and vary the dimensions of the working volum·· A/h and B/h, families of curves showing the behavior of the 2-norm and ·-norm errors along x and y are presented in Figures 26 through 29.

common mode – test object above the ground
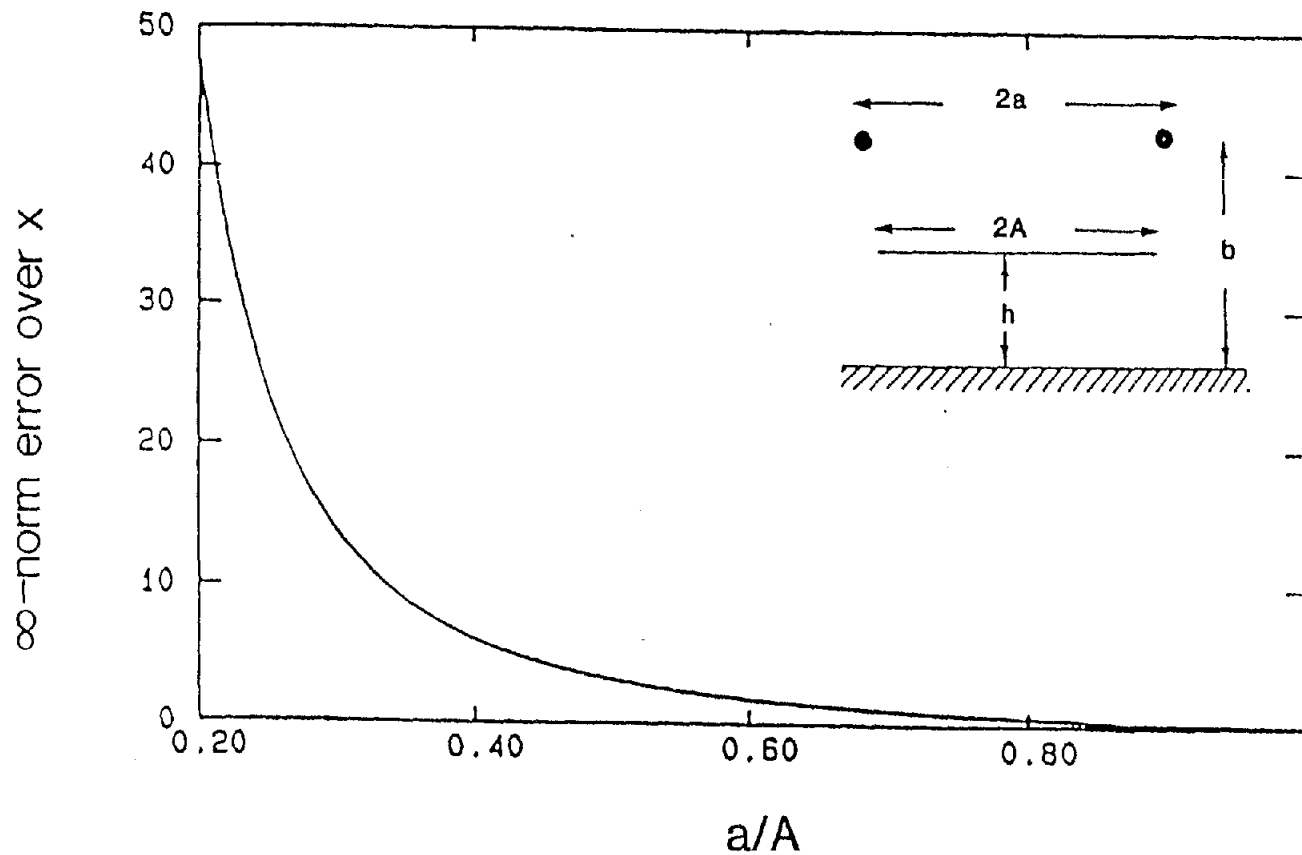
Figure 16. ∞-norm error over x; A is half the width of the working
volume (see Fig. 2) and A/h = 7.

common mode – test object above the ground
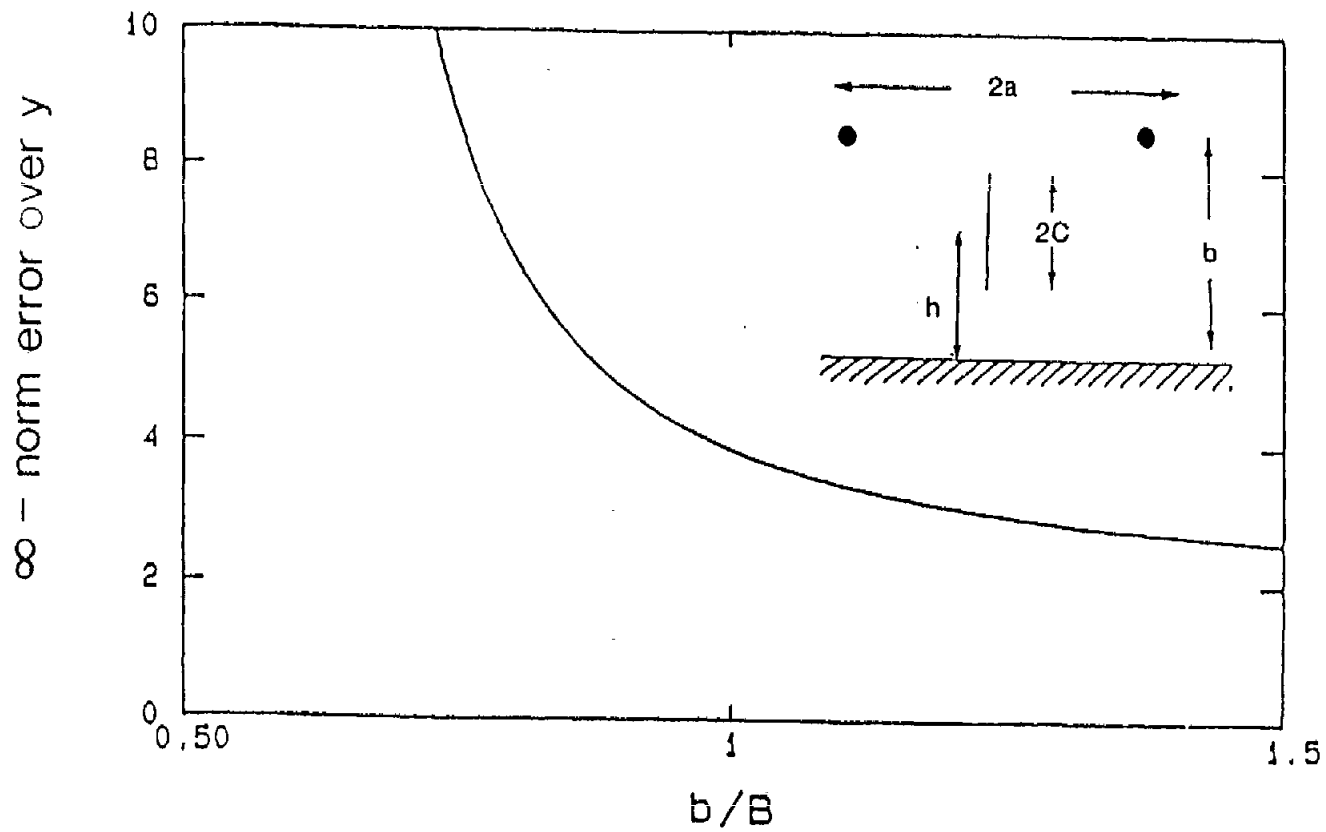
Figure 17. ∞-norm error over y; B is the height of the working volume (see Fig. 2) and B/h = 1.8.

differential mode – test object near the ground
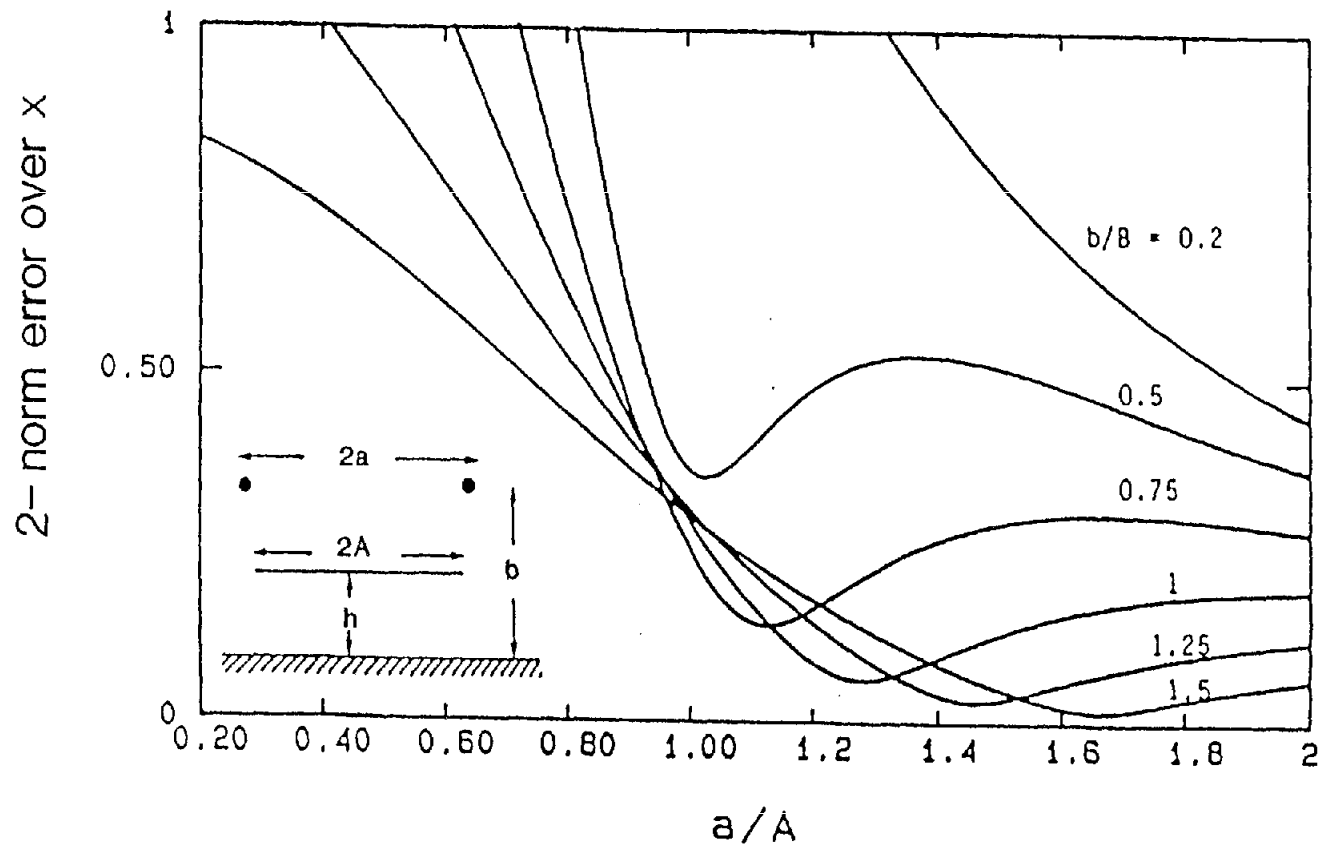
Figure 18. 2-norm error over x (from eq. A5). A is the width of the working volume (see Fig. 2) and A/h = 7. B is the height of the working volume (see Fig. 2) and B/h = 6.7.

differential mode - test object near the ground
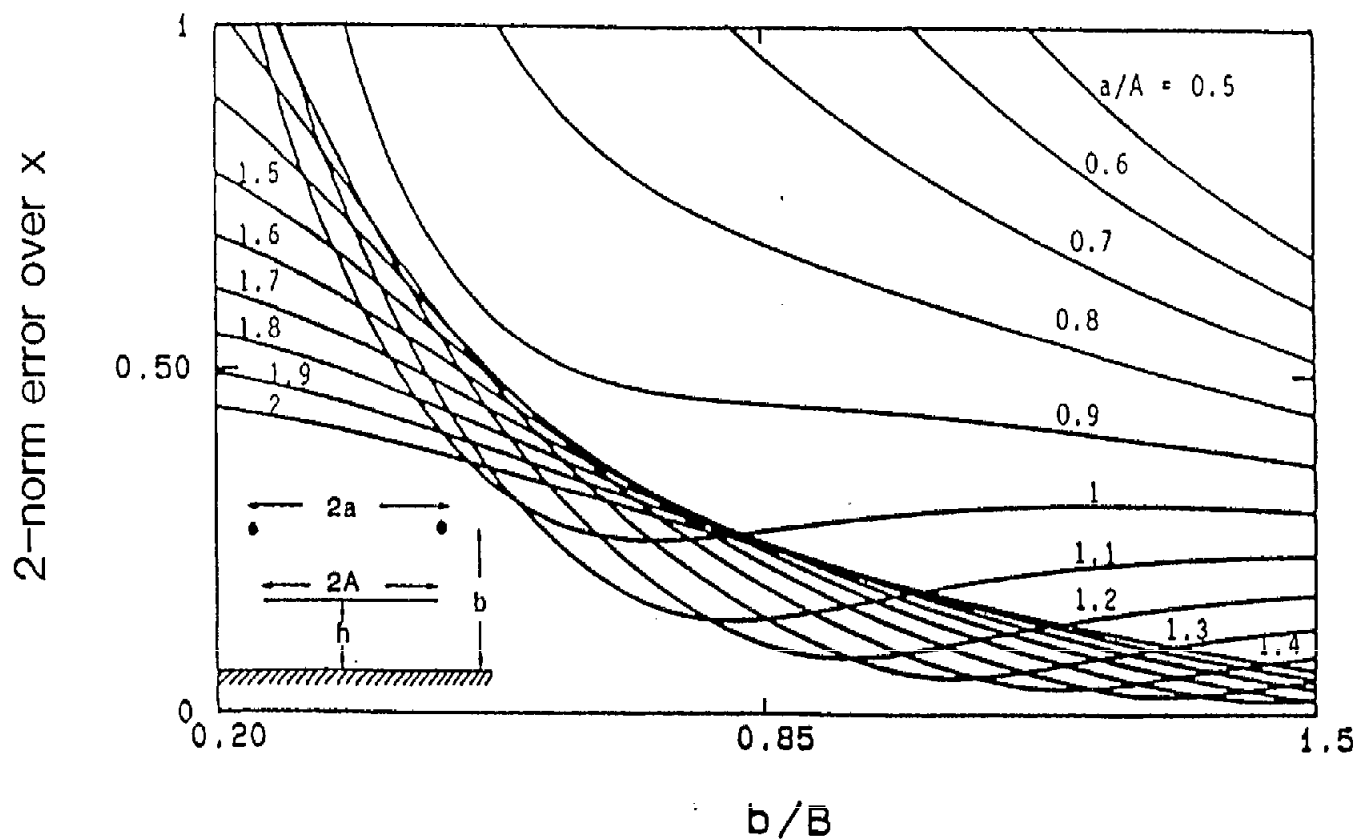
Figure 19. 2-norm error over x (from Eq. A5). B is the height of the working volume and B/h = 6.7. A is the half-width of the working volume and A/h = 7.

differential mode – test object near the ground
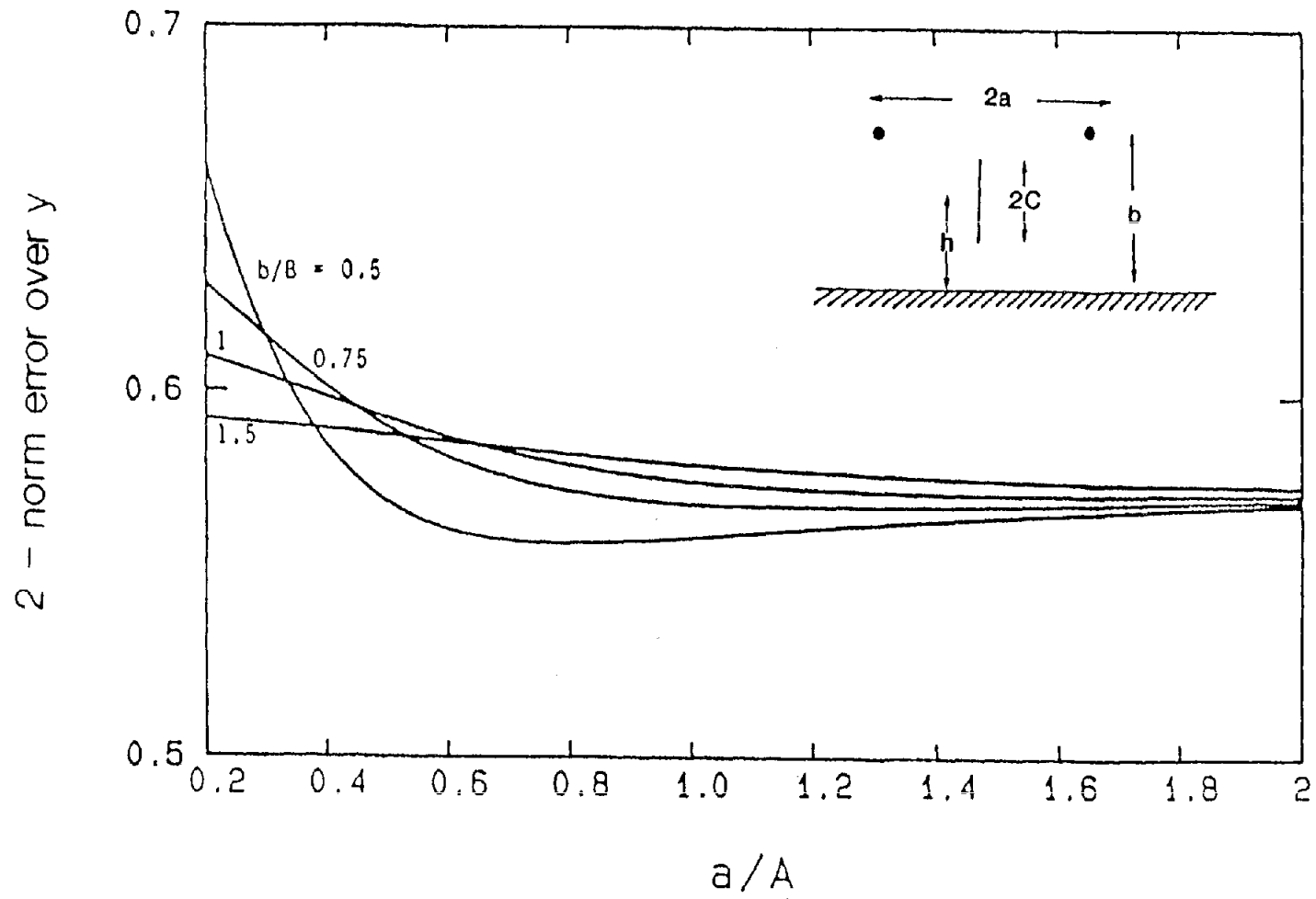
Figure 20.   2-norm error over y (from eq. A7).   A is the half-width of the working volume (see Fig. 2) and A/h = 7.

Figure 21. 2-norm error over y (from eq. A7). B is the height of
the working volume and B/h = 6.7.

differential mode – test object near the ground
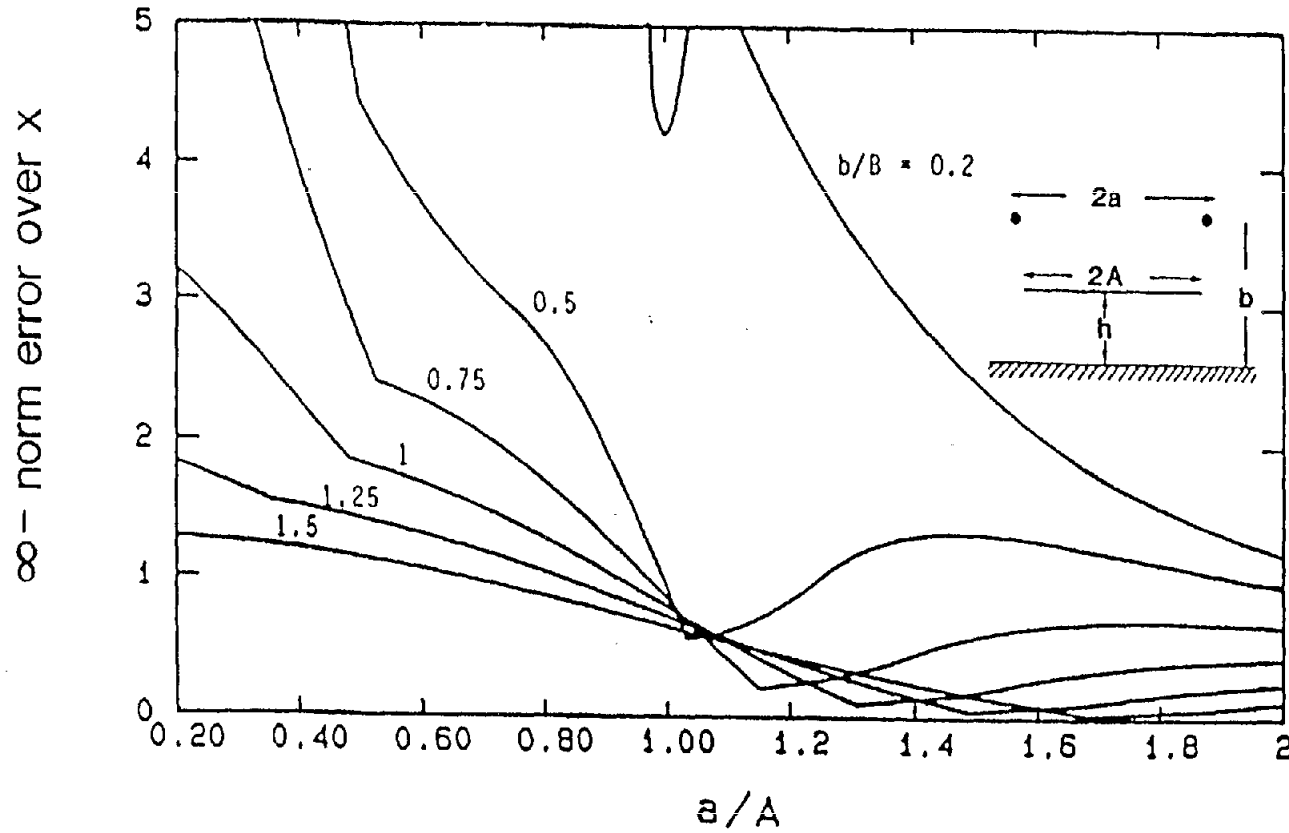
Figure 22. ∞-norm error over x. A is the half-width of the working
volume (see Fig. 2) and A/h = 7. B is the height of the working
volume (see Fig. 2) and B/h = 6.7.

differential mode − test object near the ground
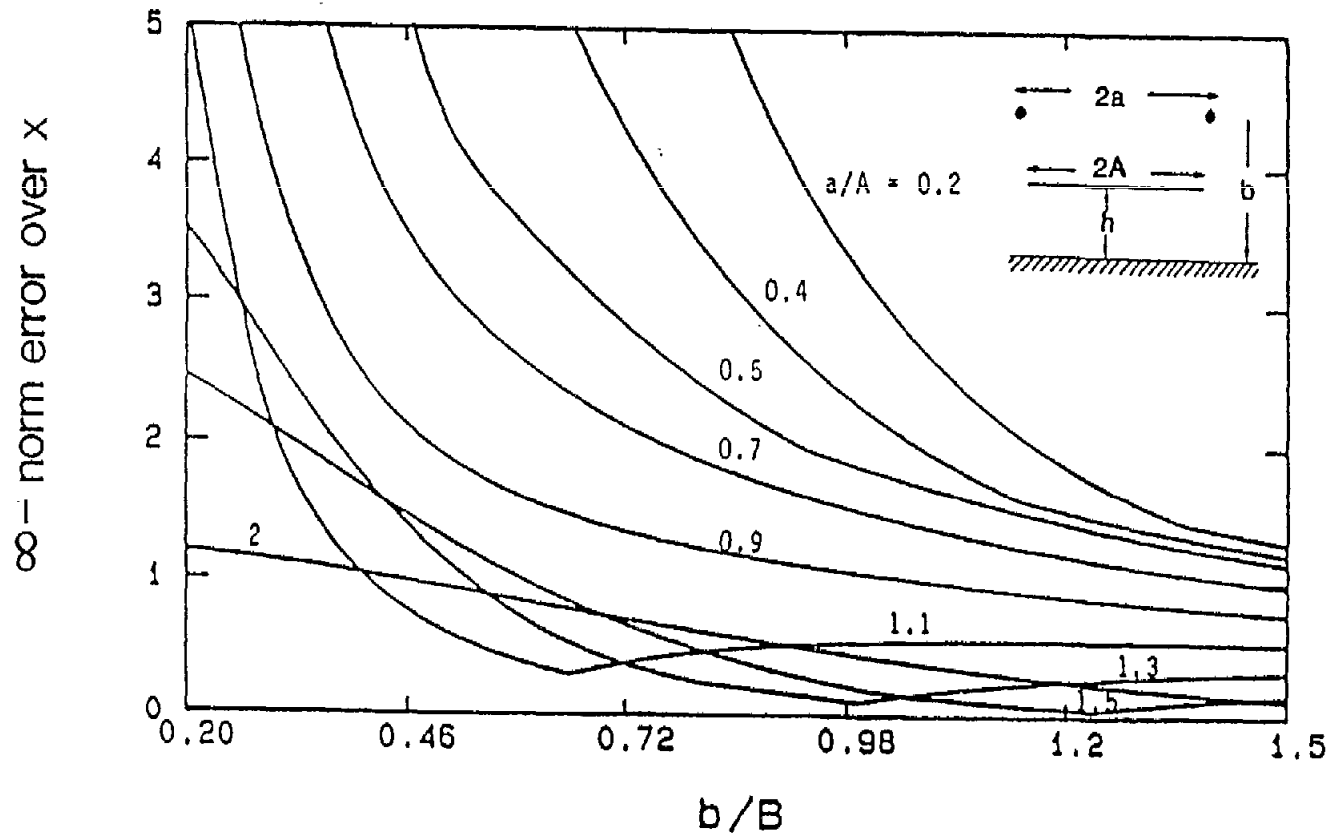
Figure 23. ∞-norm error over wings. B is the height of the working volume (see Fig. 2) and B/h = 6.7. A is the half-width of the working volume (see Fig. 2) and A/h = 7.

differential mode – test object near the ground
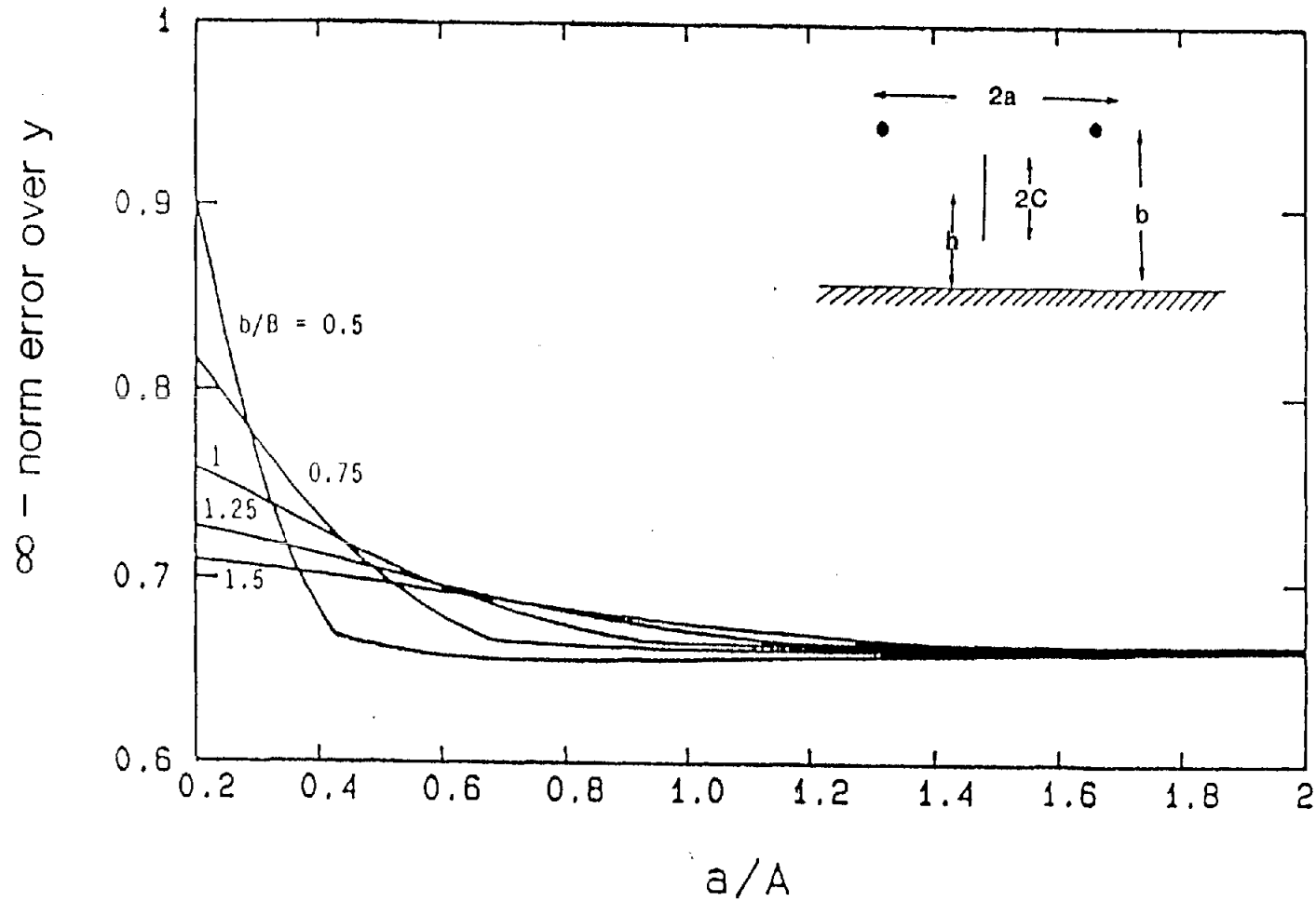
Figure 24. ∞ - norm error over fuselage. A is the half-width of the working volume (see Fig. 2) and A/h = 7. B is the height of the working volume (see Fig. 2) and B/h = 6.7.

differential mode – test object near the ground
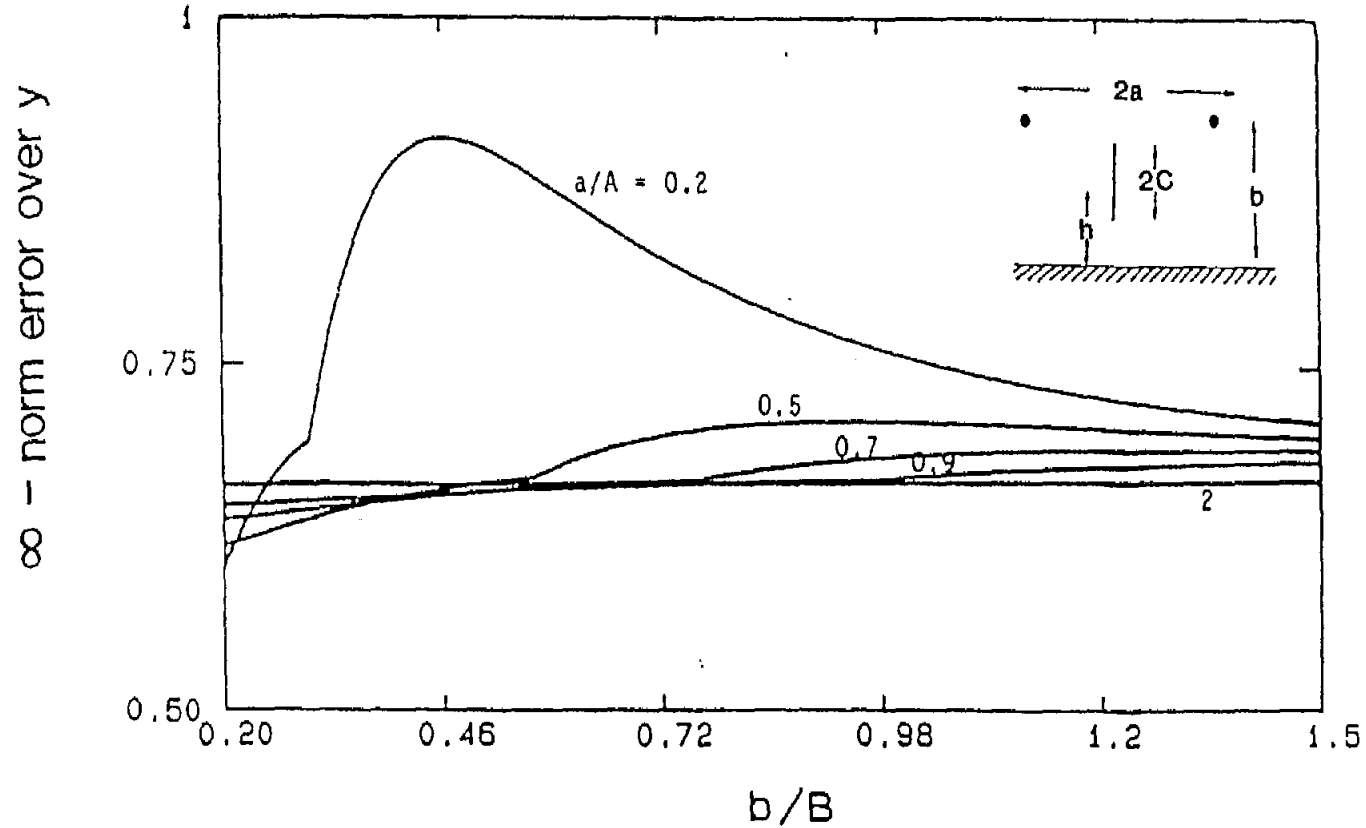
Figure 25. ∞-norm error over fuselage. A is the half-width of the working
volume (see Fig. 2) and A/h = 7. B is the height of the working
volume (see Fig. 2) and B/h = 6.7.

differential mode – test object near the ground
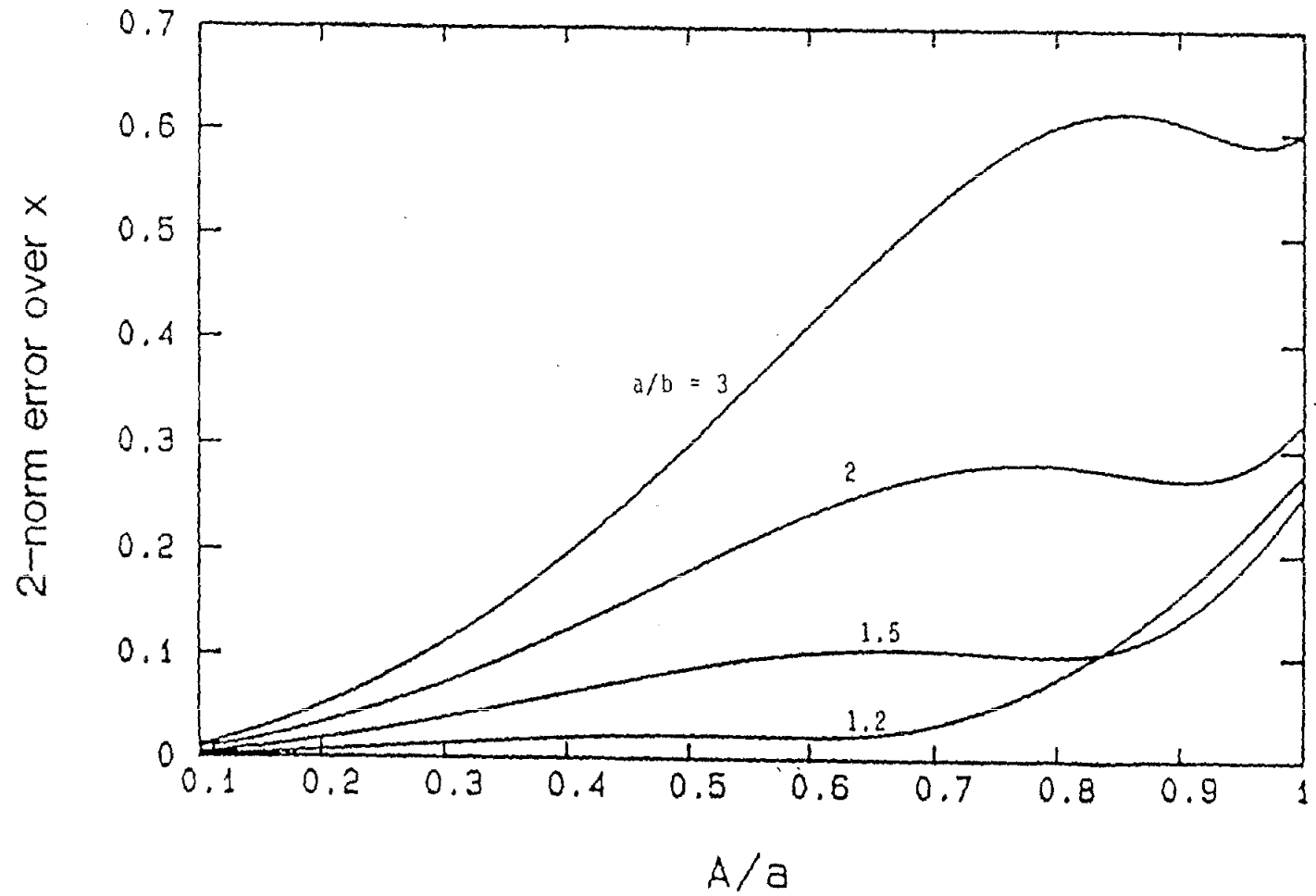
Figure 26. 2-norm error over x; a is the half-separation between the wires and a/h = 12 (fixed value).

differential mode – test object near the ground
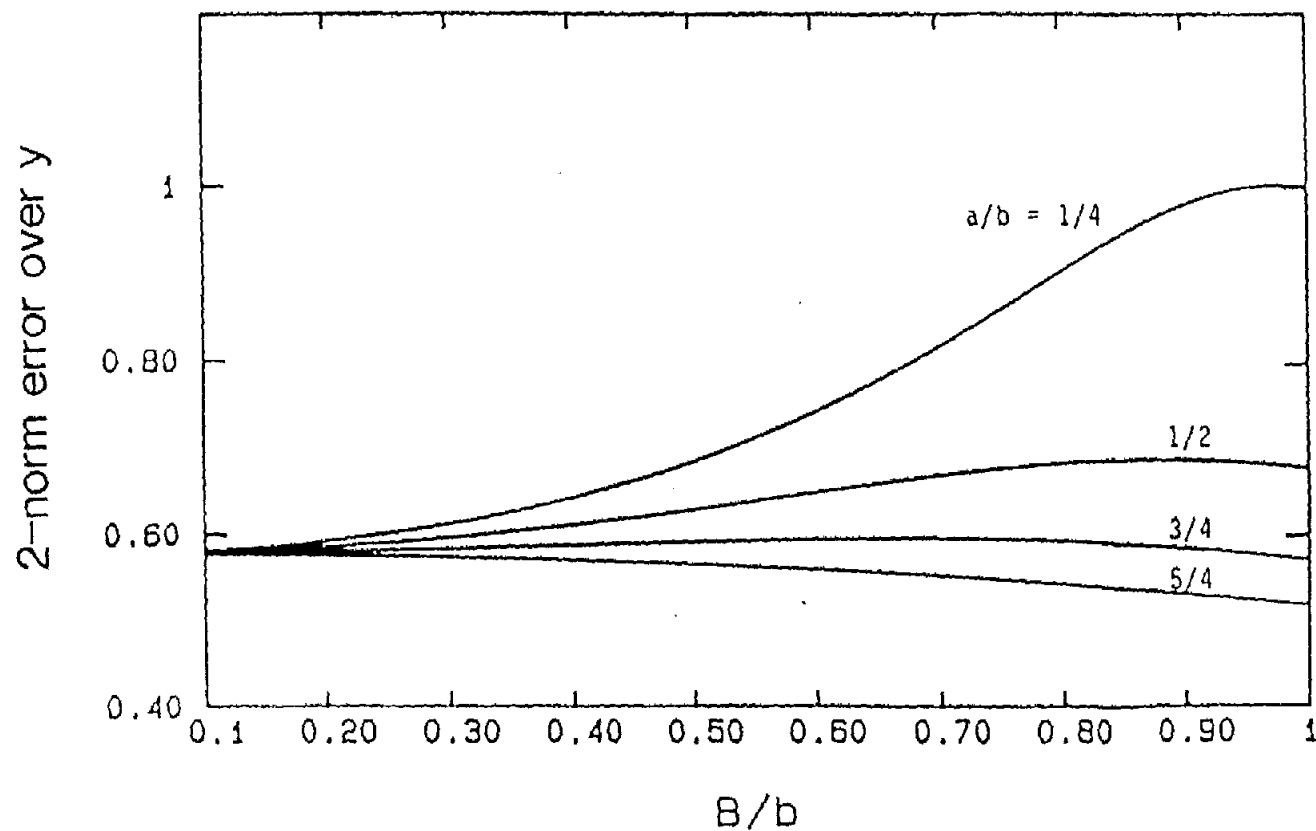
Figure 27.   2-norm error over y; b is the height of the wires above the ground
and b/h = 9 (fixed value)

differential mode – test object near the ground
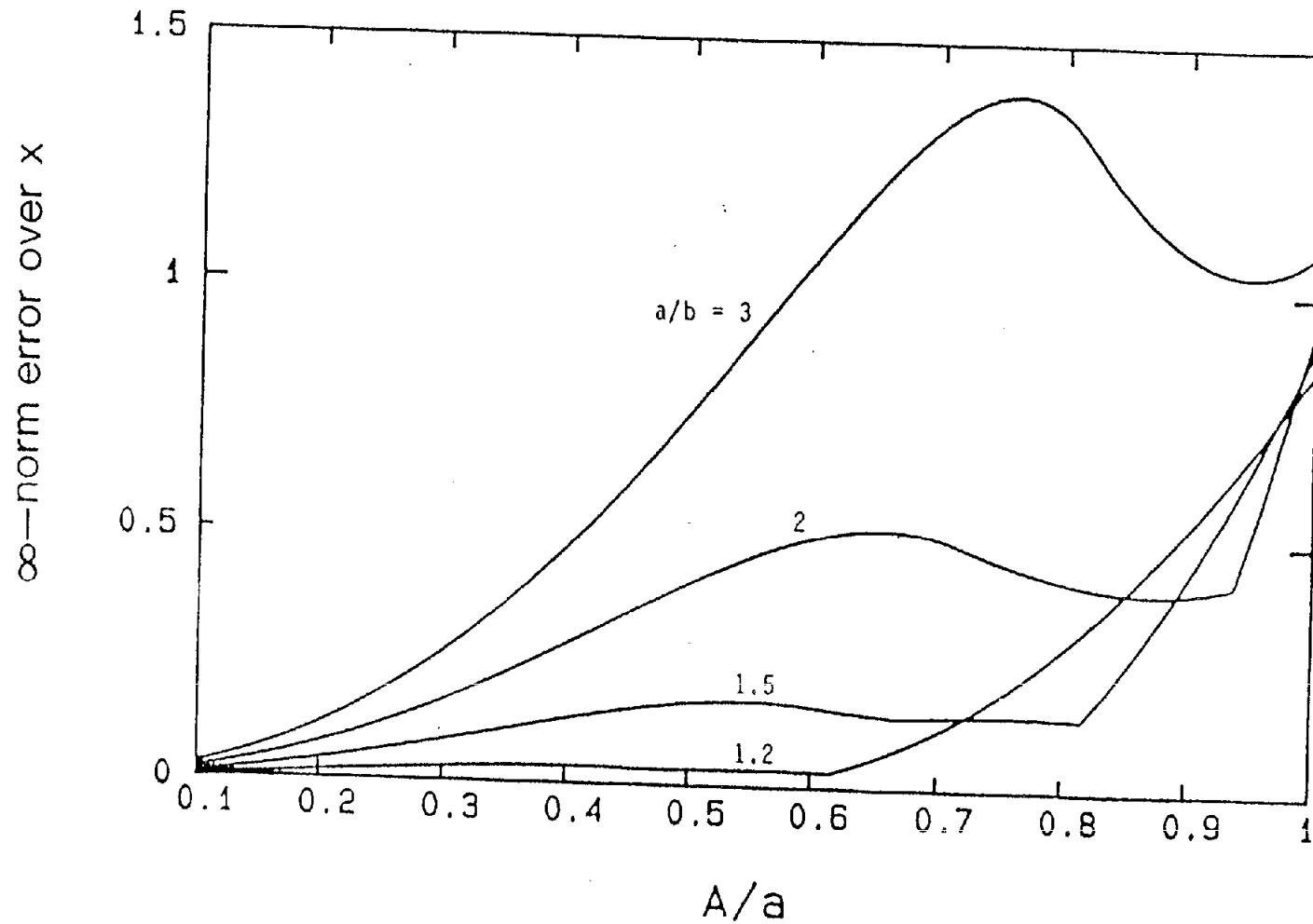
Figure 28. ∞ – norm error over x; a is the half-separation between the wires and a/h = 12 (fixed value).
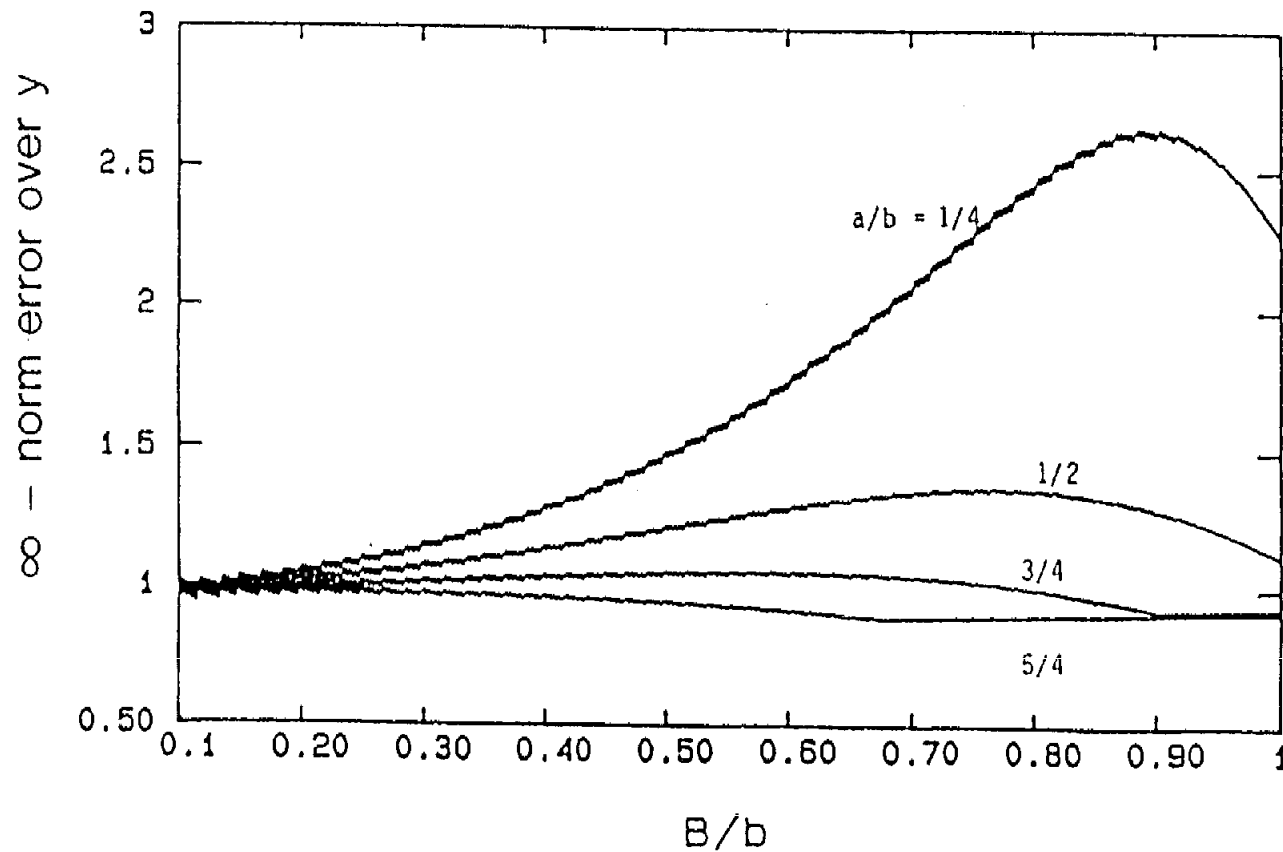
Figure 29. ∞ - norm error over y; b is the height of the wires above the ground and b/h = 9 (fixed value).

As a final remark we point out that in this case the choice a = b gives a small uniformity error and offers the advantage of a complete symmetry of the structure about both the x and y axis.

4. CASE 4: DIFFERENTIAL MODE - TEST OBJECT ABOVE THE GROUND

When the test object is located on top of a stand, in analogy with what was already stated for the common mode excitation, an optimum field uniformity in the differential mode is obtained by choosing a' and b' so that the first derivative of E_x with respect to y is zero at the point (x = 0, y = h). From Equation 2, by imposing that $\partial E_x/\partial y = 0$ at (x = 0, y = h) , the following relationship between a' and b' is obtained:

$$a'^2 = 1 - b'^2 + 2\sqrt{1 - b'^2} \tag{11}$$

$$\text{or} \quad b'^2 = -(a'^2 + 1) + 2\sqrt{a'^2 + 1} \tag{11a}$$

We note that it results that b must always be less than h.

Figures 30 and 31 illustrate the 2-norm errors computed along x and y for this case.

Figures 32 and 33 report the ∞-norm errors. Figures 34 through 37 plot the behavior of 2-norm and ∞-norm errors along x and y when a/h and b/h are fixed and A/h and B/h are varying. Figure 37 shows that the ∞-norm error is a constant equal to 1. This stems from the fact that in this case Eq. 7 becomes maximum when ξ = 0 for any value of B/b, in which case the field component E_x is zero also, as can be seen from Eq. 2. A similar behavior, although on a different range of values for B/b, can be observed in Figure 29, for the case of the test object on the ground.

5. CONCLUSIONS

We have shown that in all four cases suitable ranges of values for a and b can be determined where the uniformity error is made small. When the test object is near the ground for the common mode excitation the ration a/b = $1/\sqrt{3}$ provides the most uniform field about the center of the antenna whereas for the differential mode excitation the ratio a/b = 1 presents a small uniformity error and provides a complete symmetry of the antenna.

differential mode − test object above the ground
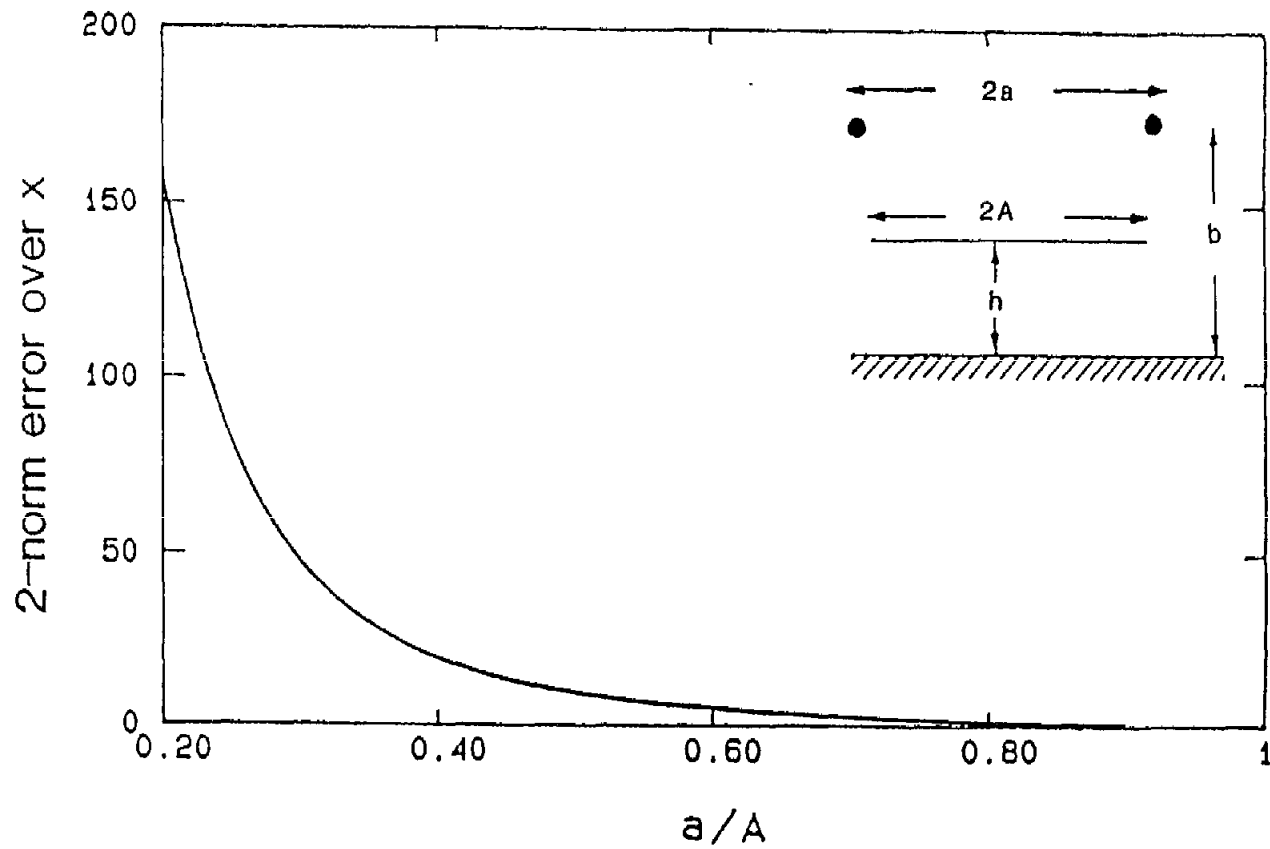
Figure 30. 2-norm error over x (from eq. A5). A is the half-width of the
working volume (see Fig.2) and A/h = 2.

differential mode – test object above the ground
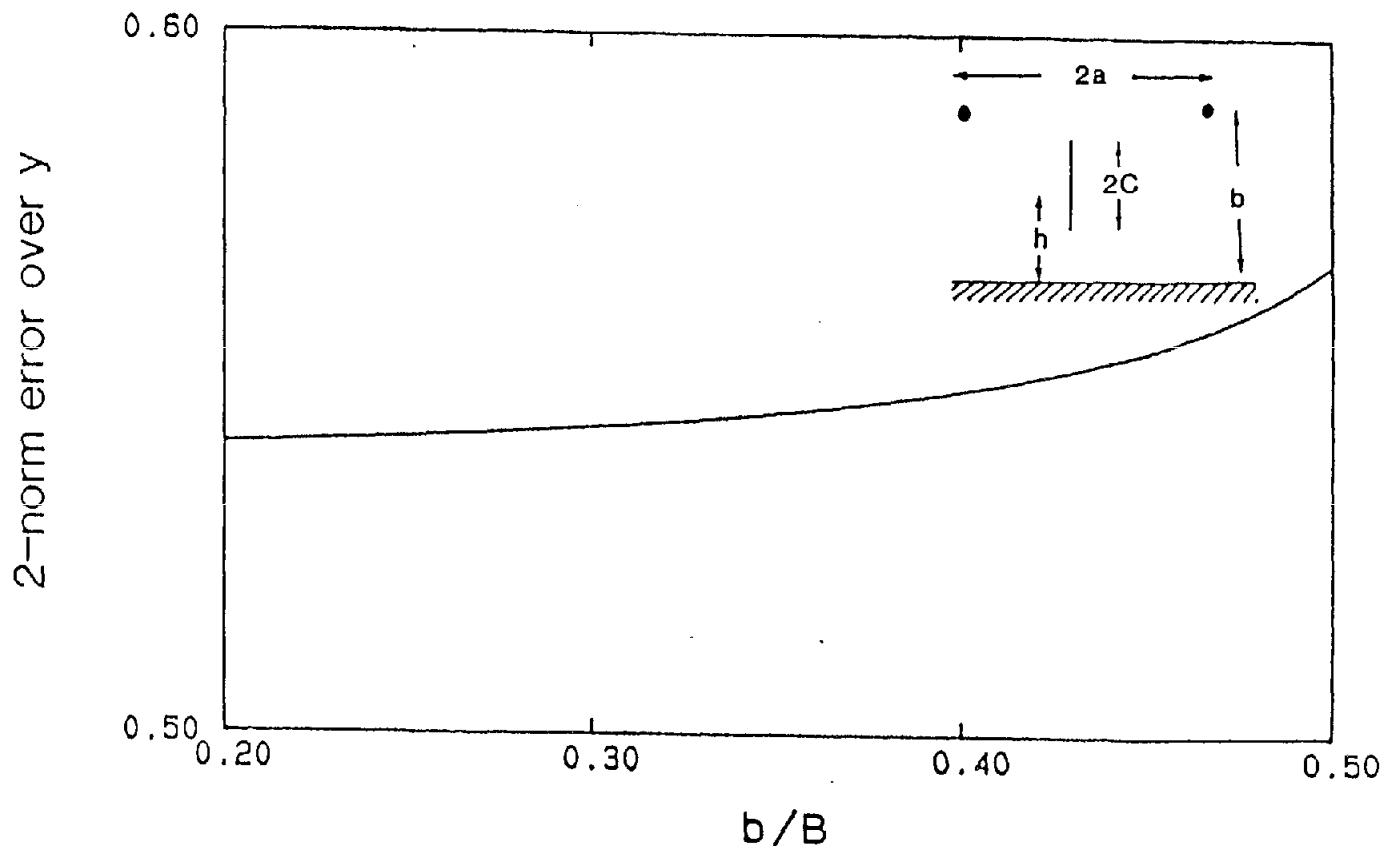
Figure 31.   2-norm error over y (from eq. A7).   B is the height of the
working volume (see Fig. 2) and B/h = 1.8.

differential mode – test object above the ground
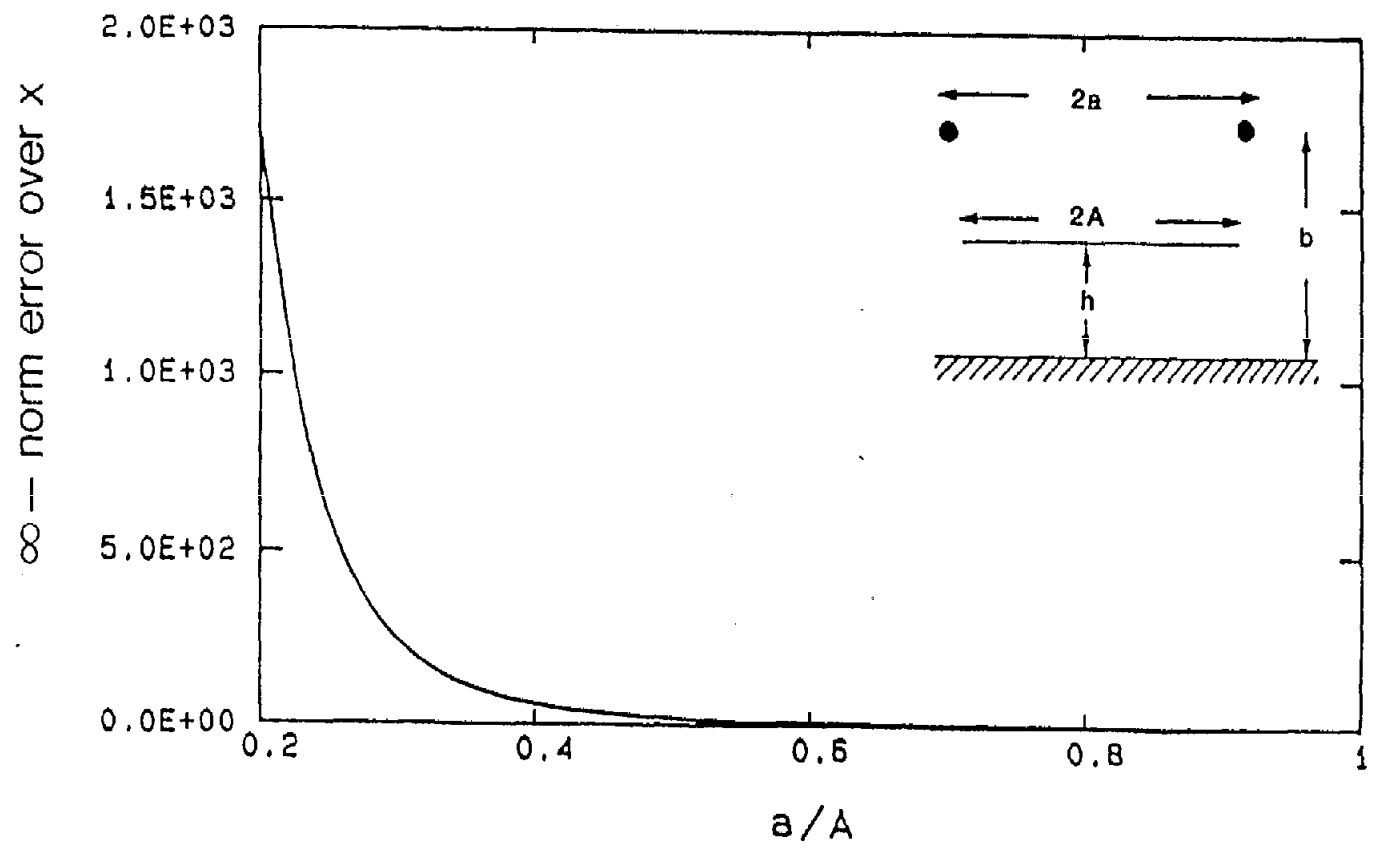
Figure 32. ∞ - norm error over x. A is the half-width of the working volume (see Fig. 2) and A/h = 2.

differential mode – test object above the ground
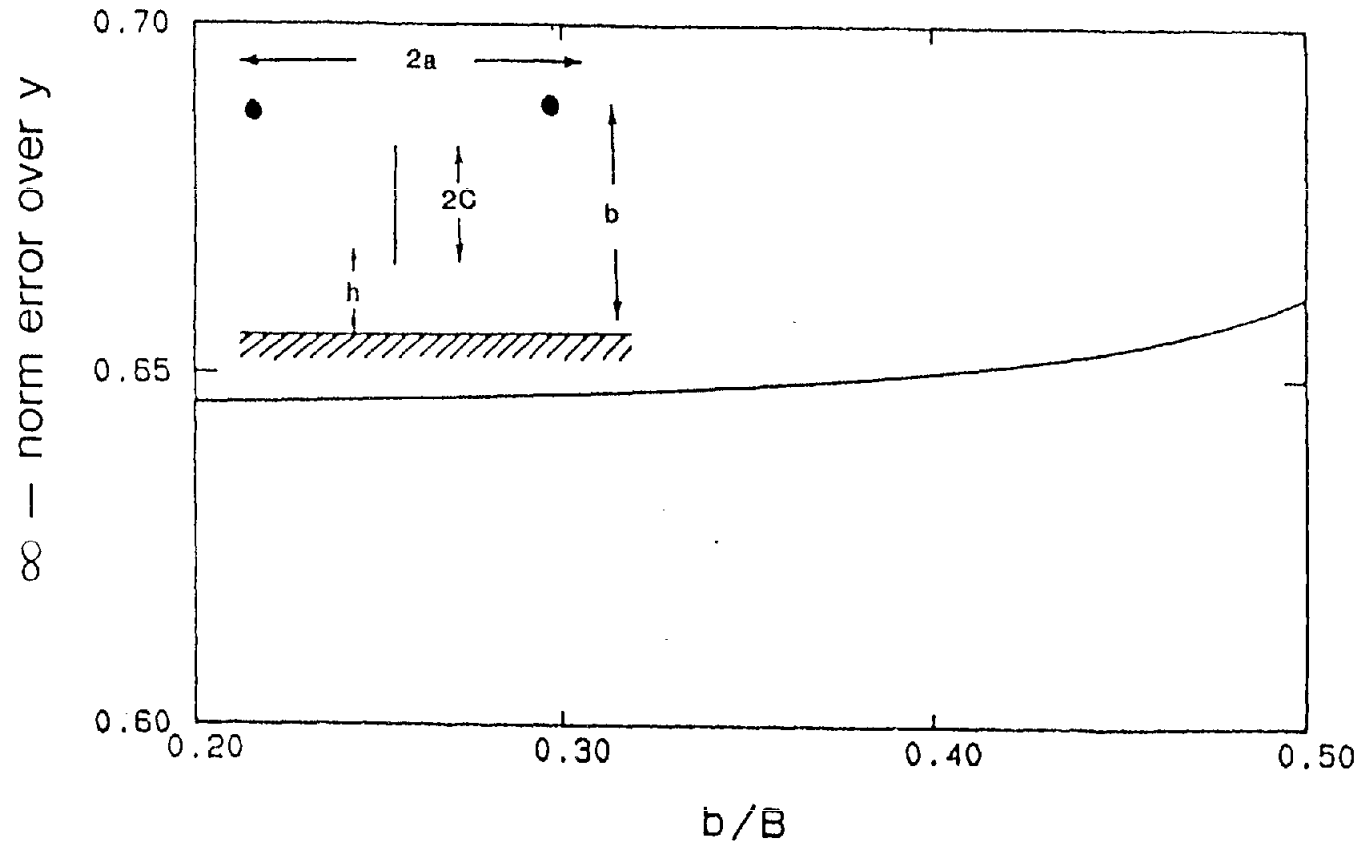
Figure 33. ∞ – norm error over y. B is the height of the working volume and B/h = 1.8.

differential mode – test object above the ground
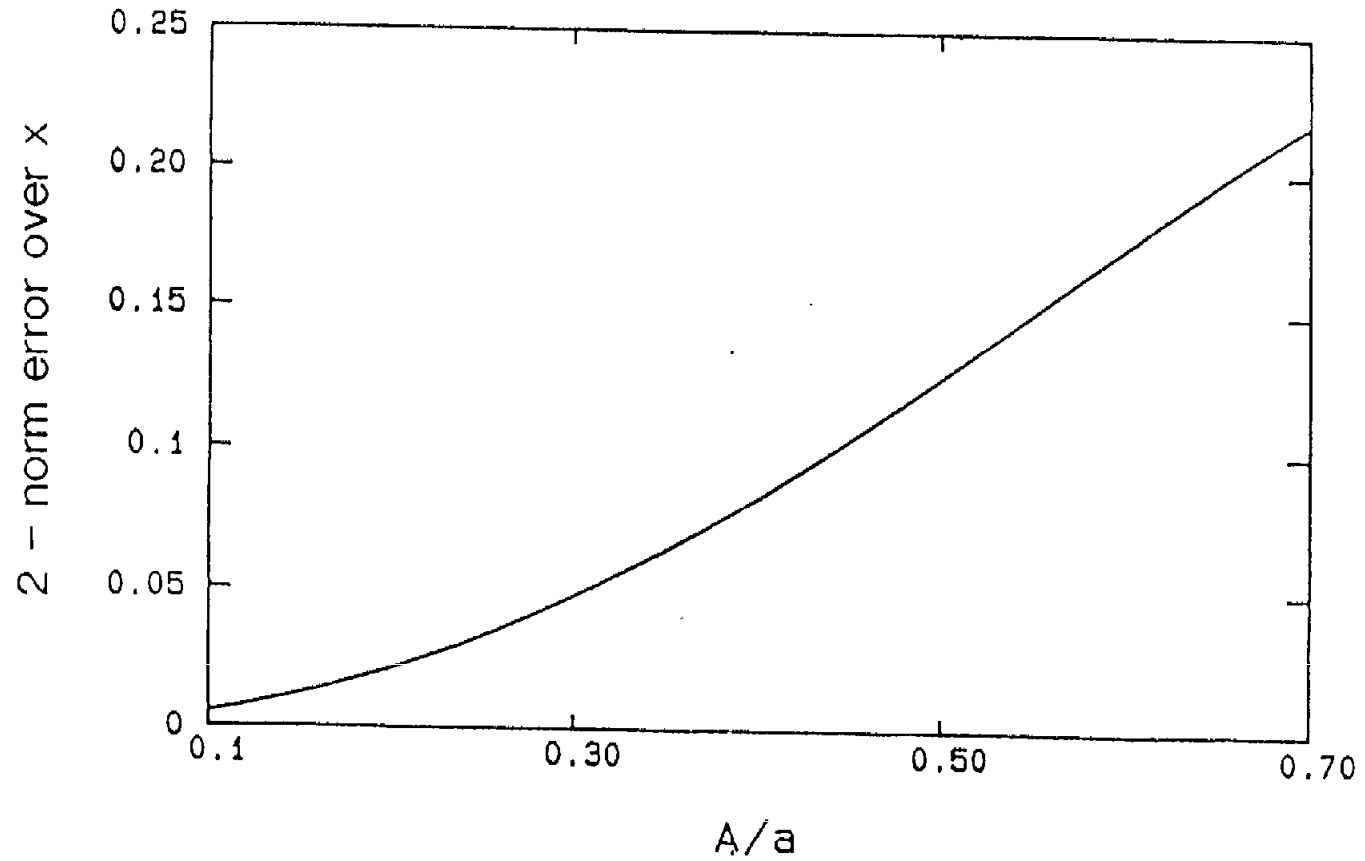
Figure 34. 2-norm error over x; a is the half-separation between the wires
and a/h is fixed at 1.5. From eq. 11a, b/h turns out to be 0.6.

differential mode – test object above the ground
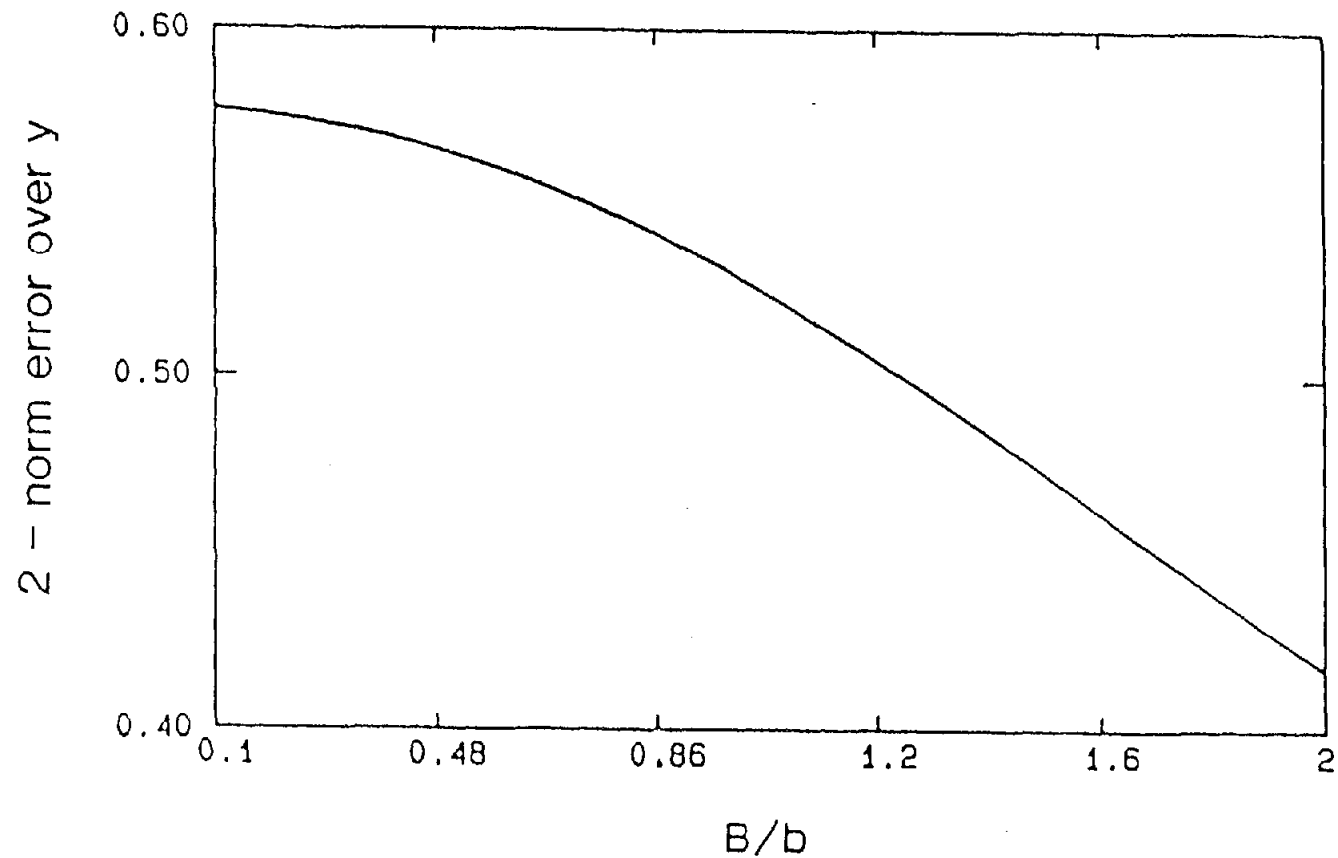
Figure 35. 2-norm error over y; b is the height of the wires above the ground and b/h is fixed at 0.6. From eq. 11, a/h is 1.5.

differential mode – test object above the ground
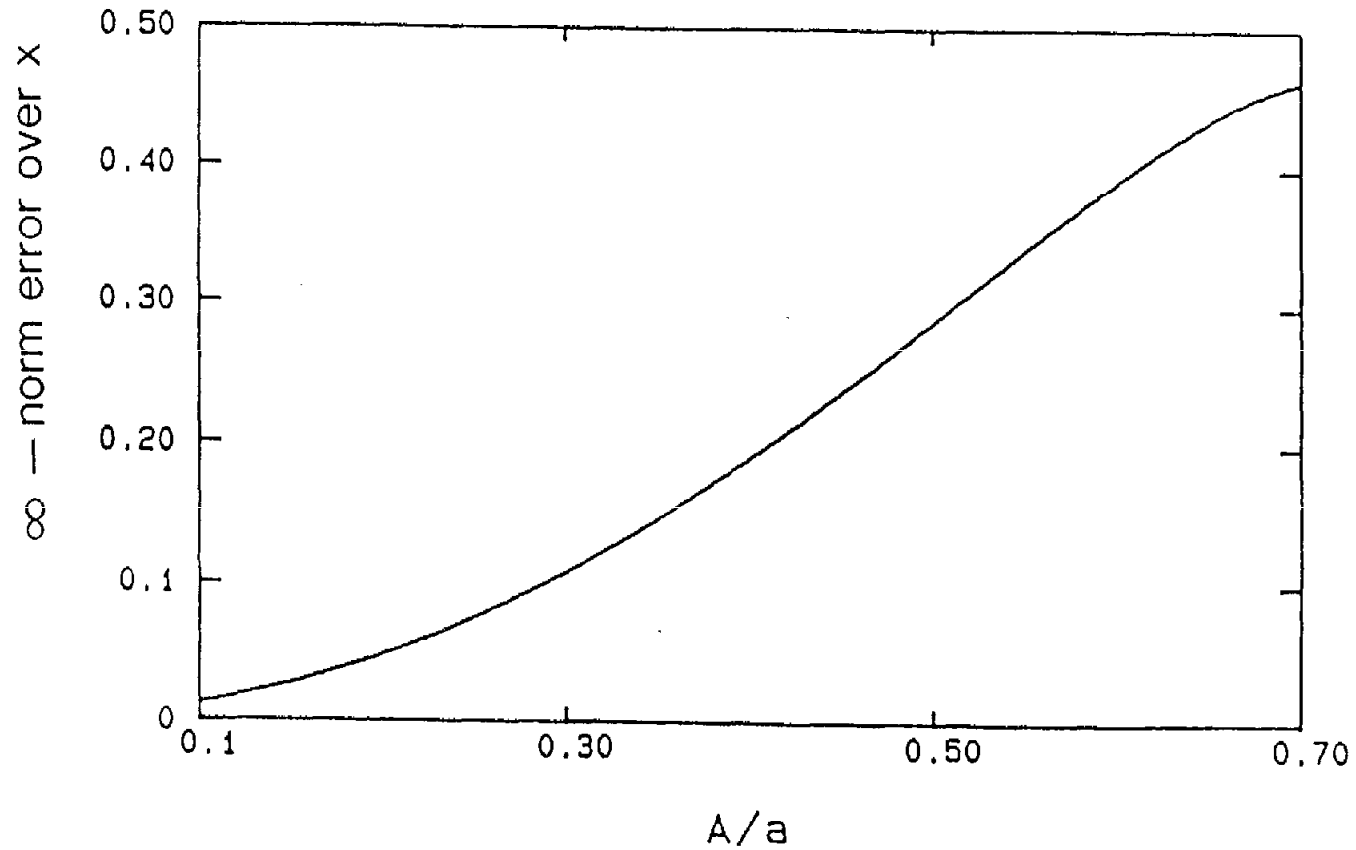
Figure 36. ∞ – norm error over x; a is the half separation between
the wires and a/h is fixed at 1.5. From eq. 11a, b/h is 0.6.

differential mode – test object above the ground
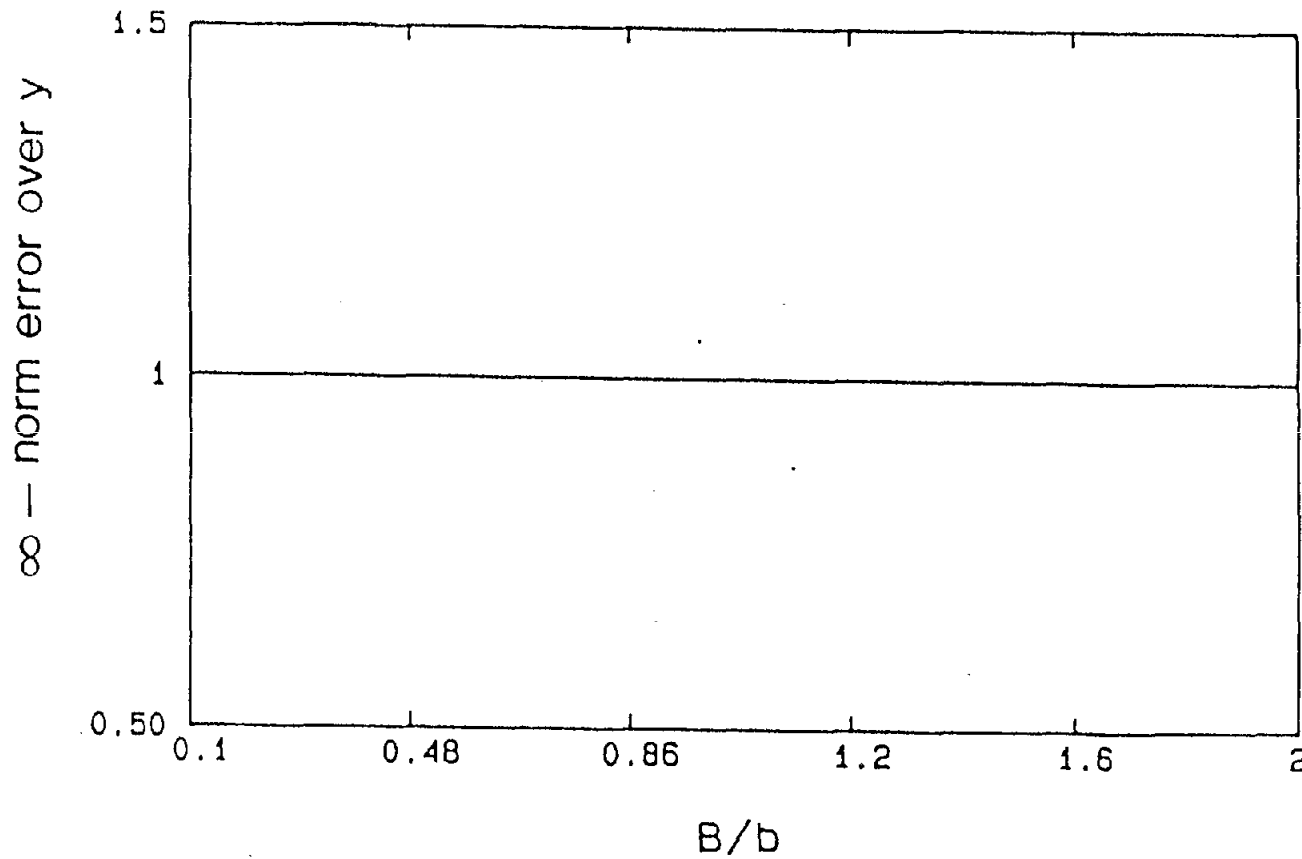
Figure 37. ∞ – norm error over y; b is the height of the wires above the ground and b/h is fixed at 0.6. From eq. ii a/h is 1.5.

IV. IMPEDANCE CALCULATIONS

So far our analysis has been concerned with a system of four line charges of radius equal to zero. However, in practice we are dealing with wires of finite radius which have equipotential surfaces (i.e., their cross sections are equipotential lines). From Equations 3 and 4 one finds that the equipotential lines associated with a system of four line charges, in the immediate neighborhood of the charges themselves, can be approximated by circles, not concentric with the (line) charges nor with one another. Therefore the same field is obtained by replacing four line charges located at $(\pm a, \pm b)$ with four wires of radius R located at $(\pm a, \pm \sqrt{b^2 + R^2})$ for the common mode, and at $(\pm \sqrt{a^2 + R^2}, \pm b)$ for the differential mode, provided a/R >> 1 and b/R >> 1. By integrating the electric field as given by Equation 1 or 2 along any contour starting on the surface of a wire at negative voltage and ending on the surface of a wire at positive voltage, and by calling V the potential difference, we found

$$V = \frac{q}{2\pi\varepsilon_o} \left\{ 2 \ln\left[\frac{b(1 + \sqrt{1 + (R/b)^2}) - R}{b(1 - \sqrt{1 + (R/b)^2}) + R}\right] + \ln\frac{[b(1 + \sqrt{1 + (R/b)^2}) - R]^2 + 4a^2}{[b(1 - \sqrt{1 + (R/b)^2}) + R]^2 + 4a^2} \right\} \quad (12)$$

for the common mode and

$$V = \frac{q}{2\pi\varepsilon_o} \left\{ 2 \ln\left[\frac{a(1 + \sqrt{1 + (R/a)^2}) - R}{a(1 - \sqrt{1 + (R/a)^2}) + R}\right] - \ln\frac{[a(1 + \sqrt{1 + (R/a)^2}) - R]^2 + 4b^2}{[a(1 - \sqrt{1 + (R/a)^2}) + R]^2 + 4b^2} \right\} \quad (13)$$

for the differential mode.

We stress that up to this point our discussion was concerned with establishing an "equivalence" between a system of four lines of charge ± q per unit length and one of four wires of radius R containing currents ±I. In reality there are only two wires above a conducting plane, the other two being their images. We now introduce the characteristic impedance (Z_c' for the common mode and Z_c'' for the differential mode) of two transmission lines operating in the TEM mode. For the common mode excitation Z_c' is the ratio of the voltage between each wire and ground (given by 1/2 of Eq. 12) to the total

50

current $2I = 2qc$ (c is the speed of light) flowing along the wires. Starting from Equation 12, approximating the second logarithm for R<<a and R<<b and normalizing to the vacuum intrinsic impedance n_o, we find

$$f'_g = \frac{V}{4In_o} = \frac{1}{4\pi} \left[\ln\left(\frac{1 + (1 + (R/b)^2)^{1/2} - R/b}{1 - (1 + (R/b)^2)^{1/2} + R/b}\right) + \frac{1}{2} \ln(1 + (b/a)^2) \right] \quad (14)$$

$$= f'_{g1} + f'_{g2} = Z'_c/n_o$$

where the nondimensional quantity f'_g is the characteristic impedance geometric factor. We stress that this result is equivalent to that previously obtained in Reference 2 and also to that presented in Reference 4. Equation 14 points out that f'_g consists of two independent terms: one, f'_{g1}, being a function of R/b alone and the other, f'_{g2}, being a function of a/b. Figure 38 plots f'_g for the two cases of the tst object near the ground and above it. The two different curves for f'_{g2} are shown.

For the differential mode Z''_c is the ratio of the voltage between the two wires (as given by Eq. 13) to the current $I = qc$ flowing along one wire, the current along the other wire being $-I$. From Equation 13, normalizing with respect to n_o, we find:

$$f''_g = \frac{V}{In_o} = \frac{1}{\pi} \left[\ln\left(\frac{1 + (1 + (R/a)^2)^{1/2} - R/a}{1 - (1 + (R/a)^2)^{1/2} + R/a}\right) - \frac{1}{2} \ln(1 + (a/b)^2) \right] \quad (15)$$

$$= f''_{g1} - f''_{g2} = Z''_c/n_o$$

which is in agreement with the results presented in Reference 4.

Again f''_g is the characteristic impedance geometric factor and it is plotted in Figures 39 and 40 for the two cases of test object on the ground and above it. Figure 39 shows two curves: f''_{g1} as a function of log (a/R) (lower scale) and f''_{g2} as a function of a/b (upper scale). Figure 40 shows two curves also but now f''_{g2} is a function of a, while the value of a/b is recovered from Equation 11. From the examination of Figures 39 and 40 it

51

Common mode impedance geometric factor
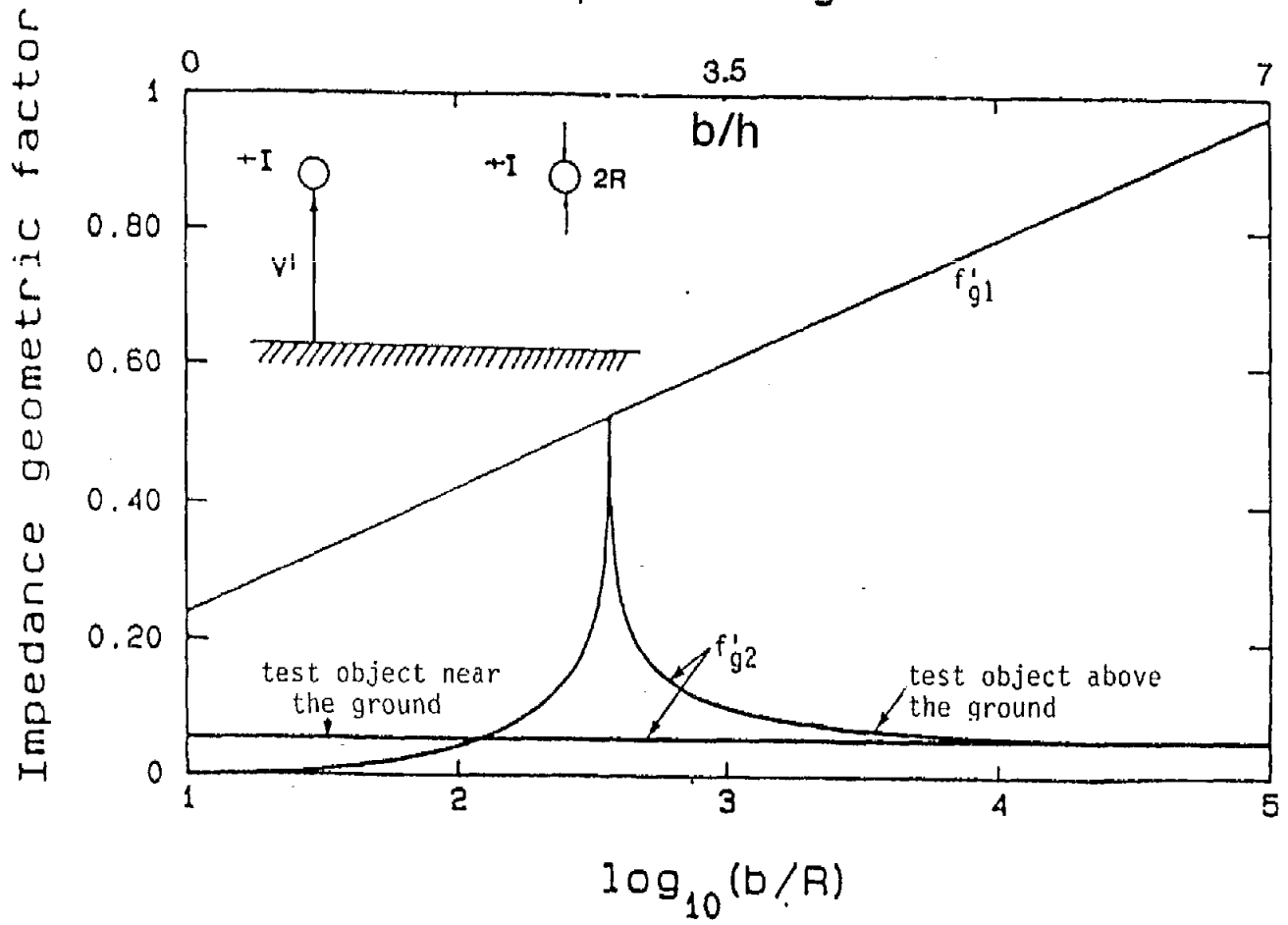
Figure 38. The lower scale (logarithmic) is for f'_{g1}. The upper scale is for f'_{g2} as a function of b.

Differential mode impedance geometric factor
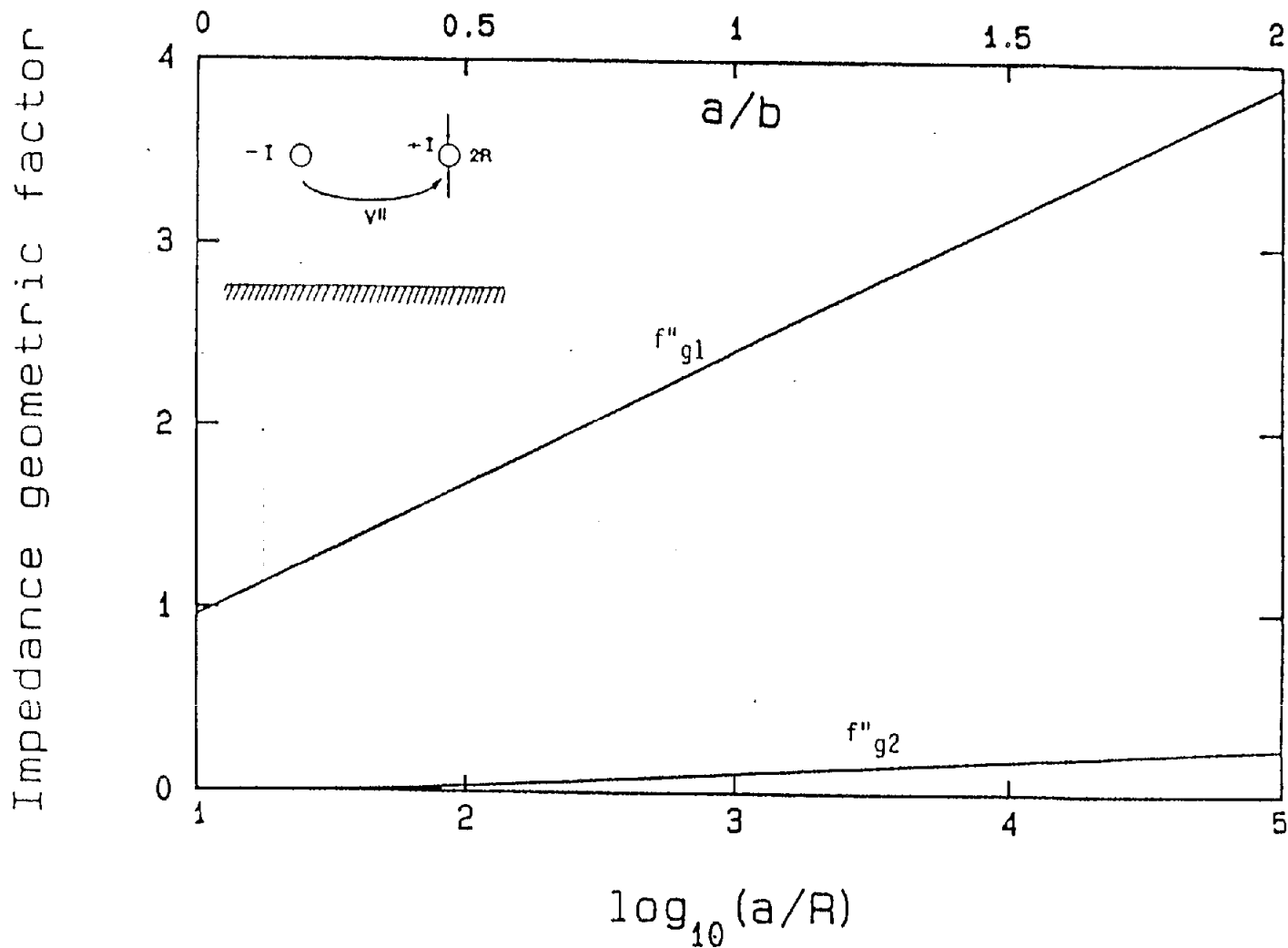
Figure 39. f''_g for the case of the test object near the ground. The lower scale (logarithmic) is for f''_{g1}, the upper scale is for f''_{g2} as a function of a/b.

Differential mode impedance geometric factor
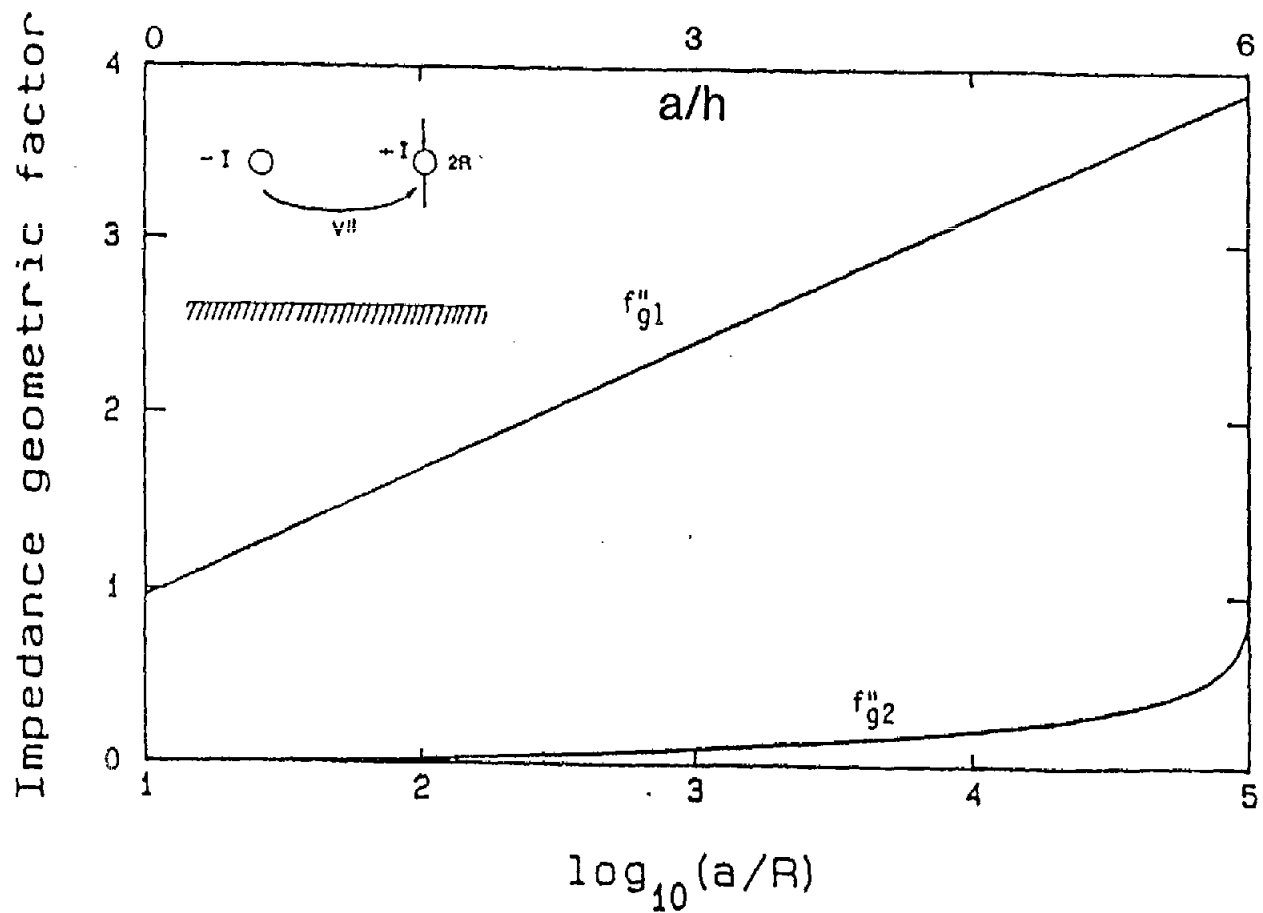
Figure 4D. f''_g for the case of the test object above the ground. The lower scale (logarithmic) is for f''_{g1}, the upper scale is for f''_{g2} as a function of a. The correspondent b can be recovered from eq. 11a.

appears that either f'_{g2} or f''_{g2} is a small quantity compared to f'_{g1} or f''_{g1}, respectively, for all the values of a and b of practical interest. Therefore, the ratios a/R or b/R are the critical quantities to look at for estimating the characteristic impedance.

Finally it is useful to relate the voltage to the source power W via the characteristic impedance, in both cases. When both the voltage and the power are r-m-s values, we have

$$\frac{V'^2}{Z'_c} = W \tag{16}$$

for the common mode excitation, where $V' = 1/2\ V$ of Equation 12. For the differential mode it is

$$\frac{V''^2}{Z''_c} = W \tag{17}$$

where V'' is given by Equation 13. From these equations and from Equations 12 and 13 it is straightforward to show that:

$$\frac{q}{2\pi\varepsilon_0} = \begin{cases} \sqrt{\dfrac{30\ W}{\pi f''_g}} & \text{differential mode} \tag{18} \\[4mm] \sqrt{\dfrac{1.87\ W}{\pi f'_g}} & \text{common mode} \tag{19} \end{cases}$$

V. FIELD DISTRIBUTION

Figures 41 through 44 show the field and equipotential lines for the four cases considered in this study.

Figure 41 refers to the common mode excitation with the test object near the ground: b is taken equal to 1 and $a = b/\sqrt{3}$, as required for optimum field configuration. Figure 42 is for the case of the test object above the ground. By making b = 1 we find from Equation 8 that a is equal to 1.16. Figure 43 deals with the differential mode excitation for the case of the test object near the ground. From Figure 18 it was inferred that the ratio $a/b \simeq 1.2$ minimizes the 2-norm error (and the ∞-norm error) along x. This ratio was used to plot Figure 43. Finally, when the test object is away from the ground, from Equation 11 it turns out that if b = 1, the value of a is 2.3. This value was used to plot Figure 44. From looking at the equipotential plots one can immediately visualize the field distribution and get a feeling for the relative intensity of the electric field at various locations. The actual value of each tube of flux is recovered by multiplying the difference Δv between any two field curves by the appropriate ratio of $q/(2\pi\varepsilon_0)$. Similarly, the value of the voltage difference between equipotentials is determined by multiplying the total voltage V by the difference Δu between any two potential lines and dividing by 4 π.

When actual field strength values are required, one should use Equations 1 and 2 along with Equations 8, 11, 18 and 19. Figures 45 through 48 show the electric field at (x = 0, y = h) for the four cases which have been discussed above as functions of a and b. We stress that the field estimate is based on a perfect impedance match and perfectly conducting ground. Nevertheless it gives the reader a rough feeling for the overall field strength and how it can be expected to vary when the wire separation is changed. Since it might be required that the field level be within a certain range, these plots permit one to choose proper values of a and b within a specified range predetermined by uniformity requirements.

common mode – test object near the ground
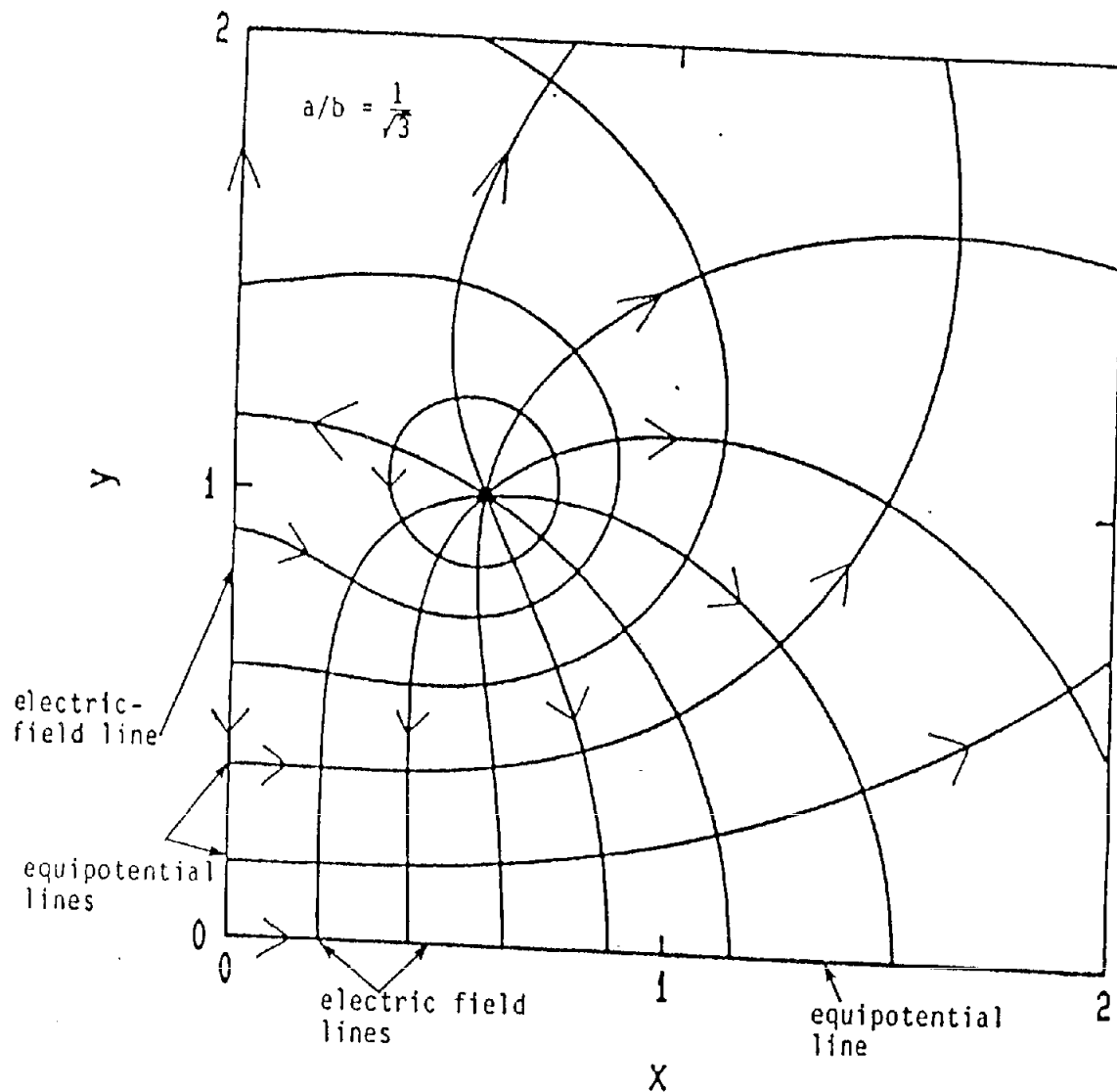
Figure 41. Field lines in half cross section of the working volume. The rest is recovered by symmetry with respect to y. The potential difference between any two adjacent lines and the value of the tube of flux is $\pi/5$.

common mode – test object above the ground

a/b = 1.16

equipotential lines

electric
field line

electric field
lines

equipotential line

X

y
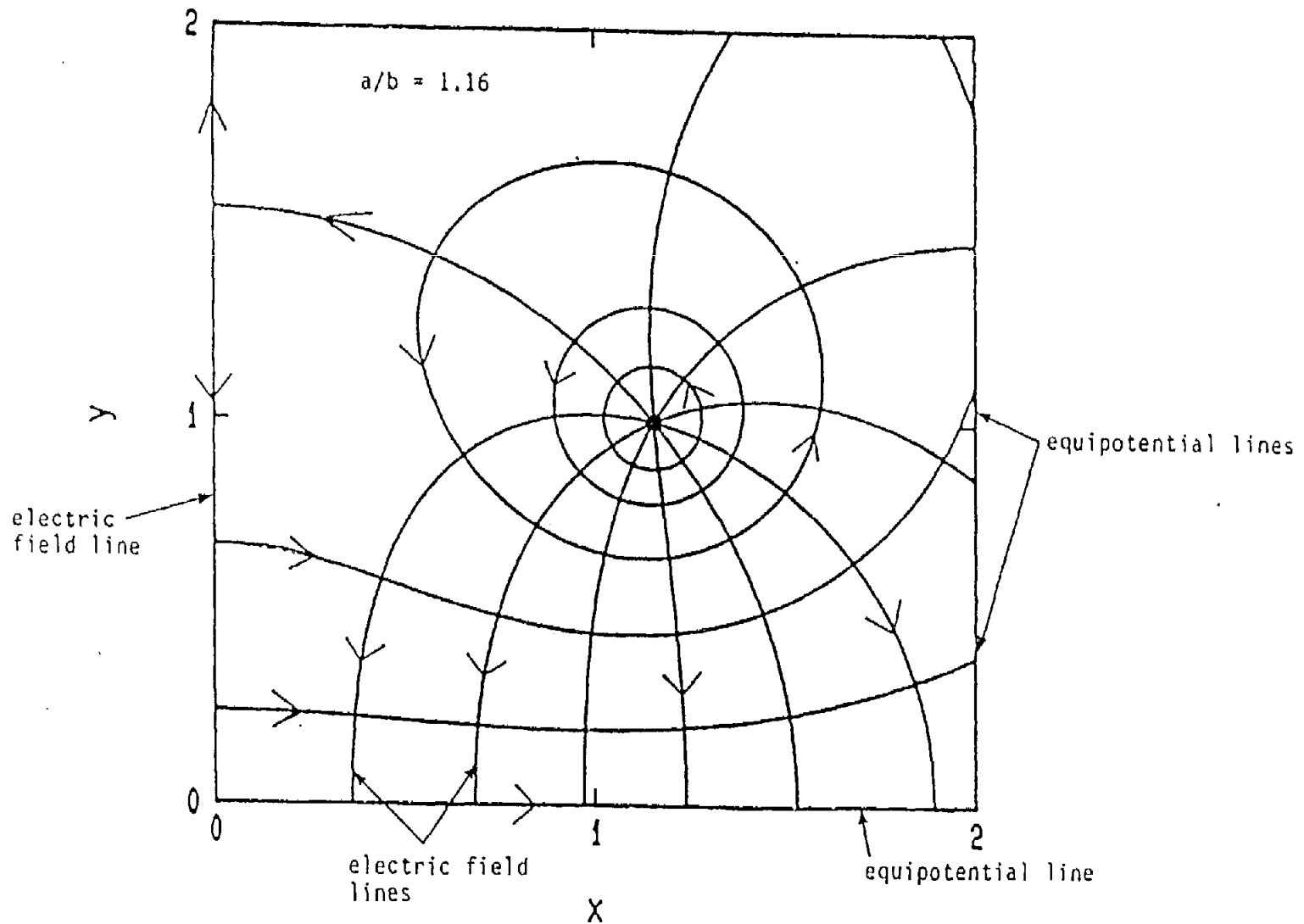
Figure 42. Field lines in half cross section of the working volume. The rest is recovered by symmetry with respect to y. The potential difference between any two adjacent lines and the value of the tube of flux is π/5.

differential mode – test object near the ground
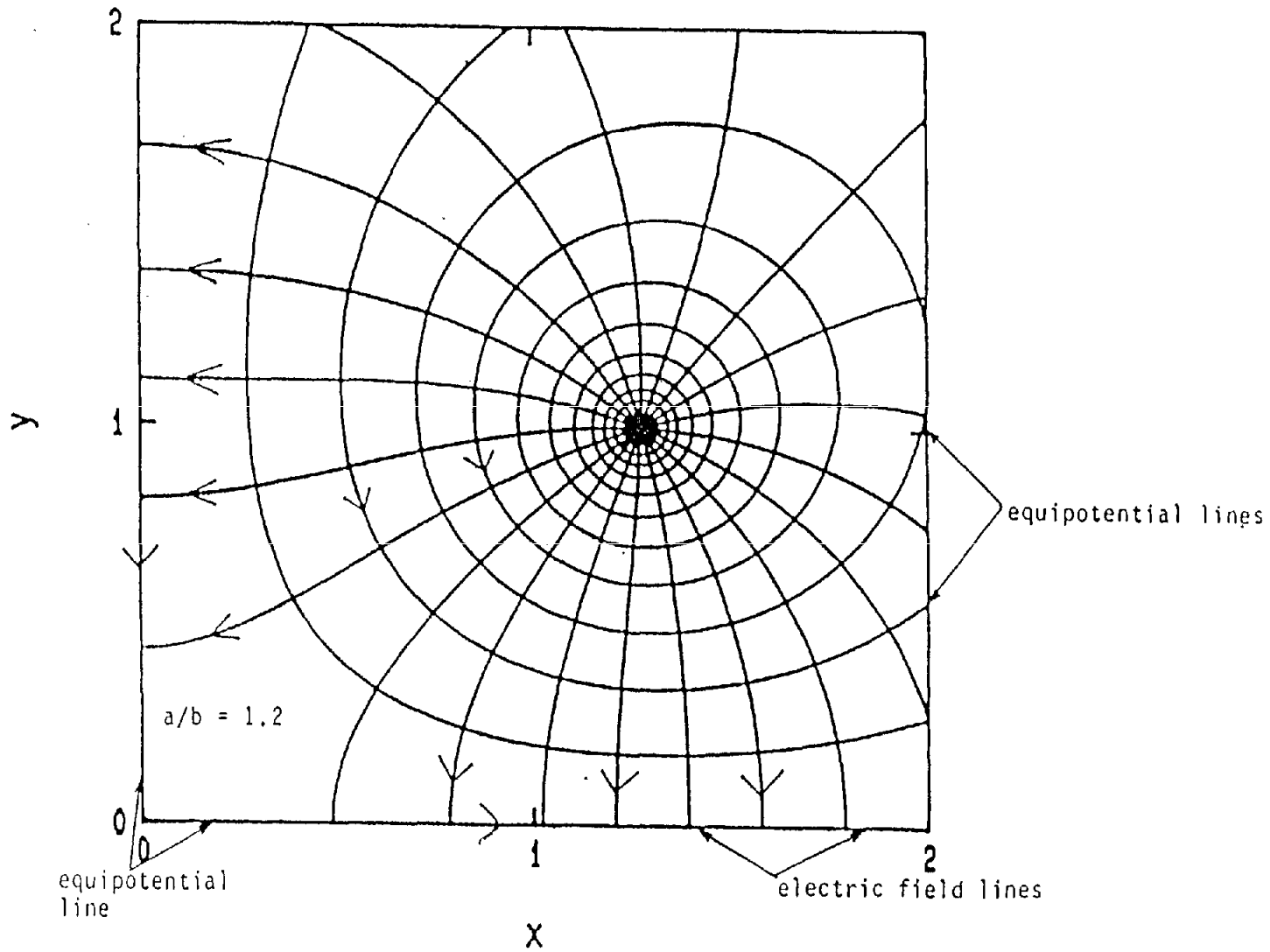
Figure 43. Field lines in half cross section of the working volume. The rest is recovered by symmetry with respect to y. The potential difference between any two adjacent lines and the value of the tube of flux is π/10.

differential mode – test object above the ground

a/b = 2.3

equipotential or magnetic field lines

equipotential lines

electric field lines

X
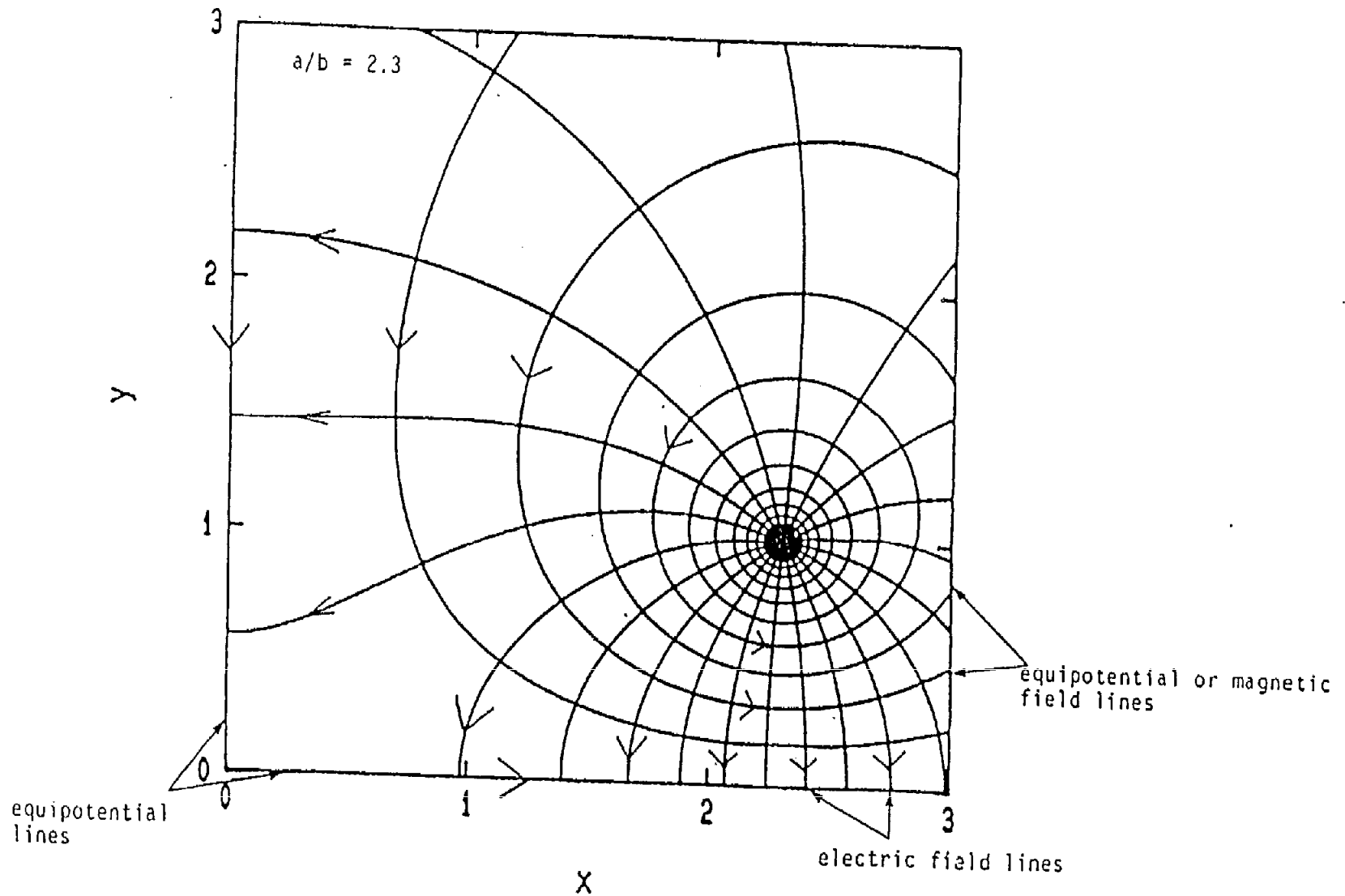
Figure 44. Field lines in half cross section of the working volume. The rest is recovered by symmetry with respect to y. The potential difference between any two adjacent lines and the value of the tube of flux is $\pi/10$.
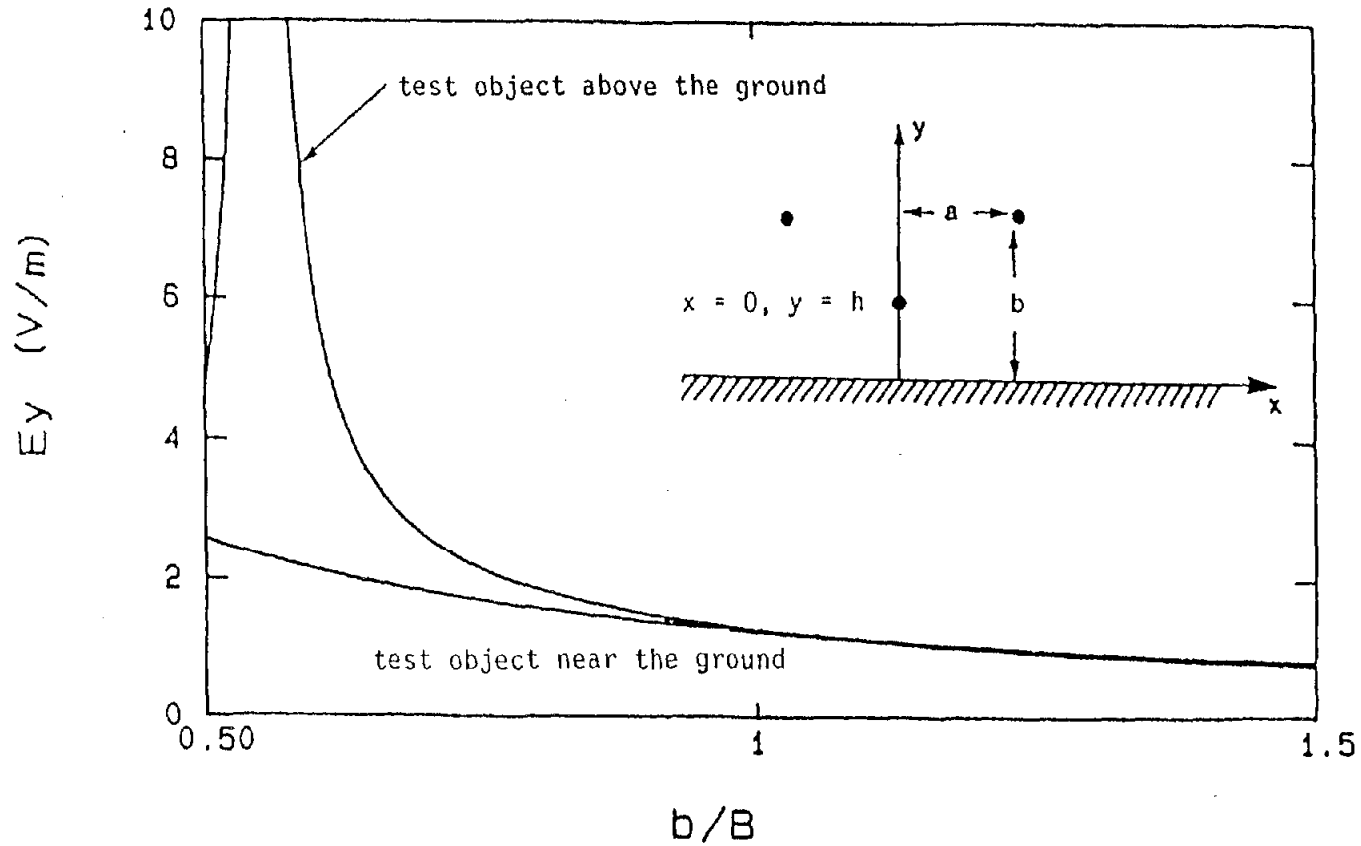
Figure 45. Absolute value of the electric field at the point x = 0, y = h (see eq. 1). B is the height of the working volume and B/h = 6.7 for the test object near the ground and 1.8 for the test object above the ground.

differential mode – test object near the ground
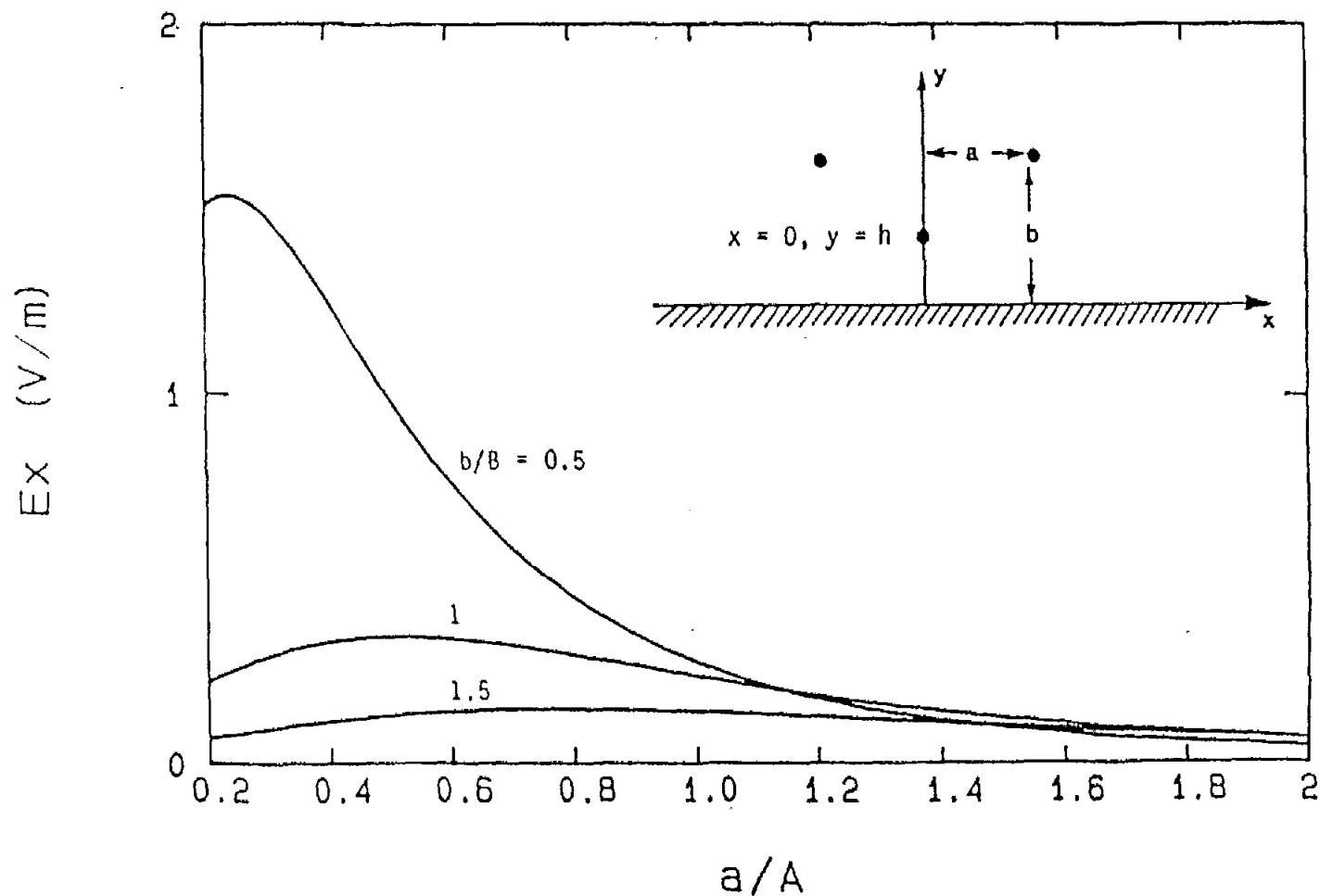
Figure 46. Absolute value of the electric field at the point x = 0, y = h (see eq. 2). A is the half-width of the working volume and A/h = 7.

differential mode – test object near the ground
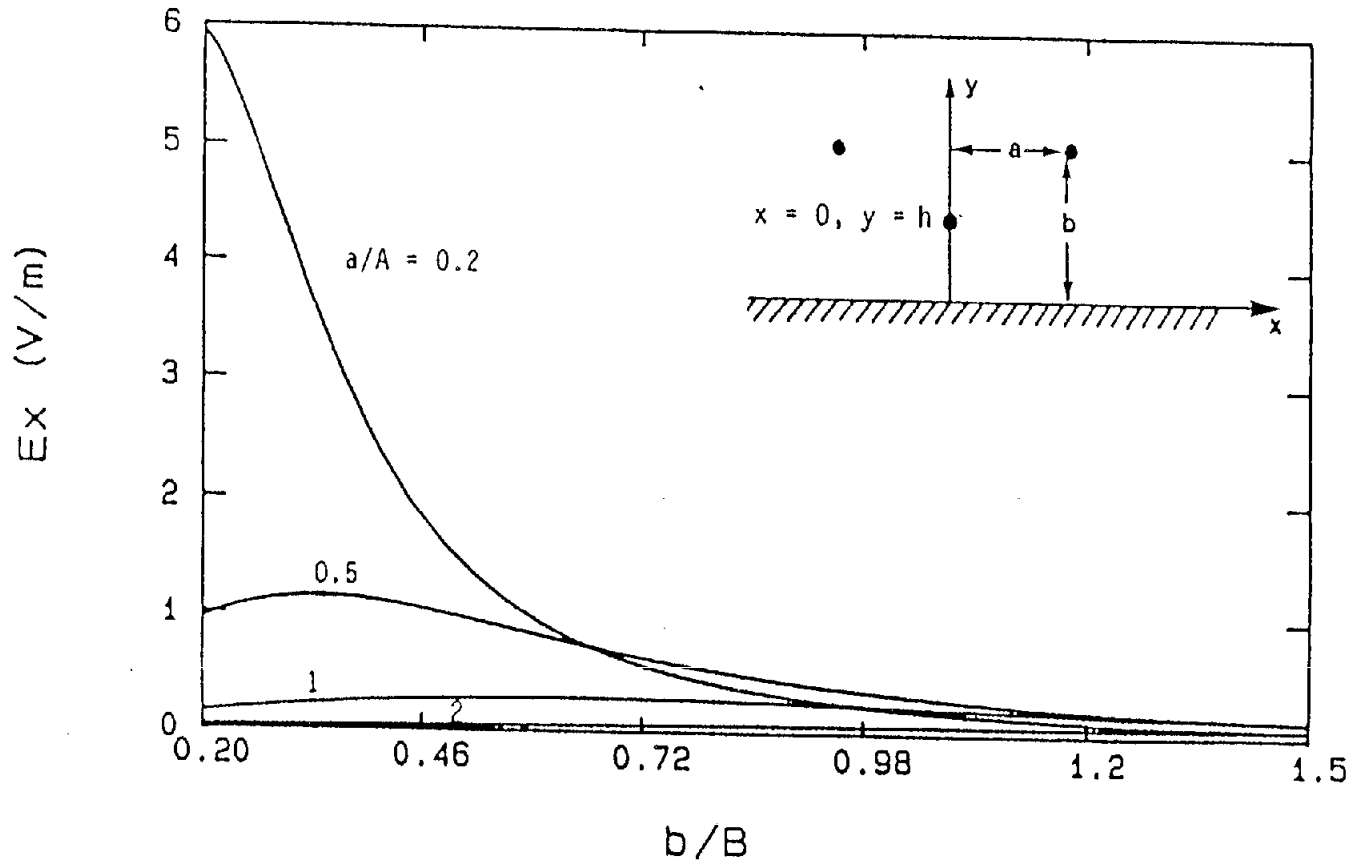
Figure 47. Absolute value of the electric field at the point x = 0, y = h (see eq. 2). B is the height of the working volume and B/h = 6.7.

differential mode – test object above the ground
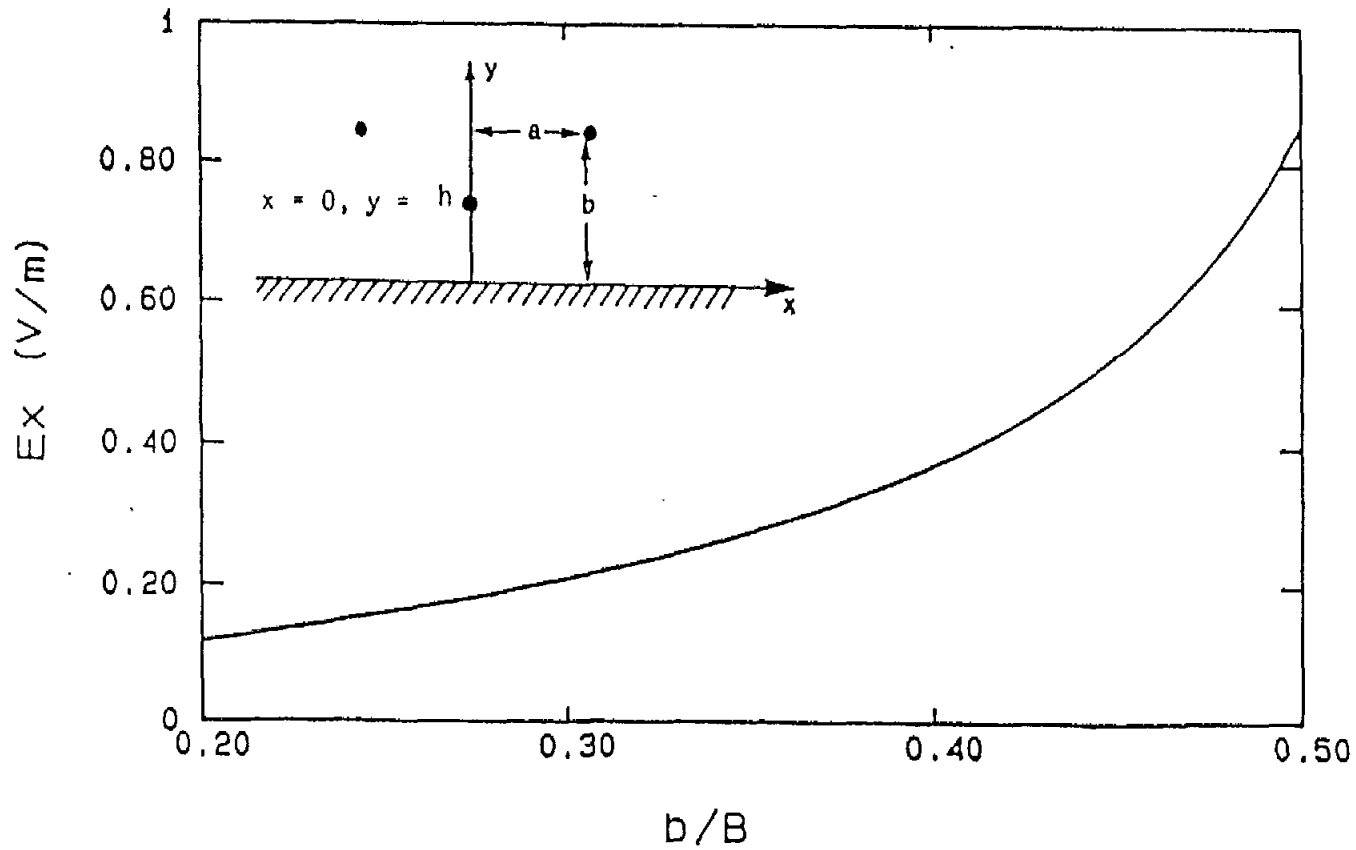
Figure 48. Absolute value of the electric field at the point x = 0, y = h
(see eq. 2). B is the height of the working volume and B/h = 1.8.

As an alternative, a nondimensional expression was derived, relating the magnitude of the electric field to the voltage source. By observing that $|E|/|H| = n_0$ anywhere for the TEM mode and $|V'|/|2I| = Z_C'$ or $|V''|/|I| = Z_C''$, we obtain from the equation for the magnetic field of four line currents, at the point $(x = 0, y = h)$

$$\frac{|H| \, b}{I} = 2f_g' \frac{|E| \, b}{V'} = \frac{b}{\pi a} \left| \frac{(b - h)/a}{1 + (b^2 - h^2)/a} + \frac{(b + h)/a}{1 + (b^2 + h^2)/a} \right| \qquad (20)$$

for the common mode and

$$\frac{|H| \, b}{I} = f_g'' \frac{|E| \, b}{V''} = \frac{b}{a \pi} \left| \frac{1}{1 + (b^2 - h^2)/a} - \frac{1}{1 + (b^2 + h^2)/a} \right| \qquad (21)$$

for the differential mode. Figures 49 through 52 plot these two functions.

common mode
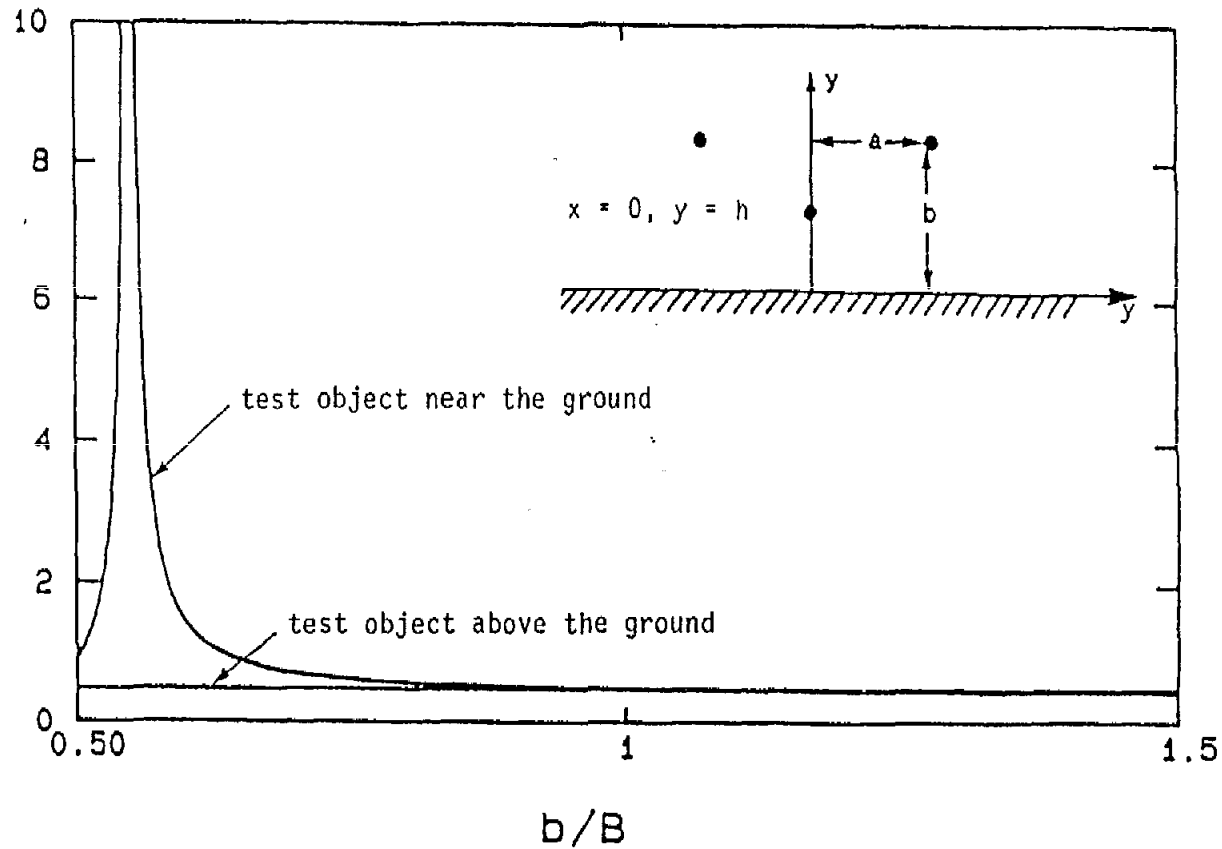
Figure 49. Non-dimensional quantity related to electric field or magnetic field at the point x = 0, y = h (see eq. 20). B is the height of the working volume and B/h = 6.7 for the object near the ground and 1.8 for the object above the ground.

differential mode – test object near the ground
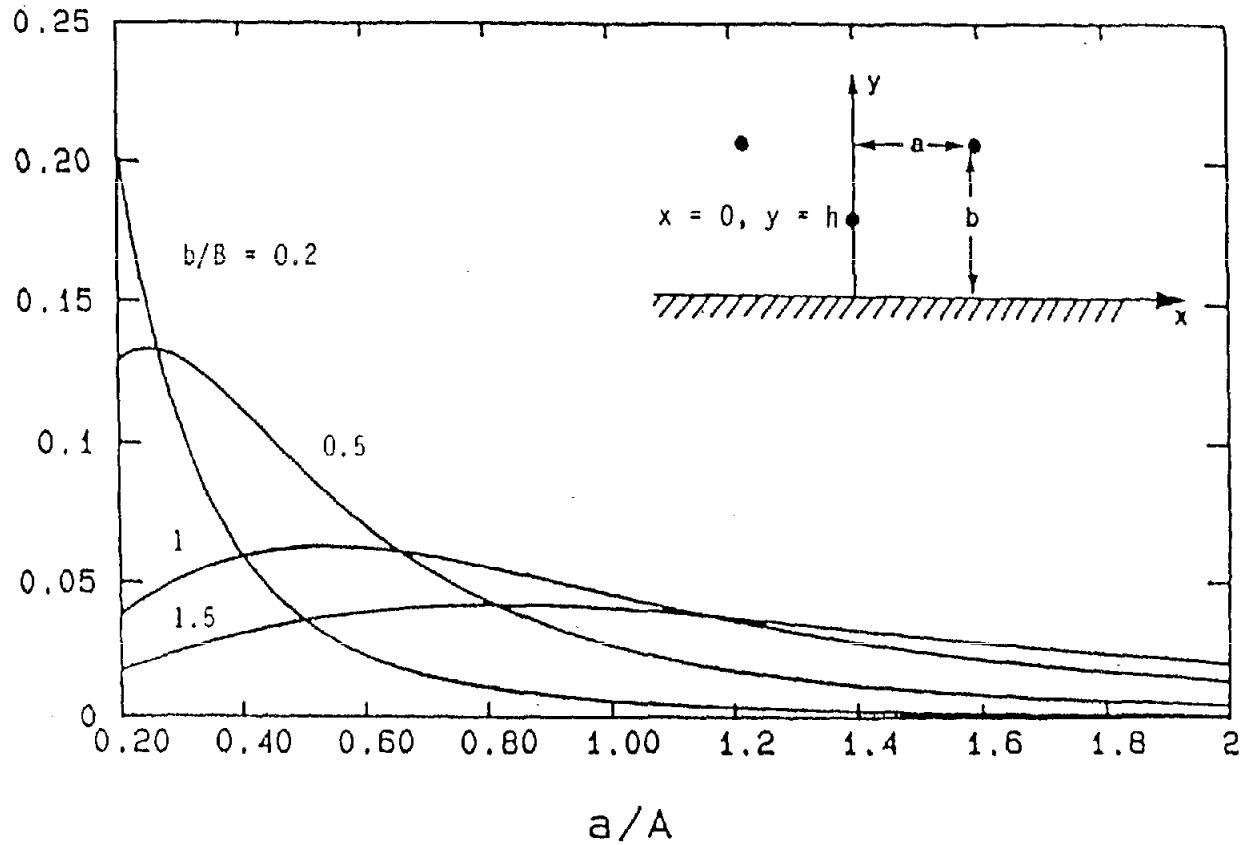
Figure 50. Non-dimensional quantity related to electric field or magnetic field at the point x = 0, y = h (see eq. 21). A is the half-width of the working volume and A/h = 7.

differential mode – test object near the ground
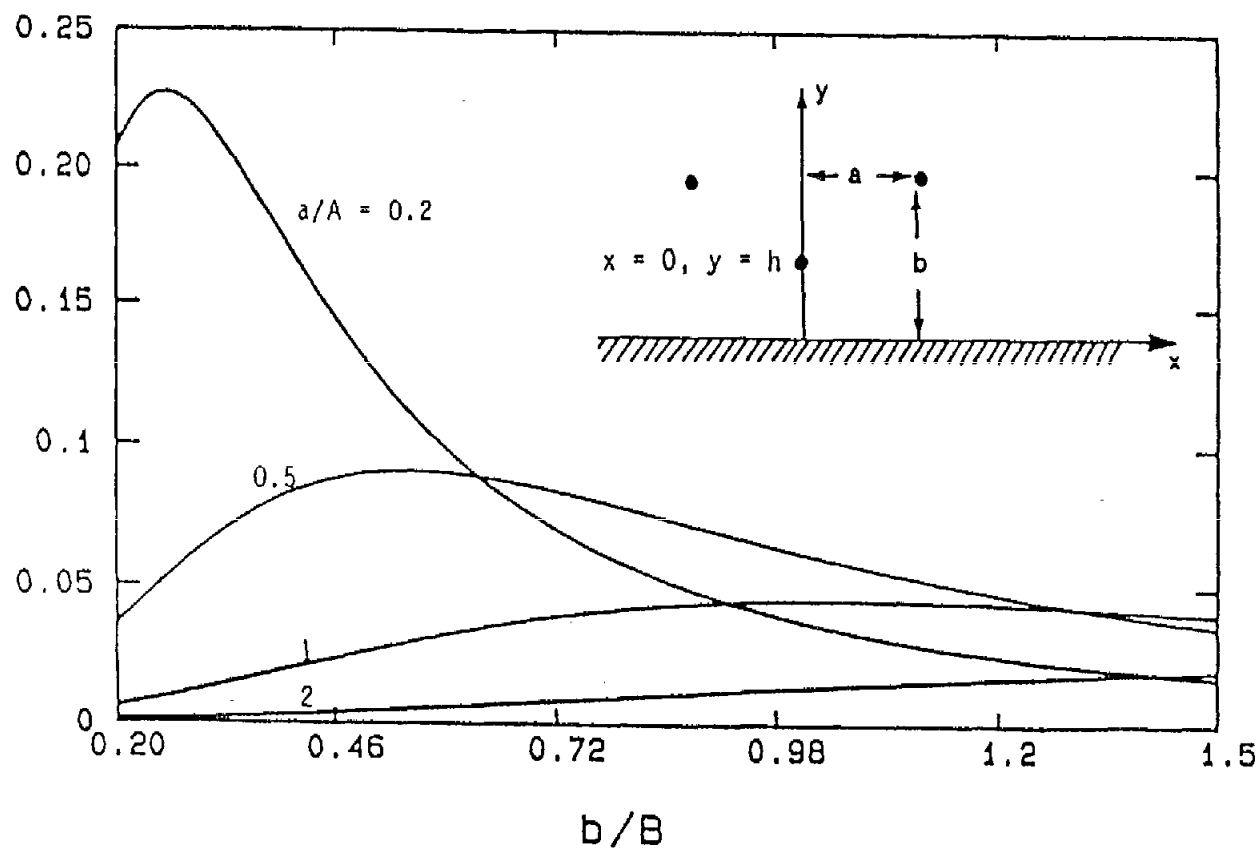
Figure 51. Non-dimensional quantity related to electric field or magnetic field at the point x = 0, y = h (see eq. 21). B is the height of the working volume and B/h = 6.7.

differential mode — test object above the ground

b/B
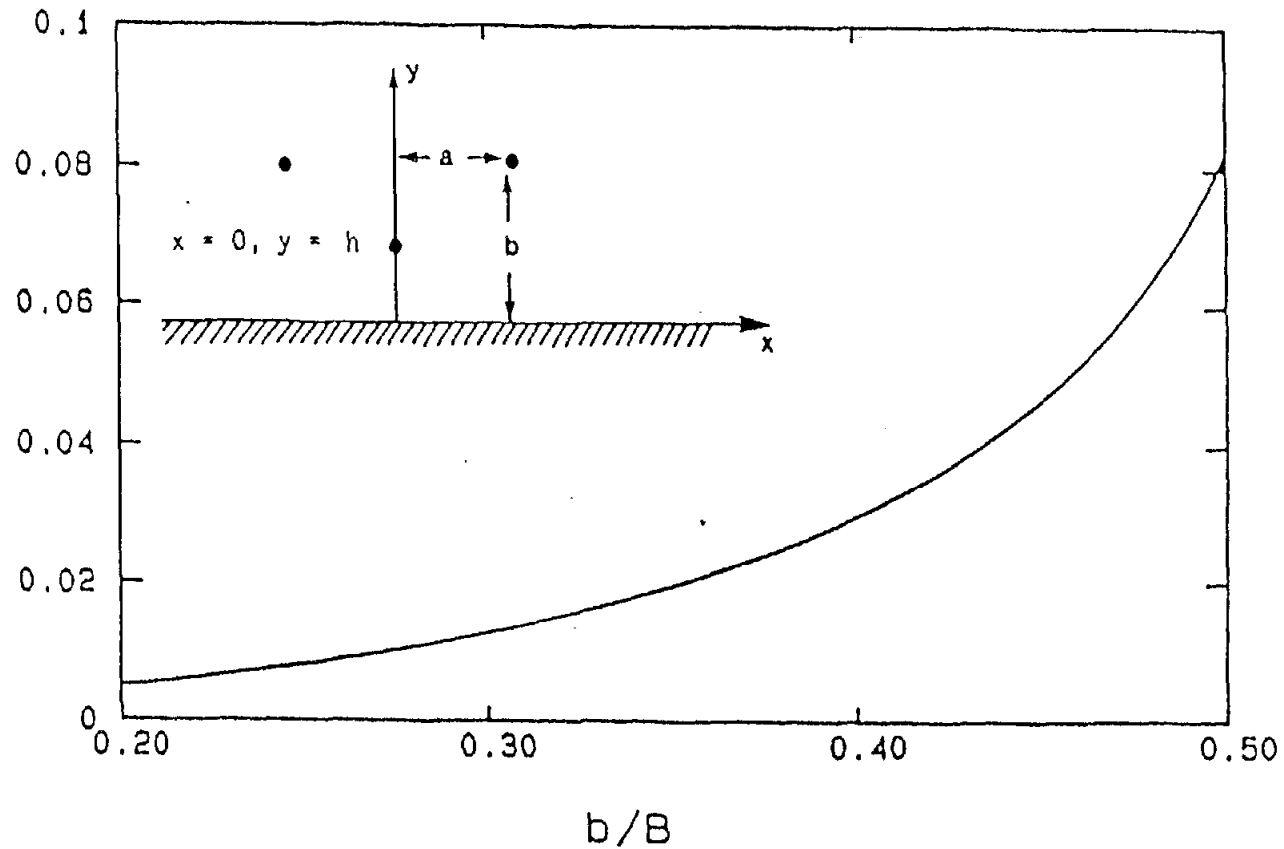
Figure 52.   Non-dimensional quantity related to electric field or magnetic field at the point x = 0, y = h   (see eq. 21).   B is the height of the working volume and B/h = 1.8.

REFERENCES

1. Baum, C.E., "Impedances and Field Distributions for Symmetrical Two Wire and Four Wire Transmission Line Simulators," Sensor and Simulation Notes, Note 27, AFWL, Kirtland AFB, June 1970.

2. Smythe, W.R., "Static and Dynamic Electricity," Chapter 5, McGraw Hill, 3rd edition, 1968.

3. Ramo, S., Whinnery, J.R., and T. Van Duzer, "Fields and Waves in Communication Electronics," Chapter 2, J. Wiley and Sons, 1965.

4. Schelkunoff, S.A. and H.T. Friis, "Antennas Theory and Practice," p. 595, Wiley, 1966.

In this appendix explicit expressions are derived for the 2-norm error for the four cases discussed in the body of the note. Starting with Equation 5, repeated below for convenience

$$F(a',b') = \{\frac{1}{D} \int_D (E_\delta(a',b',\xi) - E_\delta^{ave}(a',b'))^2 \, d\xi\}^{1/2} / E_\delta^{ave}(a',b') \quad (5)$$

the four expressions are as follows:

1. CASE 1 AND CASE 2: COMMON MODE

$$F_1(a',b') = \frac{NN_1(a',b')}{DD_1(a',b')} \quad (A1)$$

$$NN_1(a',b') = \{\frac{1}{L'} \int_0^{L'} [E_y(a',b',x') - DD_1(a',b')]^2 \, dx'\}^{1/2}$$

$$(NN_1)^2 = \frac{1}{L'} \{\frac{L_m/2}{L_m^2 + k_m^2} + \frac{L_p/2}{L_p^2 + k_m^2} + \frac{L_m/2}{L_m^2 + k_p^2} + \frac{L_p/2}{L_p^2 + k_p^2} + (DD_1^2) L'$$

$$+ \frac{1}{2k_m} [\arctan(\frac{L_m}{k_m}) + \arctan(\frac{L_p}{k_m})] + \frac{1}{2k_p} [\arctan(\frac{L_m}{k_p}) + \arctan(\frac{L_p}{k_p})]$$

$$+ (\frac{A_1 - A_2}{2}) \ln(\frac{L_m^2 + k_m^2}{a'^2 + k_m^2}) + (\frac{A_3 - A_1}{2}) \ln(\frac{L_p^2 + k_m^2}{a'^2 + k_m^2})$$

$$+ (\frac{A_4 - A_3}{2}) \ln(\frac{L_m^2 + k_p^2}{a'^2 + k_p^2}) + (\frac{A_2 - A_4}{2}) \ln(\frac{L_p^2 + k_p^2}{a'^2 + k_p^2})$$

$$+ \frac{(B_1 - C_1 - B_2 + a'(A_1 - A_2) - 2k_m DD_1)}{k_m} [\arctan(\frac{L_m}{k_m}) + \arctan(\frac{a'}{k_m})]$$

$$+ \frac{(B_1 - C_1 - C_4 - a'(A_3 - A_1) - 2k_m DD_1)}{k_m} \lceil \arctan(\frac{L_p}{k_m}) - \arctan(\frac{a'}{k_m}) \rceil$$

$$+ \frac{(B_4 + C_1 - B_3 + a'(A_4 - A_3) + 2k_p DD_1)}{k_p} \lceil \arctan(\frac{L_m}{k_p}) + \arctan(\frac{a'}{k_p}) \rceil$$

$$+ \frac{(B_4 + C_1 - C_2 - a'(A_2 - A_4) + 2k_p DD_1)}{k_p} \lceil \arctan(\frac{L_p}{k_p}) - \arctan(\frac{a'}{k_p}) \rceil \}$$

$$DD_1 = \frac{1}{L'} \int_0^{L'} E_y(a',b',x')dx' \qquad\qquad (A2)$$

$$= \frac{1}{L'} \lceil \arctan(\frac{L_m}{k_m}) + \arctan(\frac{L_p}{k_m}) - \arctan(\frac{L_m}{k_p}) - \arctan(\frac{L_m}{k_p}) \rceil$$

where we introduced

$$L' = 21/h, \; L_m = L' - a', \; L_p = L' + a', \; k_m = 1 - b', \; k_p = 1 + b'$$

$$A_1 = - k_m^2 / \lceil 2a'(a'^2 + k_m^2) \rceil, \; B_1 = k_m^2 / (a'^2 + k_m^2), \; C_1 = k_p k_m / 2b',$$

$$A_2 = - k_m k_p / \lceil 2a'(a'^2 + k_p^2) \rceil - b' / \lceil a'(a'^2 + k_p^2) \rceil \times C_2,$$

$$B_2 = k_m k_p \lceil a'^2(9k_p^2 - k_m^2) + 4b' k_p^2 + 8a'^4 \rceil / \lceil 8(a'^2 + k_p^2)(1 + a'^2)(a'^2 + b'^2) \rceil$$

$$C_2 = k_m k_p (2a'^2 - b') / \lceil 2(1 + a'^2)(b'^2 + a'^2) \rceil,$$

$$A_3 = - k_m k_p / \lceil 2a'(a'^2 + k_m^2) \rceil + b' / \lceil a'(a'^2 + k_m^2) \rceil \times C_3,$$

$$B_3 = k_m k_p \lceil a'^2(9k_m^2 - k_p^2) - 4k_m^2 b' + 8a'^4 \rceil / \lceil 8(a'^2 + k_m^2)(1 + a'^2)(a'^2 + b'^2) \rceil$$

$$C_3 = k_m k_p (2a'^2 + b') / \lceil 2(a'^2 + b'^2)(1 + a'^2) \rceil,$$

72

$$A_4 = -k_p^2 / [2a'(a'^2 + k_p^2)], \quad B_4 = k_p^2 / (a'^2 + k_p^2).$$

$$F_2(a',b') = \frac{NN_2(a',b')}{DD_2(a',b')} \qquad (A3)$$

$$NN_2(a',b') = \left\{ \frac{1}{M'' - M'} \int_{M'}^{M''} [E_y(a',b',y') - DD_2(a',b')]^2 \, dy' \right\}^{1/2}$$

$$(NN_2)^2 = \frac{1}{M'' - M'} \left\{ \frac{2M_m'}{a'^2 + M_m'^2} + \frac{2M_p'}{a'^2 + M_p'^2} - \frac{2M_m''}{a'^2 + M_m''^2} - \frac{2M_p''}{a'^2 + M_p''^2} \right.$$

$$+ \frac{2 - Q_1 - b'P_1}{a'} \left[\arctan(\frac{M_m''}{a'}) + \arctan(\frac{M_p''}{a'}) - \arctan(\frac{M_m'}{a'}) - \arctan(\frac{M_p'}{a'}) \right]$$

$$+ \frac{(DD_2'')}{M''} - \frac{(DD_2')^2}{M'} - \frac{P_1}{2} [\ln(\frac{a'^2 + M_m''^2}{a'^2 + M_m'^2}) - \ln(\frac{a'^2 + M_p''^2}{a'^2 + M_p'^2})]$$

$$\left. - \frac{2DD_2''}{M''} \ln(\frac{a'^2 + M_m''^2}{a'^2 + M_p''^2}) + \frac{2DD_2'}{M'} \ln(\frac{a'^2 + M_m'^2}{a'^2 + M_p'^2}) \right\}$$

$$DD_2 = \frac{1}{M'' - M'} \int_{M'}^{M''} E_y(a',b',y')dy' = \frac{1}{M'' - M'} [\int_0^{M''} E_y dy' - \int_0^{M'} E_y dy'] \qquad (A4)$$

$$= \frac{1}{M'' - M'} [DD_2'' - DD_2'] = \frac{1}{M'' - M'} [\ln(\frac{M_m''^2 + a'^2}{M_p''^2 + a'^2}) - \ln(\frac{M_m'^2 + a'^2}{M_p'^2 + a'^2})]$$

where we introduced

M' = either 1/3 or 9/11,   M" = either 5/3 or 13/11, M' - b' = M_m' ,

M' + b' = M_p', M" - b' = M_m'', M' + b' = M_p'', M" - M' = either 4/3 or 4/11

$$P_1 = 2(2b'^2 + a'^2)/[b'(b'^2 + a'^2)], \quad Q_1 = 4b'^2/(b'^2 + a'^2)$$

2.   CASE 3 AND CASE 4:   DIFFERENTIAL MODE

$$F_3(a',b') = \frac{NN_3(a',b')}{DD_3(a',b')} \tag{A5}$$

$$NN_3(a',b') = \left\{ \frac{1}{L'} \int_0^{L'} [E_x(a',b',x') - DD_3(a',b')]^2 \, dx' \right\}^{1/2}$$

$$(NN_3)^2 = \frac{1}{L'} \left\{ -\frac{L_m/2}{L_m^2 + k_m^2} - \frac{L_p/2}{L_p^2 + k_m^2} - \frac{L_m/2}{L_m^2 + k_p^2} - \frac{L_p/2}{L_p^2 + k_p^2} \right.$$

$$+ \frac{1}{2k_m}\left[\arctan(\frac{L_p}{k_m}) + \arctan(\frac{L_m}{k_m})\right] + \frac{1}{2k_p}\left[\arctan(\frac{L_p}{k_p}) + \arctan(\frac{L_m}{k_p})\right]$$

$$+ (DD_3)^2 L' + \frac{U_2 - U_1 + 2DD_3}{2} \ln(\frac{L_m^2 + k_m^2}{a'^2 + k_m^2}) + \frac{U_1 - U_4 - 2DD_3}{2} \ln(\frac{L_p^2 + k_m^2}{a'^2 + k_m^2})$$

$$+ \frac{U_4 - U_5 - 2DD_3}{2} \ln(\frac{L_m^2 + k_p^2}{a'^2 + k_p^2}) + \frac{U_5 - U_2 + 2DD_3}{2} \ln(\frac{L_p^2 + k_p^2}{a'^2 + k_p^2})$$

$$+ \frac{V_2 - V_1 - V_3 - a'(U_2 - U_1)}{k_m} \left[\arctan(\frac{L_m}{k_m}) - \arctan(\frac{a'}{k_m})\right]$$

$$+ \frac{Z_4 - V_1 - V_3 - a'(U_1 - U_4)}{k_m} \lceil arctan(\frac{L_p}{k_m}) - arctan(\frac{a'}{k_m}) \rceil$$

$$+ \frac{V_4 - V_5 - Z_3 + a'(U_4 - U_5)}{k_p} \lceil arctan(\frac{L_m}{k_p}) + arctan(\frac{a'}{k_p}) \rceil$$

$$+ \frac{Z_2 - V_5 - Z_3 - a'(U_5 + U_2)}{k_p} \lceil arctan(\frac{L_p}{k_p}) - arctan(\frac{a'}{k_p}) \rceil \}$$

$$DD_3 = \frac{1}{L'} \int_0^{L'} E_x(a',b',x')dx' \qquad (A6)$$

$$= \frac{1}{L'} [\frac{1}{2} ln(\frac{k_m^2 + L_p^2}{k_m^2 + L_m^2}) - \frac{1}{2} ln(\frac{k_p^2 + L_p^2}{k_p^2 + L_m^2})]$$

where we introduced:

$$U_1 = (2a'^2 + k_m^2)/\lceil 2a'(a'^2 + k_m^2) \rceil, \quad V_1 = - a'^2/(a'^2 + k_m^2)$$

$$Z_2 = \lceil (2a'^2 + k_p^2) b' - 2a'^4 \rceil/\lceil 2(a'^2 + b'^2)(1 + a'^2) \rceil,$$

$$V_2 = - 2a'^2/(a'^2 + k_p^2) - (a'^2 + k_m^2)/(a'^2 + k_p^2) \times Z_2,$$

$$U_2 = -b'/\lceil a'(a'^2 + k_p^2) \rceil \times Z_2 + (2a'^2 + k_p^2)/\lceil 2a'(a'^2 + k_p^2) \rceil, \quad V_3 = -k_m^2/2b',$$

$$Z_3 = k_p^2/2b', \quad Z_4 = \lceil -(2a'^2 + k_m^2)b' - 2a'^2 \rceil/\lceil 2(1 + a'^2)(a'^2 + b'^2) \rceil,$$

$$U_4 = b'/\lceil a'(a'^2 + k_m^2) \rceil \times Z_4 + (2a'^2 + k_m^2)/\lceil 2a'(a'^2 + k_m^2) \rceil,$$

$$V_4 = -2a'^2/(a'^2 + k_m^2) - (a'^2 + k_p^2)/(a'^2 + k_m^2) \times Z_4,$$

$$U_5 = (2a'^2 + k_p^2)/[2a'(a'^2 + k_p^2)], \quad V_5 = a'^2/(a'^2 + k_p^2).$$

$$F_4(a',b') = \frac{NN_4(a',b')}{DD_4(a',b')} \tag{A7}$$

$$NN_4 = \left\{ \frac{1}{M'' - M'} \int_{M'}^{M''} [E_x(a',b',y') - DD_4(a',b')]^2 \, dy' \right\}^{1/2}$$

$$(NN_4)^2 = \frac{1}{M'' - M'} \left\{ \frac{2M_m''}{a'^2 + M_m''^2} + \frac{2M_p''}{a'^2 + M_p''^2} - \frac{2M_m'}{a'^2 + M_m'^2} - \frac{2M_p'}{a'^2 + M_p'^2} \right.$$

$$+ \left(\frac{2 - E_1 b' - H_1}{a'} \right) \left[\arctan\left(\frac{M_m''}{a'}\right) + \arctan\left(\frac{M_p''}{a'}\right) - \arctan\left(\frac{M_m'}{a'}\right) - \arctan\left(\frac{M_p'}{a'}\right) \right]$$

$$- 4 \frac{DD_4''}{M''} \left[\arctan\left(\frac{M_m''}{a'}\right) - \arctan\left(\frac{M_p''}{a'}\right) \right] + 4 \frac{DD_4'}{M'} \left[\arctan\left(\frac{M_m'}{a'}\right) - \arctan\left(\frac{M_p'}{a'}\right) \right]$$

$$\left. - \frac{E_1}{2} \left[\ln\left(\frac{M_m''^2 + a'^2}{M_m'^2 + a'^2}\right) - \ln\left(\frac{M_p''^2 + a'^2}{M_p'^2 + a'^2}\right) \right] \right\}$$

$$DD_4 = \frac{1}{M'' - M'} \int_{M'}^{M''} E_x(a',b',y') \, dy' = \frac{1}{M'' - M'} \left[\int_0^{M''} E_x dy' - \int_0^{M'} E_x dy' \right] \tag{A8}$$

$$= \frac{1}{M'' - M'} [DD_4'' - DD_4']$$

$$= \frac{2}{M'' - M'} \left[\arctan\left(\frac{M_m''}{a'}\right) - \arctan\left(\frac{M_p''}{a'}\right) - \arctan\left(\frac{M_m'}{a'}\right) + \arctan\left(\frac{M_p'}{a'}\right) \right]$$

where we introduced

$$M_m'' = M'' - b', \quad M_p'' = M'' + b', \quad M_p' = M' + b', \quad M_m' = M' + b',$$

$$E_1 = -2a'^2/[b'(b'^2 + a'^2)], \quad H_1 = 4a'^2/(a'^2 + b'^2).$$